STUDIES OF AN ATMOSPHERIC FLUIDIZED BED COMBUSTOR USING COTTON STALK

A thesis submitted in fulfillment of the requirements for the award of degree of

Doctor of Philosophy
in
Mechanical Engineering

Submitted By

RAJEEV KAMAL SHARMA
(Reg. No. 950808004)

DEPARTMENT OF MECHANICAL ENGINEERING
THAPAR INSTITUTE OF ENGINEERING AND TECHNOLOGY
PATIALA – 147004
PUNJAB, INDIA
JULY, 2018

CERTIFICATE

Certified that the thesis entitled **"STUDIES OF AN ATMOSPHERIC FLUIDIZED BED COMBUSTOR USING COTTON STALK"** which is being submitted by **MR. RAJEEV KAMAL SHARMA, Registration No. - 950808004,** to Thapar Institute of Engineering and Technology, Patiala in fulfillment for the award of Doctor of Philosophy in Mechanical Engineering is a record of bonafide research work carried out by him under my guidance and supervision. The matter presented in this thesis has not been submitted either partially or fully to any other University or Institution for the award of any other degree.

S.K. Mohapatra

Senior Professor

Department of Mechanical Engineering

Thapar Institute of Engineering and Technology

Patiala

ACKNOWLEDGEMENT

Words are never comparable to actions those performed by humans but are the only way to pay regards. During the time of presentation of my thesis, it is worthwhile to remember almighty for filling me with all my strength that helped me to complete the present research work successfully.

It's my pleasure to pay regards and special thanks to my esteemed and eminent supervisor **Dr. S. K. Mohapatra**, Senior Professor, Department of Mechanical Engineering, Thapar Institute of Engineering and Technology, Patiala, Punjab, India for all the support, encouragement, guidance and profound efforts without which it was not possible to attain the desired level of achievement.

I would appreciate the support provided by the officials at Malwa Power Plant Limited (MPPL), Sri Mukatsar Sahib, India, during the sample collection and data sharing. I would also like to thank Sophisticated Analytical Instruments Laboratories (SAI), Thapar Institute of Engineering and Technology, Patiala, Punajb, India and Civil Engineering Department, RIMT-IET, Mandi Gobindgarh, Punjab, India for testing of various samples.

Heartiest thanks to my family who supported me all the way. All the inspirations from my parents Mr. Ravinder Nath Sharma and Ms. Saroj Sharma made it possible to complete the present work. A special thanks to my wife Ms. Preeti Sharma for her help and patience throughout my PhD work. I thank to my younger brother Dr. Sanjeev Kamal Sharma and his wife Ms. Mamta Sharma who spared me at the time of thesis preparation and remained resourceful. A loving thanks to four kids - Armaan, Vardaan, Sushant and Ishant who worked as stress busters at the time of mental fatigue.

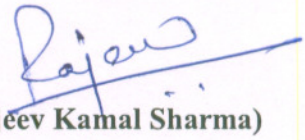

(Rajeev Kamal Sharma)

ABSTRACT

In the present work, combustion characteristics of cotton stalk based 7.5 MW atmospheric fluidized bed combustor at Malwa power plant limited (MPPL), Muktsar Sahib, Punjab, India have been studied. Operational data and various fuel samples have been collected from the plant site. A solid population balance model for fuel with wide size particle distribution (cotton stalk with particle size ranging between 0.75 mm to 80 mm) has been developed and optimized. Bed carbon load and carbon utilization efficiency are found to be rising with increase in fuel particle size modulus and distribution modulus. The solid population balance model has been optimized for maximum carbon utilization efficiency and minimum elutriation rate using multi-response optimization method. Fuel particle diameter, fuel feed rate and fractional excess air have been selected as input parameters and their optimal values are found to be 15 mm, 1.5 kg/s and 0.3 respectively.

A three-phase exit gas composition model (considering bubble growth along bed height) has been developed. Model can predict exit gas composition from the fluidized bed combustor (FBC) using cotton stalk. It has been found that oxygen conversion decreases with rise in fractional excess air supply.

First law of thermodynamics (energy) and second law of thermodynamics (exergy) based thermodynamic model has been developed and optimized in the present work. It has been found that the boiler is the source of maximum exergy destruction. The thermodynamic model has been optimized for overall plant exergy efficiency and complete cycle exergy destruction using multi-response optimization method. Turbine inlet steam pressure, turbine inlet steam temperature and fuel feed rate have been selected as input parameters and their optimal values are found to be 65 bar, 470˚C and 1.5 kg/s respectively.

A brake-even analysis based economic study for maximum profit from the plant has also been conducted. In addition, agglomeration behavior of the cotton stalk under fluidized bed conditions has been studied experimentally.

TABLE OF CONTENTS

LIST OF FIGURES

LIST OF TABLES

NOMENCLATURE

A_{att}	Dimensionless attrition constant
A_o	Cross sectional area of the bed, cm^2
C_{avg}	Average concentration of exit gas, g-mol/cm^3
C_b	Oxygen concentration in bubble phase, g-mol/cm^3
C_{cw}	Oxygen concentration in cloud-wake phase, g-mol/cm^3
C_e	Oxygen concentration in emulsion phase, g-mol/cm^3
C_o	Inlet oxygen molar concentration, g-mol/cm^3
c_p	Specific heat at constant pressure, J/kg-K
c_{p_g}	Specific heat of exhaust gases at constant pressure, J/kg-K
D_g	Gas diffusivity, cm^2/s
d_B	Bubble diameter, cm
d_{bed}	Bed diameter, cm
d_p	Fuel particle diameter, cm
$d_{p_{mean}}$	Size modulus, cm
$d(d_p)/dt$	Cotton stalk particle shrinkage rate, g/s
E	Energy, kJ
E_x	Exergy, kJ
E_x^{tm}	Thermo-mechanical exergy, kJ
E_x^{ch}	Chemical exergy, kJ
E_{xair}	Fractional excess air
$\dot{E}_{x_D}$	Exergy destruction rate, kW
$E_{x_{fuel}}$	Specific exergy of fuel, kJ/kg
$\dot{E}_{x,P}$	Exergy of the products, kW
$\dot{E}_{x,R}$	Exergy of the reactants, kW
$\dot{F}_o$	Total carbon feed rate, g/s
$\dot{F}_1$	Overflow rate, g/s
$\dot{F}_2$	Carry over rate, g/s
$F(d_p)$	Distribution function
F_e	Evaporation factor

$\dot{F}_{ME}$	Actual molar feed rate of fluidizing air, g-mol/s
$\dot{F}_{MTH}$	Chemically correct molar feed rate of fluidizing air, g-mol/s
F_r	Froude number
f_{cw}	Cloud-wake phase fraction in the bed
$f(d_p)$	Density function
g	Acceleration due to gravity, cm/s^2
H_{mf}	Bed height at minimum fluidization, cm
h	Specific enthalpy, kJ/kg
h_o	Enthalpy at ambient conditions, kJ
$(K_{bc})_b$	Bubble to cloud-wake gas interchange coefficient, s^{-1}
$(K_{ce})_b$	Cloud-wake to emulsion gas interchange coefficient, s^{-1}
K_s	Intrinsic reaction rate constant, cm/s
$K^*(d_p)$	Elutriation rate constant, g/cm^2-s
$\dot{K}(d_p)$	Elutriation rate, s^{-1}
LHV	Lower heating value, kJ/kg
M_c	Molecular weight of carbon
m	Distribution modulus
$\dot{m}$	Mass flow rate, kg/s
m_a	Evaporation capacity, kg of steam/ kg of fuel
m_e	Equivalent evaporation, kg of steam/ kg of fuel
$\dot{m}_{fuel}$	Fuel mass flow rate, kg/s
P_{av}	Average combustor pressure, atm
Q	Heat, kJ
R	Gas Constant, atm-cm^3/g-mol-K
R_{et}	Reynolds number based on terminal velocity
r	Correlation coefficient
S_H	Sherwood number
s	Specific entropy, kJ/kg-K
T	Absolute temperature, K
T_b	Bed temperature, K

T_o	Ambient temperature, K
U_b	Gas velocity through bubble phase, cm/s
U_{cw}	Gas velocity through cloud-wake phase, cm/s
U_e	Gas velocity through emulsion phase, cm/s
U_{mf}	Minimum gas velocity, cm^2/s
U_o	Superficial gas velocity, cm/s
U_T	Terminal velocity, cm/s
u_b	Absolute velocity of crowd of bubbles, cm/s
u_{br}	Single bubble rise velocity, cm/s
$\dot{V}_g$	Volumetric flow rate, cm^3/s
$\dot{W}$	Work, kJ
W_c	Bed carbon load, g
$\dot{W}_{\text{cooton stalk}}$	Cotton stalk feed rate, g/s
XC	Carbon weight (%)
XH	Hydrogen weight (%)
XO	Oxygen weight (%)
XS	Sulphur weight (%)
XV	Volatile matter weight (%)
XW	Moisture weight (%)
Y_1	Weight of empty silica crucible and lid (g)
Y_2	Weight of cotton stalk, silica crucible and lid before heating (g)
Y_3	Weight of cotton stalk, silica crucible and lid after heating (g)
Y_4	Weight of cotton stalk after moisture removal, silica crucible and lid before heating (g)
Y_5	Weight of cotton stalk after moisture removal, silica crucible and lid after heating (g)
Y_6	Weight of ash and silica crucible after heating (g)
Z	Bed height, cm

Greek symbols

λ_c	Heat conductivity, W/mK
ε_b	Volume fraction of bubbles in the bed

ε_{mf}	Bed voidage at minimum fluidization
ρ_g	Gas density, g/cm^3
ρ_p	Density of cotton stalk, g/cm^3
μ_g	Gas viscosity, g/cm/s
η	Efficiency

Subscript

b	Bubble phase
e	Emulsion phase
g	Gas phase
mf	Minimum fluidization

Abbreviations

ASTM	American society for testing and materials
C	Carbon
CEP	Condenser extraction pump
CO	Carbon monoxide
CO_2	Carbon monoxide
FWP	Feed water pump
H	Hydrogen
LHV	Lower heating value, kJ/kg
N	Nitrogen
O	Oxygen
P	Phosphorus
PSD	Particle size distribution
RIMT	Regional Institute of Management and Technology
S	Sulphur
SEM	Scanning Electron Microscope

Chapter 1

INTRODUCTION

India consumes about 3.4% of the total global energy generation [1]. By 2030, the electricity demand in India is expected to cross 960,000 MW [1]. Out of the total electricity consumed, coal-based thermal power plants, hydroelectric power plants, nuclear power plants, and non-utilities supply 70.25%, 14.24%, 1.68%, and 13.83% respectively [1]. This shows that India largely depends on coal for electricity generation. But coal shortages, delay in coal transportation, its lower calorific value, and high ash content cause disruptions in energy generation. In India, every day around 0.8 million tons of coal is extracted. At this rate, the coal reserves are expected to last over in the next 100 years. The situation is not different in rest of the world.

The oil shocks of 1973 and 1979 along with the fear of losing coal reserves forced the researchers all over the world to think about energy self-sufficiency and alternate to fossil fuels. The only option left was moving for large-scale adoption and development of renewable energy sources. This was the beginning of a new era for renewable energy sources. The development of renewable energy sources became an integral part of the development plans worldwide. Biomass, small hydropower plants, wind, and solar emerged as primary renewable energy sources. Most of these sources are location specific except for biomass, which is available in different forms throughout the world.

1.1. Biomass – a potential source of energy

Biomass is the biological material produced from living or non-living organisms. It is one of the oldest forms of renewable energy and is in use for thousands of years. Wood is the primary source of biomass, crop residues such as wheat straw, cotton stalk, rice husk, mustard husk, and sugarcane residue along with municipal and animal wastes are its other sources. Biomass

is used mainly for cooking and power generation. The biomass energy potentials in various regions of the world are shown in Table 1.1.

Table 1.1. Global biomass energy potential

Region	Biomass energy potentials (EJ/ year)	
	Woody	**Non-woody***
Asia	7.7	13.7
Latin America	5.9	15.6
North America	12.8	7.1
Former USSR	5.4	4.6
Africa	5.4	16.0
The Middle East	0.4	0.3
Europe	4.0	4.9
World	41.6	62.2

Modified from [2].
* Non-woody = Energy crops + straw.

1.1.1. Importance of efficient biomass utilization

Biomass utilization for power generation increases energy security, decreases problems associated with biomass waste management and reduces the load on fossil fuels. Also, it can be a source of revenue generation. If managed sustainably, biomass reduces carbon emission. Biomass is also called carbon-neutral energy source as the carbon dioxide produced upon its burning equals carbon dioxide consumed during its growth. This is known as zero-carbon emission cycle as shown in Figure 1.1.

1.1.2. Biomass status in India

In India, about 147,610 MW of renewable energy is estimated [1]. Figure 1.2 shows different forms of renewable energy available in India. Among the renewable energy reserves, the biomass is locally available and is easily convertible into more useful form with lower capital

investment. Agro residues, agro-industry residues, forest residues, and energy plants are the various types of biomass used in India. According to Ministry of New and Renewable Energy (MNRE) annual report, 60 million metric tons of surplus agro and forest residues are available for electricity generation, and 13 GW of electricity generation is possible in India from surplus biomass.

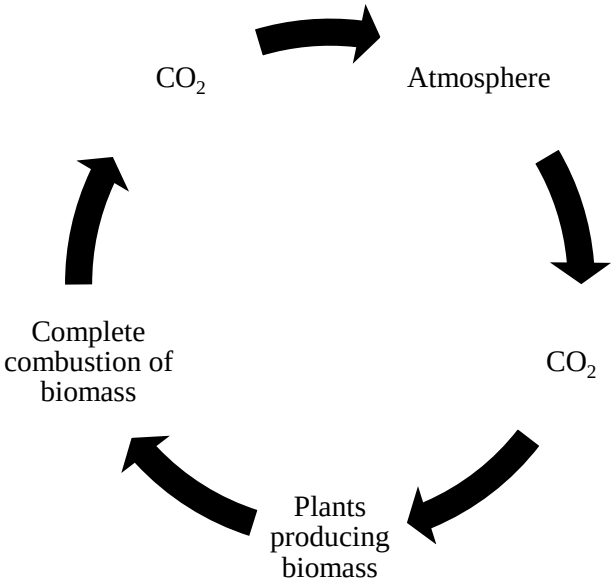

Figure 1.1. Zero carbon emission cycle (modified from [2])

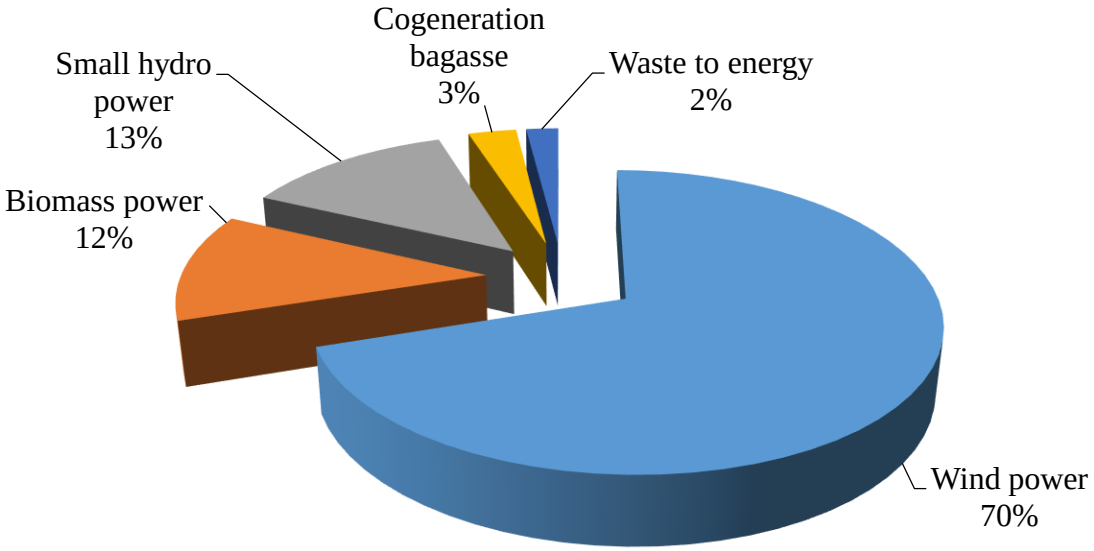

Figure 1.2. Renewable energy potential in India (modified from [1])

1.1.3. Biomass status in Punjab

Punjab has been put on forefront after the green revolution (1965-1972), when wheat production increased three times. The increase in production of other crops has also been impressive. Punjab is also called the food granary of India. It is spread over 50,360 km^2 and is located 30° 4' N latitude and 75° 5' E longitude. Punjab contributes 55% of rice, 22% of wheat, and 25% of cotton to total country's production, whereas, it has merely 1.5% of the total cultivable land. The state uses 84% of the entire geographical area for agriculture, producing around 40.14 metric tons of agricultural and industrial biomass residues annually. 71% of crop residue is consumed in different forms and 29% is left as surplus. 1.464 GW of energy can be produced from the net surplus crop residue [3]. Independent biomass-based thermal power plants and cogeneration plants have been recently commissioned in Punjab for converting biomass into energy. Table 1.2 shows the biomass-based thermal power plants currently operating and under implementation in Punjab. The state aims to generate 15% (5,400 MW) of its power requirement from renewable energy sources by 2022.

It can be concluded from the above discussion that biomass can be a massive source of energy generation in India and there is a requirement of efficient technologies for its conversion into energy.

1.2. Biomass to energy conversion technologies

Direct firing, biomass gasification, biomass co-firing with coal, anaerobic digestion, and ethanol production are the technologies in use for producing useful energy from biomass [4]. Direct firing is the most common technology in use. Biomass burns in the combustor and generates heat in the presence of air. Heat converts water into steam in the boiler. Steam is used to run steam turbine producing mechanical work. Mechanical work is further converted into electricity using an electric generator. Direct firing is inefficient but is simple in use.

Table 1.2. Biomass based power plants in Punjab

S. no.	Name and location of the plant	Plant capacity (MW)	Month of establishment
1	Jalkheri power private limited, village Jalkheri, Fatehgarh Sahib.	10.0	January 1992
2	Malwa power plant limited, village Gulabewala, Sri Muktsar Sahib.	7.5	May 2005
3	Dee development engineers private limited, village Gaddadhob, Ferozepur.	8.0	February 2009
4	Universal biomass energy private limited, village Channu, Sri Muktsar Sahib.	14.5	October 2009
5	Punjab biomass power private limited, Patiala.	12.0	June 2010
6	Green planet energy private limited, Hoshiarpur.	6.0	March 2012
7	Green planet energy private limited, Jalandhar.	6.0	February 2013
8	Viaton energy private limited, Mansa.	10.0	July 2013
9	Green planet energy private limited, village Binjon, Hoshiarpur.	4.0	Under implementation
10	Green planet energy private limited, village Bir, Jalandhar.	4.0	Under implementation
11	Green planet energy private limited, village Manuke Gill, Moga.	6.0	Under implementation

Source: Punjab energy development authorities, Chandigarh (U.T.), India.

Biomass gasification is another efficient, promising, and advanced technique. In this, biomass is converted into a gas having energy content lower than natural gas. Gas generated from biomass is used to produce heat and run gas turbines. Biomass gasification is still under

developing stage. Biomass co-firing with coal in a thermal power plant is another option to convert biomass into useful energy. This method is also very efficient and is extensively used.

Pile, stoker, suspension, and fluidized bed combustion are the different technologies of direct firing in use to convert biomass into energy. Among these, fluidized bed combustion is the most popular and best suited. Fluidized bed combustor works upon the principle of fluidization as discussed in the next section.

1.3. Science of fluidization

Fluidization is a phenomenon of reducing friction between the bed particles using some counter forces such that the bed behaves like a flowing fluid [5]. Fluidizing gas like air or inert gas is made to flow in the direction opposite to the direction of friction. The drag exerted by the fluidizing gas is the counter force acting against friction. Bed particles are suspended when the drag balances the friction. The bed material particles suspended in the fluid neither move out of the combustor nor settle down in the bed. Fluidizing gas moves upward in bubbles form and movement of fluidizing gas mixes the bed material particles well. This increases the surface area available for heat transfer. Alumina and silica are the commonly used bed materials in FBC. Vigorous movement of bed material particles makes the heat transfer process more efficient. Bed material particles also act as a thermal reservoir. Due to this property of bed material, combustor temperature does not change rapidly with the change of plant load or operating conditions.

Fluidization was introduced in 1942, when the first fluidized catalytic cracking plant was set up in Baton Rouge, Louisiana. In 1948, Fluidization was noticed by researchers when Wilhelm and Kwauk [6] categorized it as aggregative and particulate fluidization. In 1961, Davidson [7] proposed the theoretical concept of bubble formation which was confirmed experimentally by Row and Partridge [8] in 1963. The theories of fluidization and fluidized

bed were published in the book written by Kunii and Levenspiel [9] and its design theory was explained by Yue et al. [10]. After this, the development of fluidization science was prolonged for next forty years. At present, fluidization has found applications in coal and biomass-based thermal power plants, petroleum refineries, pharmaceutical industries, agriculture food sectors and lots more. Figure 1.3 shows the different phases of fluidization [11].

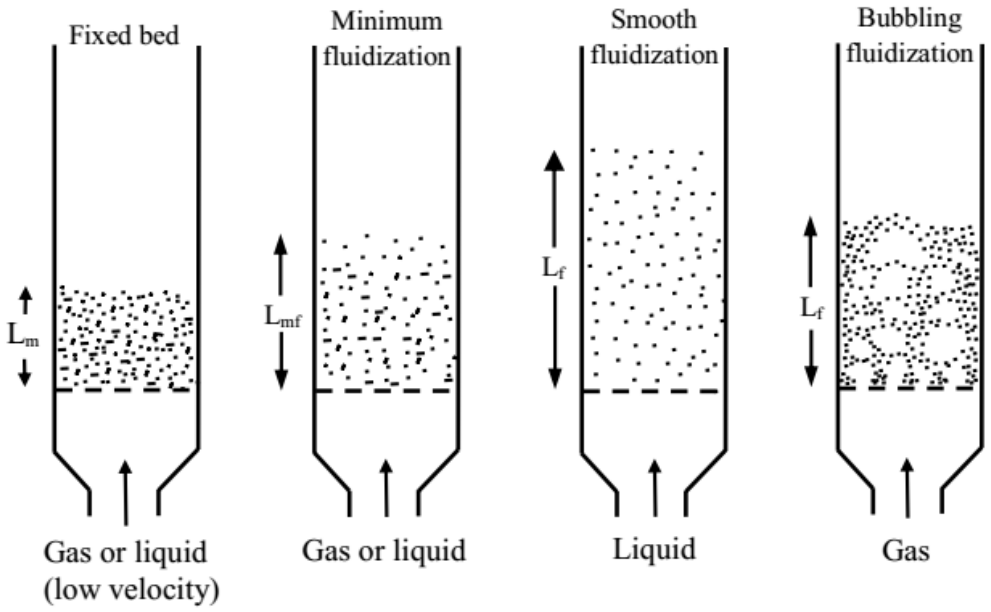

Figure 1.3. Phases of fluidization (adapted from [11])

1.4. Fluidized bed combustor

A fluidized bed combustor works on the principle of fluidization. Fuel flexibility, improved heat transfer rate, efficient combustion, isothermal combustion, and low NO_x emission make fluidized bed combustor as one of the most preferred options for converting biomass into useful energy. Biomass of any type and moisture content up to 55% can be fed into the preheated bed with an efficiency in the range of 80-85%. In an FBC, chemical reactants can be introduced into the bed to remove harmful gases like SO_x.

All types of fluidized bed combustors consist of fuel feeding, fluidizing air distribution, heat transfer, and ash removal systems. Fuel feeding systems can be under-bed or

over-bed type. The under-bed feeding system is used for fuel particles having the size ranging from 6 to 10 mm. For large size particles, over-bed fuel feeding system is used where screw conveyors carry fuel from storage point to the combustor. Modern combustors are fitted with both types of fuel feeding systems.

Fluidized bed air distribution system consists of a distributor plate having many holes fitted with tuyere or cap type nozzles. The distributor plate ensures the uniform distribution of the fluidizing air in the bed so that inventory in the bed is under constant turbulence. This also reduces the possibility of agglomeration or clinker formation.

Heat transfer in the bed takes place from bed material to water tubes passing through the bed. Heat transfer rate depends upon the height of the bed, positioning of the water tubes, bed temperature, bed pressure, gas velocity, fuel particle size, and distributor plate design.

Ash removal system of FBC consists of the subsystems for the removal of fly ash and bottom ash. In fluidized bed combustors, fly ash and bottom ash are 55% to 65% and 35% to 45% respectively. Fly ash removal from flue gases is performed in preheaters, economizer, and finally in the dust collectors. Electrostatic precipitators, cyclones, bag filters are some common types of the dust collectors. Bottom ash is removed as overflow from the bed or from the combustor's bottom. Overflow ash removal is required to maintain the necessary bed height. Agglomeration or clinker formation is a crucial problem encountered in fluidized bed combustors. Agglomerates or clinkers are removed from the bed bottom as and when needed to avoid defluidization of the bed.

Fluidized bed combustors are classified as follows:

- Atmospheric fluidized bed combustor
- Circulating fluidized bed combustor
- Pressurized fluidized bed combustor

1.4.1. Atmospheric fluidized bed combustor

Atmospheric Fluidized Bed Combustor (AFBC) is the most important type of fluidized bed combustor. Variety of fuels like agricultural wastes, forest wastes, municipal wastes, animal wastes, and even inferior quality coal can be burnt efficiently in an atmospheric fluidized bed combustor. AFBC finds wide applications in energy and cogeneration industries. Figure 1.4 shows the general arrangement of an AFBC.

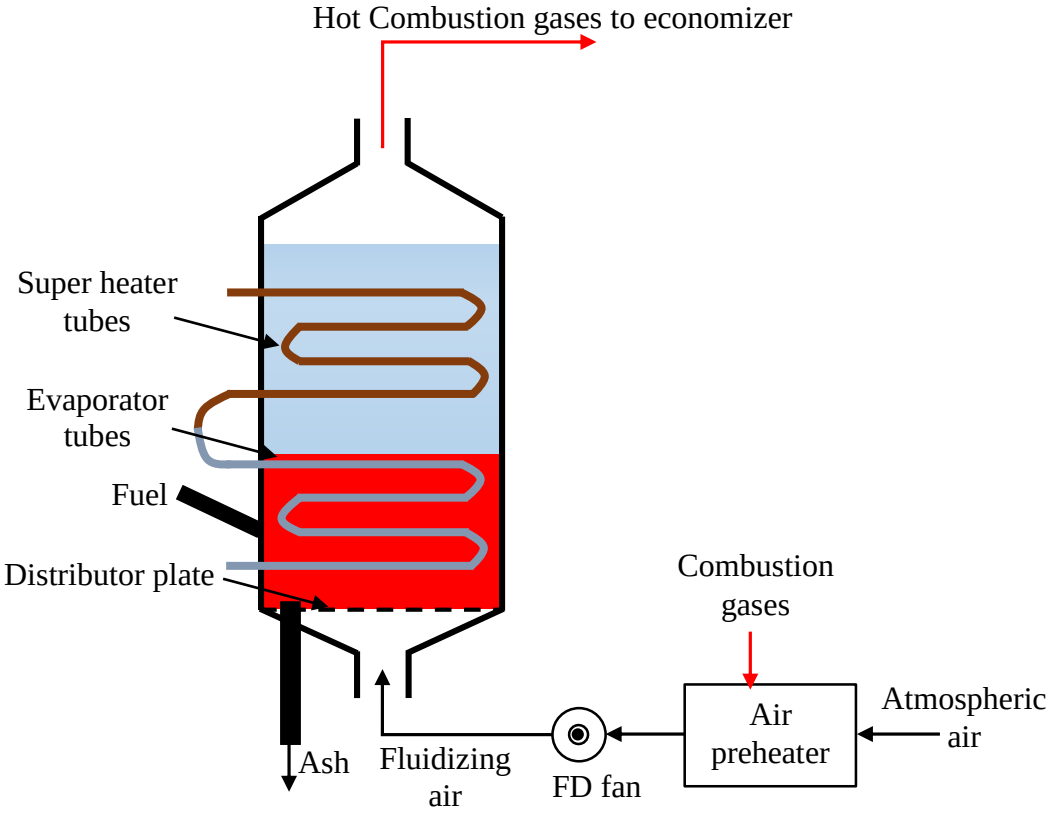

Figure 1.4. Atmospheric fluidized bed combustor (modified from [11])

An AFBC bed is an inventory of fuel particles, inert bed material particles, and limestone (as sorbent). Atmospheric air (preheated by exhaust flue gases in an air preheater) is pressurized in Forced Draft (FD) fan and is supplied to the combustor through the distributor plate containing number of nozzles.

Pressurized preheated atmospheric air acts as fluidizing as well as combustion air. Fluidizing air is supplied at velocities between 1 to 4 m/sec and its supply rate determines the

amount of the fuel that can be burnt in the combustor. Type of the fuel and fuel supply system decide about the feed size of the fuel particle. Smaller size fuel particles such as rice husk and mustard husk are supplied in the original shape and size, whereas longer fuel particles such as cotton stalk and wheat straw are cut into appropriate size before supplying to the combustor. Larger size particles can be supplied as briquettes also. Briquettes may be of different size and shapes.

AFBC is preheated to a temperature above 600°C by burning kerosene or furnace oil. Once the required temperature is attained, kerosene or furnace oil supply is gradually reduced and fuel supply is gradually increased. Kerosene or furnace oil supply is stopped once the combustion is sustained by the fuel only and the bed becomes nearly isothermal. Water filled evaporator tubes pass through the bed and the water is heated by the hot gases in the bed. Water heated in the evaporator tubes is passed through the super-heater tubes (positioned in the upper portion of the combustor) producing superheated steam. Superheated steam is collected in the steam drum. The hot gases produced in the combustor rise to the evaporator, super-heater, economizer, particulate collector, and the air preheaters before being exhausted through the chimney to the atmosphere. AFBC operates in 800°C to 850°C temperature range. Agglomeration is one of the most critical reasons responsible for the defluidization of an AFBC. Agglomeration can be controlled by maintaining bed temperature below 850°C. In this temperature range, Sulphur retention is also more efficient.

1.4.2. Circulating fluidized bed combustor

Circulating fluidized bed combustors (Figure 1.5) are used where plant capacity ranges from medium to large, SO_x/NO_x emission control is important, and inferior quality fuel is to be used. Fuel along with limestone are supplied into the combustor and bed inventory is fluidized by the fluidizing air. Primary fluidizing air is supplied through nozzles mounted in the distributor

plate and secondary air is supplied at locations above the plate. The fuel is burnt at low temperature producing heat, Sulphur dioxide and nitrogen oxide (NO_x). Sulphur dioxide is absorbed by limestone and ammonia is injected in the hot gases at the combustor outlet to reduce NO_x emission.

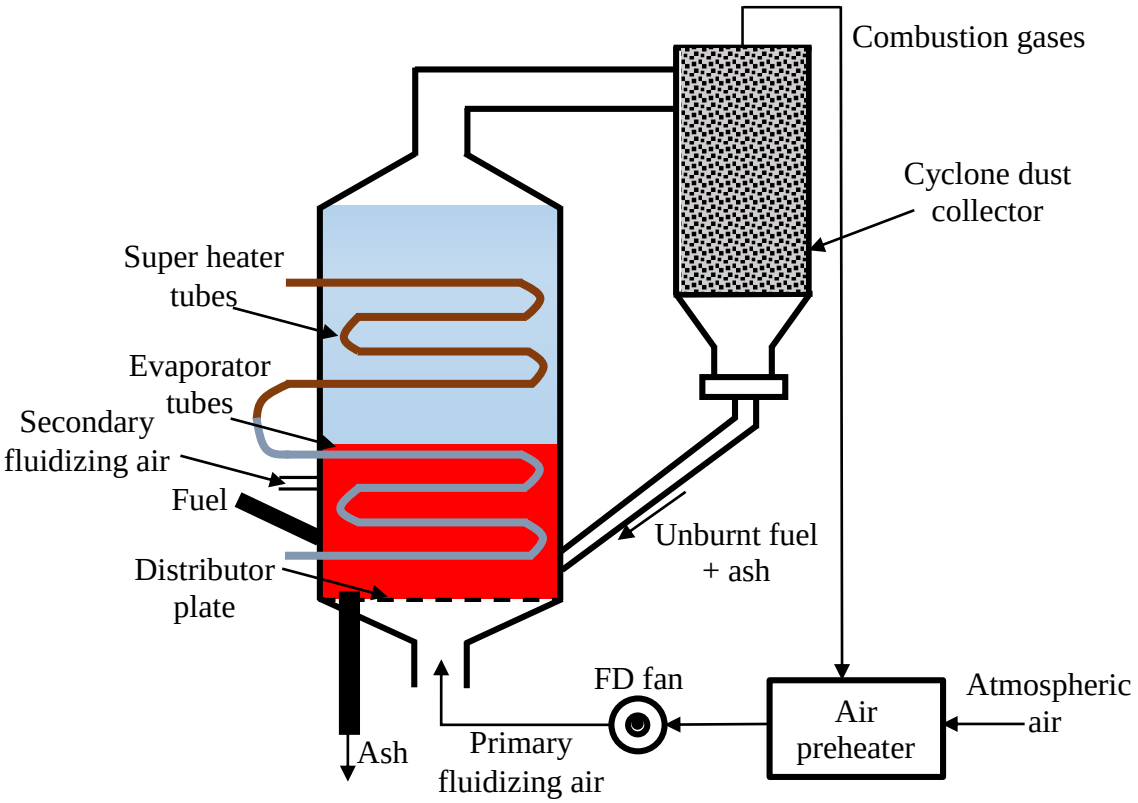

Figure 1.5. Circulating fluidized bed combustor (modified from [12])

Water tubes are parallel to the flue gases flow direction and this arrangement reduces the erosion rate of hot surfaces in the combustor. The fluidizing air velocity and fines (5 to 10% of total fuel supplied) elutriating with fluidizing air in CFBC are higher in comparison to AFBC. To recover elutriating fuel particles, cyclone dust collector is used. Cyclone dust collector separates unburnt fuel and ash from flue gases and return them to the combustor. This increases the combustion efficiency of the combustor. Fuel particles residence time and bed turbulence control fluidized bed combustor's temperature. Fuel residence time increases for taller combustors, which in turn increases combustion efficiency. Sorbent residence time is

also increased in the taller combustors leading to cleaner flue gas emission. Two-point entry of fluidizing air as primary and secondary air increases turbulence in the bed. High turbulence and recirculation of fuel particles using cyclone separator make the bed temperature uniform throughout the combustor. Low bed temperature also reduces the NO_x formation.

1.4.3. Pressurized fluidized bed combustor

Pressurized Fluidized Bed Combustor (PFBC) is mainly used for combined cycle power generation or cogeneration. In combined cycle power generation, both steam and gas turbines are operated by steam from boiler drum and high-pressure exhaust gases respectively. Such systems are 5 to 8% more efficient than conventional systems. The combustor in PFBC operates at a pressure ranging from 17 bar to 20 bar. Condensate is preheated using exhaust from the gas turbine and is supplied to the boiler drum as feed water.

1.5. Advantages of fluidized bed combustor

Fluidized bed combustors have the following advantages over conventional boilers:

- Fluidized bed combustors have higher combustion efficiency even with the high ash content fuels. Overall efficiency varies between 80% to 90%. Turbulence created by fluidizing air increases the surface area for heat transfer. Due to this, the dimensions of fluidized bed combustor are lesser in comparison to conventional boilers.
- Fuel flexibility is one of the biggest advantages of FBC. Any fuel having high ash content, low calorific values, high moisture content (up to 55%), and low carbon content up to 1% can be burnt independently or can be co-fired with crushed coal or other fuels in a fluidized bed combustor.
- Fine fuel particles such as coal below 6 mm size can be fed and burnt in FBC very efficiently. Fine fuel particles are difficult to burn in conventional boilers.

- Biomass of any size (as small as rice husk and as large as cotton stalk and wheat straw) can be burnt efficiently in FBC.
- SO_2 emission can be reduced efficiently by adding limestone in the bed material. Low bed temperature reduces NO_x formation significantly.
- Excess air requirement reduces in FBC systems due to the turbulence created by fluidizing air in the bed. Each fuel particle has sufficient oxygen for its burning which reduces the amount of CO in the exhaust gases.
- FBC can adjust quickly to load changes due to heat storage by the inert bed materials.

Fluidized bed combustors have certain drawbacks such as N_2O and agglomeration formation at low temperatures.

1.6. Characteristics of cotton stalk

The cotton plant is cultivated in tropical/ subtropical areas around the world, including Africa, India, and United States of America. It is a fluffy and soft fiber, growing in a boll around its seed. The cotton plant is of Gossypium genus and is of Malvaceae family. Cotton fiber is pure cellulose. Cotton is mostly spun into threads and used for making fabric. The invention of cotton gin lowered its production cost and increased use of cotton worldwide. About 25 million tons of cotton is produced annually around the world and China, India, United States, Pakistan, Brazil, Australia, and Turkey being its major producers. Japan, Korea, Russia, and Taiwan are primary importers of cotton. Gossypium barbadense (staple cotton), Gossypium hirsutum (upland cotton), Gossypium herbaceum (levant cotton), and Gossypium arboretum (tree cotton) are main types of cotton, out of which Gossypium arboretum is cultivated in India and Pakistan. White, brown, pink, and green are four natural colors of cotton. It is cultivated in areas having enough sunlight, moderate rainfall, and heavy soil.

After harvesting of cotton from its plant, it is left with a stem which is called cotton

stalk. The cotton stalk is burnt in the fields leading to environmental pollution. However, for the past few years, the cotton stalk after drying is used as fuel in an FBC. Figure 1.6 shows the picture of cotton plant taken from the fields in Sri Muktsar Sahib, Punjab, India.

Figure 1.6. Cotton plant picture taken from the fields in Sri Muktsar Sahib, Punjab, India

The cotton stalk is 10-100 mm long with the natural packing density of 100-130 kg/m^3 (≈ 1/8th of bituminous coal) and real packing density of about 450 kg/m^3 (≈ 1/4th of bituminous coal) [13]. Gross calorific value of cotton stalk is around 16.9 MJ/kg. It is difficult to transport and process cotton stalk as it cannot be fluidized alone in an FBC. Suitable bed material like silica or alumina is required to fluidize cotton stalk. Cotton stalk combustion in FBC has attracted many researchers due to its potential of fulfilling energy requirements in the rural areas. Sun et al. [14] investigated the fluidizing characteristics of the cotton stalk with alumina. The different variables include lengths of cotton stalk, superficial velocity of fluidizing air, and diameter of alumina particles. Alumina with particle size 0.6 to 1 mm has been found suitable for best fluidization of the cotton stalk.

1.7. Motivation of work

The cotton stalk is the waste agri-biomass left in the fields. Annually, about 22-25 metric tons of the cotton stalk is produced in India, most of which is burnt in open fields causing air

pollution. The cotton stalk has relatively high gross calorific value in comparison to other agri-wastes. The cotton stalk can be fed into fluidized bed combustors and the power generated from fluidized bed combustor based thermal power plant can be used to fulfill the electricity demands in rural areas. Providing cotton stalk in a thermal power plant boosts the economy of the region and leads to rural employment. Motivated by benefits of using cotton stalk in FBC for power generation, the focus of current work is on the study of cotton stalk's combustion characteristics in an atmospheric fluidized bed combustor.

1.8. Objectives

The main aim of the present work is to develop a mathematical model for a cotton stalk based atmospheric fluidized bed combustor. Following are the objectives of the study:

1. To develop and optimize a solid population balance model for wide particle size distribution biomass fuels such as cotton stalk ranging between 0.075 mm to 80 mm. Fuel particle size effect will be analyzed on the following parameters:
    - Carbon Utilization Efficiency (CUE)
    - Carryover rate
    - Bed Carbon Load (BCL)
    - Elutriation rate and particle shrinkage rate
2. To develop an exit gas composition model (for bubble growth with fluidized bed height) to study the effect of fractional excess air supply (0.1 to 0.5) on the followings:
    - Percentage of carbon dioxide and oxygen in the exit flue gases
    - Overall reaction rate constant
    - Expanded bed height
3. To develop the first law of thermodynamics (energy) and the second law of thermodynamics (exergy) based thermodynamic model for the plant under study. The

model will be optimized for minimum exergy destruction and maximum exergy efficiency using multi-response optimization method.

4. To conduct economic assessment of the plant using break-even analysis method.
5. To study cotton stalk agglomeration behavior under fluidized bed conditions.

1.9. Organization of thesis

The dissertation is divided into six parts.

Chapter 1 was regarding the introduction of biomass scenario in India and Punjab. Problems associated with biomass waste disposal, fluidized bed combustor as an efficient way of utilizing biomass wastes for energy generation and advantages of fluidized bed combustor over conventional combustors have been discussed. Motivation of work has also been highlighted. At the end of the chapter, objectives of the present work have been shown.

Chapter 2 provides an extensive literature review of mathematical modeling of atmospheric fluidized bed combustors. Literature review covers previous work done by researchers on solid population modeling, oxygen mass balance modeling, and thermo-economic modeling of coal and biomass fluidized bed combustors. At the end of the chapter, gaps in the literature have been discussed followed by the problem formulation.

Chapter 3 explains the description of the system under consideration. 7.5 MW Malwa power plant located in the cotton belt of Punjab at village Gulabewala, district Shri Muktsar Sahib, Punjab, India is selected for validation of the models developed. The details of the collection of fuel samples, readings from the plant site, and results obtained from the various test conducted for fuel samples are provided. At the end of the chapter, discussion and investigation regarding the problem of agglomeration while using cotton stalk under condition similar to fluidized bed are presented.

Chapter 4 deals with the mathematical modeling of the fluidized bed combustor.

Models for solid population and exit gas composition along with thermo-economic model are developed. Optimization of solid population model and thermo-economic model is also presented in this chapter.

Chapter 5 presents the results obtained from the mathematical model. The model results are validated with plant data. Optimization results of solid population model and thermo-economic model are discussed. The results of cotton stalk's agglomeration study are discussed at the end of the chapter.

Chapter 6 is about the conclusions drawn from the work and recommendations for future work. At the end of the thesis, references used in the present work are listed.

Chapter 2

LITERATURE REVIEW

Problem formulation is always based on extensive literature review. In this chapter, literature review on efforts of researchers in modeling FBC using biomass as fuel and survey on fluidized bed combustor modeling is presented which includes the discussion on basics of two-phase and three-phase mathematical modeling. Literature review on thermo-economic modeling of fluidized bed combustor based thermal power plants is also presented in this chapter. Literature review on various theories and models available on agglomeration is also presented. The chapter is concluded with the gaps found in the literature and problem formulation.

2.1. Basics of fluidized bed combustor mathematical modeling

In the initial development stages, two-phase fluidized bed combustor mathematical models are found in literature. The word 'phase', as defined by Geldart [15], is a region that may contain both gas and solid particles. One phase is different from other by the amount of solids (% by volume), characteristics, and appearance. Different models use different meanings of word 'phase'. The bed is supposed to be composed of a particulate or dense phase and a bubble phase. Dense phase consists of solid particles and gas. Bubble phase consists of voids with no solid particles. In some other models, an additional phase namely cloud wake phase is also considered. Cloud wake phase is supposed to be associated with bubble phase and having the same gas composition as that of the bubble. A bubble is assumed to be surrounded by cloud. Figure 2.1(a) shows two-phase and Figure 2.1(b) shows interactions between these phases. Models based on the three-phase theory of fluidization have also been found in the literature. In these models, separate different phases are considered as shown in Figure 2.1(c). From the literature, it is found that while developing fluidized bed mathematical model the following fundamentals must be taken care of:

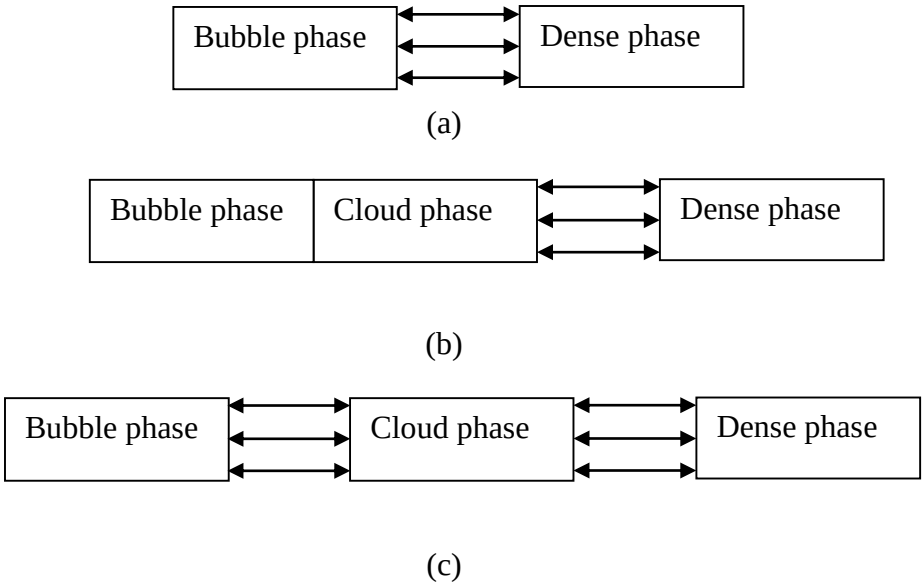

Figure 2.1. Interaction between phases (modified from [15])

(i) During fluidized bed combustion, the particle experiences change in its density and shape due to its shrinkage. Particle shrinkage is due to particle's combustion and attrition both. The model must consider particle shrinkage due to combustion and attrition while calculating particle shrinkage rate.

(ii) Combustion in a fluidized bed is a complex phenomenon and model must be based on either single film theory of combustion or double film theory of combustion. The combustion of a single particle takes place as per the following reactions:

$$C + O_2 \longrightarrow CO_2 \quad (2.1)$$

$$2C + O_2 \longrightarrow 2CO \quad (2.2)$$

$$CO_2 + C \longrightarrow 2CO \quad (2.3)$$

$$2CO + O_2 \longrightarrow 2CO_2 \quad (2.4)$$

Equations (2.1), (2.2), and (2.3) are assumed to be taking place at the internal or external char particle surface and are heterogeneous. Equation (2.4) takes place outside or inside the boundary layer around the particle and is homogeneous.

(iii) The bubble diameter and rise velocity of the crowd of bubbles and a single bubble is always changing. These must be calculated precisely as they have a significant impact on model output.

(iv) The exchange of gas and particles between and within the different phases must be considered.

(v) The particle size distribution within the bed affects its performance significantly. Elutriation rate, shrinkage rate, bed carbon load, and carbon utilization efficiency depend largely upon the fuel particle size distribution. Hence, the accuracy of the model depends mainly upon particle size distribution.

It has been found that importance of developing mathematical models for fluidized bed combustors is increasing since last two decades. Researchers are validating experimental results obtained during experimentation on fluidized bed combustors by comparing them with their mathematical models. Hydrodynamic parameters like minimum fluidization velocity, bed pressure drops, bubble parameters, and heat transfer characteristics of biomass mixed with sand have also been investigated by researchers [16-19]. Work has also been reported on CFD analysis of fluidized bed reactors, gasifiers, and combustors [20-21].

In literature, there are two different theories of combustion of single char particle. According to single film theory of combustion, oxygen diffusion takes place across a stationary film, and it reaches char surface. Oxygen reacts with carbon following equations (2.1) and (2.2), producing CO and CO_2 respectively. CO produced at char surface is converted into CO_2 according to equation (2.4). Figure 2.2 shows the conversion of O_2, CO, and variation of CO_2 concentration during combustion according to single film theory. Figure 2.3 shows double film theory of fluidization [15]. According to double film theory of combustion, oxygen does not reach the surface of char particle. Oxygen is consumed before it reaches the char surface according to equation (2.4) and CO_2 is produced. CO_2 reacts with carbon at char surface

according to equation (2.3) and CO is produced. CO diffuses away from the char surface and reacts with incoming O_2 producing CO_2 following equation (2.4). One half of CO_2 diffuses outwards and one half diffuses towards the char surface for reacting with C and forming CO.

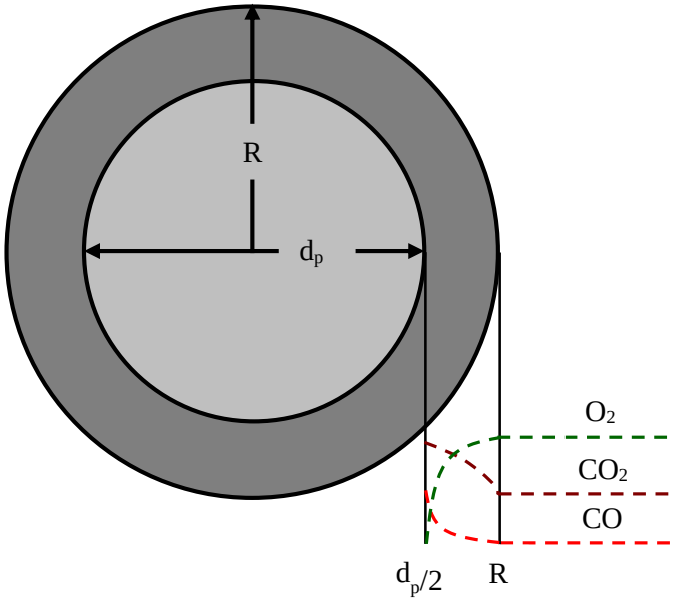

Figure 2.2. Single film theory of combustion (adapted from [15])

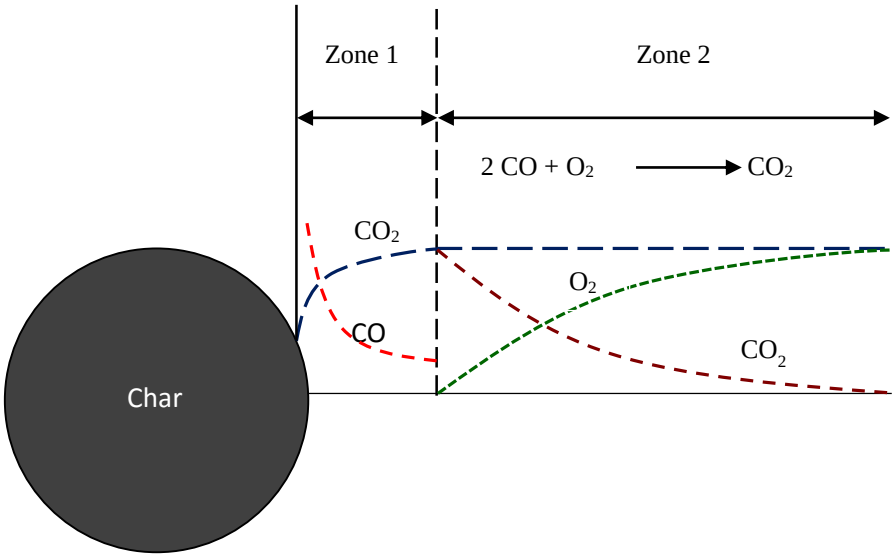

Figure 2.3. Double film theory of combustion (modified from [15])

2.2. Fluidized bed combustion models

Yagi and Kunii [22] made the first attempt to model a fluidized bed combustor without considering the existence of bubble phase. They considered both fixed size carbon particle and shrinking carbon particle for developing equations for their combustion. Yagi and Kunii [22] developed solid population balance equation and bed carbon load equation. They compared model results with lab scale results and found their model results to be reasonably matching with lab-scale results. This model became popular but had certain limitations.

(i) The model was only for single fixed size carbon particle.

(ii) The model was applicable only for isothermal bed.

(iii) The model results were not validated with industrial scale fluidized bed combustor.

(iv) The conversion of carbon into carbon oxide was only considered and conversion of carbon into carbon monoxide was neglected.

The concept of two-phase fluidization theory was introduced by Toomey and Johnstone [23]. They proposed that volumetric flow rate ($\dot{V}_g$) of rising bubbles through an FBC is equal to the gas flowing in excess to the amount required for minimum fluidization.

$$\frac{\dot{V}_g}{A_o} = U_o - U_{mf} \tag{2.5}$$

A simple model for a circular and solid free rising bubble was proposed by Davidson and Harrison [24]. In emulsion phase, gas was assumed to flow as an incompressible fluid. It was concluded that the pressure in the upper part of the bubble is higher and in the lower part of the bubble is lesser than the surroundings. Due to this, the gas enters the bubble from its bottom and comes out at the top. The assumption of circular shaped bubble by Davidson and Harrison [24] was not practical, but even then it presented a good insight into the bubble behavior in the FBC.

In continuation to the work done by Toomey and Johnstone [23], Grace and Clift [25] summarized the experiments to estimate the volumetric flow rate of bubbles in a fluidized bed and suggested the following equation for the same:

$$\frac{\dot{V}_g}{A_o} = U_o - K.U_{mf} \tag{2.6}$$

where *K* is a constant.

They found that in all the experiments the value of *K* is well above unity (1.0 to 8.27). This showed that Toomey and Johnstone [23] overestimated the volumetric flow rate of bubbles. Many researchers have tried to explore the reason behind the overestimation. Some researchers [26-29] have highlighted an increase in gas interstitial velocity in the particulate or dense phase above the minimum fluidization velocity, while others [30-35] have supported through flow inside the bubbles as a reason behind this. This gave a modified two-phase theory of fluidization [30]:

$$\frac{\dot{V}_g}{A_o} = U_o - (1 + n\varepsilon_b)U_{mf} \tag{2.7}$$

By putting $n = 0$ in equation (2.7), the original postulate of the two-phase theory of fluidization can be obtained. In equation (2.7), it is assumed that the gas velocity in the particulate or dense phase remains U_{mf} and the gas rises with a mean velocity of $(1 + n)U_{mf}$ in the voids relative to the bubble's boundary. The value of n as observed in literature or calculated after measurement of $\dot{V}_g$ and ε_b has been found to be almost positive and varies over a wide range. But the value of n has been found to be dependent on superficial gas velocity within a system. So the modified two-phase theory which has been developed with an intention to improve the original two-phase theory of fluidization in itself is an oversimplification.

Avedesian and Davidson [35] worked on calculating the bubble diameter for a hot fluidized bed of inert material. This was the first attempt to use the two-phase theory of fluidization. Later this approach became the base for subsequent development. They assumed perfect mixing of emulsion phase and derived the expression for bubble diameter. Avedesian

and Davidson [35] found that bubble diameter remained constant along the bed height. They further assumed that oxygen diffusion rate to the particle controls combustion rate. Considering the first order reaction kinetics, Avedesian and Davidson [35] derived an expression for oxygen molar flow rate to a char surface.

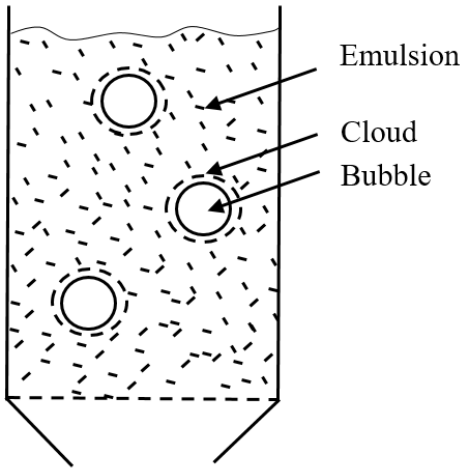

Figure 2.4. Three-phases of fluidization (modified from [23])

Kunii and Levenspiel [36] proposed three-phase theory of fluidization, where they consider cloud as a separate phase (Figure 2.4). Their study was based on two cases viz. when emulsion gas rises quicker than the bubble or when bubble rises quicker than emulsion gas. In first case, emulsion gases enter the bubble from the bottom and comes out from its top generating a ring circulating within the bubble. In the second case, emulsion gas leaves at bubble top, sweep around it, and travels to the bubble bottom. The region surrounding bubble covered by the emulsion gas is called 'cloud'. Bubbles are concave in shape and the region just below the bubble is called wake. Gas flow patterns within and around the bubble as proposed by Kunii and Levenspiel [36] are shown in Figure 2.5.

In the initial times, only two-phase fluidized bed combustion models were found and very few researchers considered the existence of three-phases of fluidization [36-37]. Few two-phase mathematical models also assumed plug flow in both the phases [38], while some other

models assumed mixed flow in the dense and bubble phase [39-41]. Some models assumed dense phase to be well mixed and bubble phase to be in plug flow [42-44].

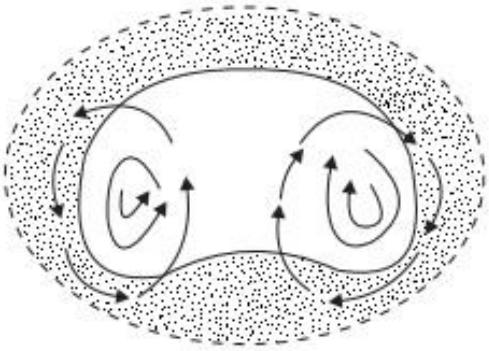

Figure 2.5. Gas flow pattern within and around the bubble (modified from [36])

Bukur and Nasif [45] studied bubble growth effect by coalescence on some performance parameters of FBC. They used two-phase model considering changing bubble size with bed height as suggested by Orcutt et al. [46] for all the calculations. Darton et al. [47] studied the bed height effect at minimum fluidization on conversion. Darton et al. [47] calculated three different effective bubble diameters, viz. (i) an integral average bubble diameter (d_{B_1}) (ii) bubble diameter giving bed height equal to as given by model (d_{B_2}), and (iii) bubble diameter (d_{B_3}) giving the same number of mass transfer units as obtained from the model and found that $d_{B_1} > d_{B_2} > d_{B_3}$. They found that results provided by d_{B_2} were more favorable than results given by d_{B_1} and d_{B_3}.

A two-phase mathematical model for 1 MW waste wood fired AFBC was developed by Khan et al. [48], assuming bed to be consisting of emulsion phase and bubble phase only. This model is one of the few models found in literature which considered wide particle size distribution of waste wood and the actual boiler feed was taken into account. Khan et al. [48] attempted to predict the variation of exit gas composition in dense bed and freeboard with boiler height, fluidization velocity, bed voidage, and bed temperature. They found that oxygen

consumption and carbon dioxide concentration increases along with the boiler height. The mathematical model included the effect of devolatization, fragmentation of char, and char attrition. Khan et al. [48] concluded that the gas hydrodynamics has a very dominating effect on the exit gas composition and boiler performance. Using these parameters, system performance can be optimized.

Chavarie et al. [49] studied the effect of hydrodynamics of two-phases on a fluidized bed reactor performance. The study was mainly focused on bubble size, bubble flow rate, and bubble frequencies in a two dimensional fluidized bed.

Okasha [50] studied rice straw stage combustion in a 300 mm internal diameter and 3300 mm high lab scale AFBC. Rice straw was supplied as pallets of cylindrical shape (10 mm to 15 mm long and 10 mm to 12 mm diameter). Primary as well as the secondary air was supplied to the combustor with secondary air inlet at about 1500 mm above primary air inlet. Okasha [50] found that at the higher temperature range (850°C to 950°C), stage combustion reduces NO_x emission to a great extent. The staged operation was found to have a negligible effect on SO_2 emission. Combustion efficiency increased with increase in secondary air supply.

Reddy and Mohapatra [51] developed three-phase exit gas composition model for a 10 MW coal-fired AFBC. The fluidized bed was considered to consist of equivalent stages in series and gas exchange was assumed to take place in all three-phases in each stage. Reddy and Mohapatra [51] compared exit gas composition predicted by the model with the actual plant data and found that model predictions were in good agreement with the plant data. It was concluded that oxygen concentration decrease in bubble, cloud, and emulsion phase along bed height. It was also found that in an FBC plant, oxygen conversion decreases with increase in excess air supply.

Cano et al. [52] presented an FBC model for a single char particle. This model was unique as it combined shrinking char and shrinking particle features representing carbon

combustion and attrition of ash layer depleted by carbon respectively. The non-uniform temperature profile in the char particle generated due to the thermal resistance offered by the ash layer and un-reacted core was also included in this model. Equations for oxygen concentration variation at core surface and the external surface for a single granular sludge (GS) particle were developed. Cano et al. [52] validated model for fluidized combustion using pelletized sewage sludge. Model's conceptual framework is represented in Figure 2.6. Cano et al. [52] compared the calculated and experimental particle radii and found good agreement between model and experimental results.

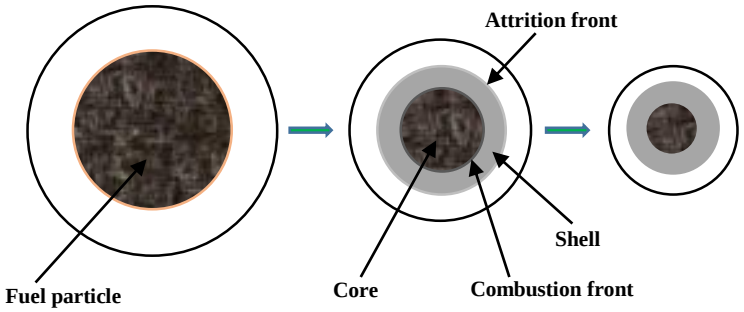

Figure 2.6. Conceptual framework of FBC for a single char particle (modified from [52])

Komatina et al. [53] developed a mathematical model for describing devolatization rate and heat transfer for a single coal particle. Model was tested for different thermal properties of coal (C_p and λ_c) and compared coal temperature during devolatization measured experimentally with the model predictions. The bed temperature was varied between 300°C to 850°C. Coal of two different ranks: brown coal bogovina and lignite Kosovo was tested in the experimental test rig. The model and experimental results were found in good agreement for brown coal at C_p = 1200 J/kg-K, λ_c = 0.20 W/m-K, and for lignite at C_p = 1100 J/kg-K, λ_c = 0.17 W/m-K.

Ergudenler et al. [54] developed a homogeneous kinetic-free equilibrium model for a cereal straw-fired fluidized bed gasifier. The model predicted the normalized production rate of the produced gas under different operating conditions, reactor temperature, higher heating

value, and composition without involving complex reaction kinetics. Model predictions improved significantly while taking tar formation into account. It was suggested that model can be further enhanced by considering char conversion in freeboard region of the gasifier.

Okasha [55] developed a mathematical model for BFBC using straw-bitumen pallets. The combustor was divided into dense, splashing, and freeboard zones. The model considered char elutriation, volatile release, ejection of particles from the bed, and post-combustion above the bed. Okasha [55] developed mass and energy equations for both splashing and freeboard sectors of the combustor. The model predicted that amount of heat released in the dense bed, splash zone, and freeboard is 60%, 33%, and 7% of total released heat respectively. Approximately 53% of volatiles released burns within the bed. Combustion efficiency was found to be always greater than 99.5%.

Singh et al. [56] developed a solid population, an exit gas composition model, and studied agglomeration problem for a 10 MW rice husk based atmospheric fluidized bed power plant. The three-phase theory of fluidization was followed and burning of rice husk particle was assumed to be following single film theory. It was found that in flue gases, amount of carbon dioxide decreased and amount of oxygen increased with increase in excess air and increase in moisture content of the fuel.

Natale et al. [57] developed an unsteady particle size distribution model for a fluidized bed wood gasifier. The model included chemical reactions, abrasion, elutriation, and fragmentation during gasification of wood. They coupled the particle size distribution model with a two-phase, three zone model for predicting the producer gas composition and compared the outcome of the model with that of the gasifier.

2.3. Fluidized bed thermo-economic models

Thermal power plant energy analysis and exergy analysis are important to evaluate its thermodynamic performance. It has been found that there are number of models dealing with

the thermal and economic analysis of thermal power plant [58-62], but a very limited number of thermo-economic models [63] have been developed for the biomass-based thermal power plant. Energy analysis and exergy analysis are based on the first law of thermodynamics and second law of thermodynamics respectively. The performance analysis of most of the thermal power plants is carried out through energy analysis only, but most of the times it provides the insufficient information about the plant's performance. The energy analysis does not take into account the surrounding properties and cannot differentiate between the energy quantity and its quality.

To overcome the limitations of the first law of thermodynamics, the second law of thermodynamics based exergy analysis has become a more useful tool in the hands of researchers for the design, performance analysis, and optimization of the thermal power plants. Using exergy analysis, not only the magnitude, causes, and location of the irreversibility can be determined but the assessment of plant's individual component efficiency can also be done. Exergy analysis gives the true efficiency of an engineering system, using which efforts can be made to find the scope of improvement (Dincer et al. [64]). In literature, exergy analysis has been applied to individual components and combined systems as well.

Wright et al. [65] conducted a technical and economic analysis of one large and two medium size biomass-based thermal power plants located in the UK. They found LHV efficiency of the medium thermal power plants to be 30% and large thermal power plant to be 35%. The difference in LHV efficiency is due to the higher superheated steam condition in the large thermal power plant. CO_2 was found to be lower in the large thermal power plant.

Rosen [66] compared nuclear and coal-fired steam power plants on the basis of their energy and exergy analysis. ASPEN+ software was used for exergy analysis. It was found that although exergy and energy efficiencies are the same for nuclear thermal plant and similar for a coal-fired thermal power plant, energy analysis could not identify the cause and location of

inefficiencies systematically, whereas exergy analysis could do it very efficiently. It was found that energy losses are mainly associated with heat rejections such as heat rejection in condenser and exergy losses are primarily associated with consumptions mainly in the reactors. It was concluded that devices with the highest thermodynamic losses have the maximum scope for improvement in efficiency, efforts must be put on increasing the efficiencies of nuclear reactor and combustor of nuclear power plant and coal-fired thermal power plants, respectively.

Kwak et al. [67] performed exergo-economic analyses of a 500 MW combined cycle thermal power plant. They applied energy and mass-energy conservation laws to each component of the plant. An exergy costing method was used to the combined cycle thermal power plant for estimating the cost of unit production of electricity from steam and gas turbines. Exergy losses from each component and overall system were calculated in term of cost losses. The computer program developed can be used for any other energy system. For this maintenance cost, salvage values, and initial investments of each component are required.

Sengupta et al. [68] performed exergy analysis for 210 MW coal based thermal power plant. For the analyses, the complete thermal plant cycle was divided into three zones: (i) turbo-generator with inlet and outlet, (ii) condenser, turbo-generator, regenerative heaters, and all feed pumps, (iii) the complete cycle with the condenser, boiler, feed pumps, turbo-generator, and plant auxiliaries. This was done to estimate the contribution of various parts of the plant in exergy destructions. The exergy efficiency was calculated at different conditions such as varying loads, condenser pressures, with different turbine governing settings, and with and without regenerative heaters. Effects of condenser pressure (76 mm and 89 mm Hg (abs.)) on exergy efficiency were studied. Regenerative heaters were disconnected to study the effect on exergy efficiency. It was found that in the power plant the boiler was the main irreversibility source. Exergy destruction in the boiler was of the order of 60%. They found that irreversibility in the plant increased at part load conditions and the effect is reflected more with the decrease

in the plant load. Exergy efficiency increased with decrease in the back pressure of condenser. Exergy efficiency showed increment on the high-pressure heaters removal when the boiler is not included. Whereas exergy efficiency decreased when the boiler is also considered. Under part load conditions it was observed that exergy efficiency improved when steam pressure before control valve of the turbine is kept in sliding mode.

Peng et al. [69] studied the performance of a 300 MW solar-hybrid coal-fired thermal power plant. They disclosed the irreversibility of energy conversion of the thermal power plant using EUD method. Exergy destruction of each process has also been calculated and it was higher for the solar only thermal power plant. For solar-hybrid coal thermal power plant, minimum exergy destructions were found in the steam turbine and solar feed-water heater. It was concluded that solar-hybrid coal-fired thermal plants work better than solar-only thermal power plants even under off-design conditions.

Verkhivker and Kosoy [70] analyzed the performance of conventional power plant on the exergy basis quantitatively. The analyses showed that exergy destructions are mainly due to chemical transformation of exergy into heat. They found that exergy destructions decrease when the thermodynamic parameter values of the working fluid are increased and the temperature difference across the net heaters is decreased.

Table 2.1 shows a number of studies on the exergy and energy performance analysis of coal-based power plants. It has been observed in these studies that the different researchers used various parameter definitions. For example, a few are using lower heating value in the thermal efficiency calculations, whereas the others are using higher heating value for the same. However, the reported literature on the energy and exergy performance analysis of biomass-based thermal power plants is very limited. So, combined utilization of the energy and the exergy analysis is of more interest. Plant efficiency has significant impact on energy savings, which in turn influences the profits earned from the plant.

Table 2.1. Literature review on the energy and exergy performance analysis of the power plants

Author(s)	Plant details	Fuel used	Discussion
Aljundi [58]	3x66 MW Al-Hussein power plant, Jordan.	Diesel, Oil	Energy analysis showed that condenser is the source of maximum energy loss, whereas exergy analysis showed that the maximum exergy loss takes place at the boiler.
Rosen [66]	8x500MW (presently decommissioned) coal-fired Nanticoke Generating Station, Ontario and 4x516 MW & 2x515 MW (presently decommissioned) Pickering Nuclear Generating Station, Ontario.	Coal and nuclear	Analysis of both the coal-fired and the nuclear power stations supports the fact that the exergy analysis provides a better estimation of the plant performance in comparison to the energy analysis.
Sengupta et al. [68]	210 MW thermal power plant, India.	Coal	The boiler is the major source of the irreversibility. Irreversibility increase with part load.
Oktay [71]	2x160 MW FBC thermal power plant, Turkey.	Coal	Exergy efficiencies and irreversibilities of plant components (pumps, steam turbine, steam generator, etc.) along with their improvement factors are calculated.
Kopac and Hilachi [72]	2x150 MW Catalagzi Coal Power Plant, Turkey.	Anthracite Coal	Used energy analysis for determining the heat loss of each component and exergy analysis for determining the exergy destruction rates of the whole plant for different ambient temperatures (5–35 °C). Concluded that ambient temperature had a

			high impact on the changes of the irreversibility of the boiler.
Mitrovic et al. [73]	348.5 MW Kostolac steam power plant, Serbia.	Coal	The maximum energy losses were observed in the condenser and the maximum exergy losses were observed in the boiler.
Erdem et al. [74]	Nine thermal power plants, Turkey.	Coal	Highlighted the importance of the energy and the exergy analysis of the thermal plants by comparing the energy and the exergy analysis of thermal plants.
Regulagadda et al. [75]	32 MW Tecpro power systems Limited, Chennai, India.	Coal	Suggested that the maximum efforts must be put on improving the boiler's performance as the maximum exergy destruction occurred at the boiler in the power plant.

A few decades ago, due to low fuel prices, low costs involved in their transportation, and minor capital expenditure, the economic analysis of the plant was not given due importance. But, with increasing fuel prices and the capital expenditure involved in setting up a thermal power plant, the importance of the economic analysis has also increased. Exergy efficiency of the plant has a substantial impact on its economics. A thermodynamic theory of economics considering first and the second law of thermodynamics has been presented by Bryant [76]. Table 2.2 shows literature available on the economic analysis of the coal-based thermal power plants. The economic analysis of a biomass-based power plant is different from those running on fossil fuels. The cost of fossil fuels is controlled by the international market, whereas, for the biomass-based power plants, the biomass is collected from nearby areas. The

plant authorities can also generate the biomass from the land taken on lease and cultivating high calorific value crops.

Table 2.2. Literature review on the economic analysis of the power plant

Author(s)	Plant details	Discussion
Thakur et al. [60]	26 state-owned electric utilities, India	Evaluated the performance by using the non-parametric technique of the Data Development Analysis (DEA) approach. Suggested various ways of increasing the performance.
Hashem [61]	1.3 MW gas turbine cogeneration plant, Arab gulf area.	Used break-even method to evaluate the fixed cost and variable cost effects on the break-even points in term of operating hours.
Wright et al. [65]	3 biomass-based thermal power plants, UK	Compared one large and two small biomass-based thermal power plants. Concluded higher superheated steam conditions as the reason for higher LHV efficiency of the larger plant.
Liu et al. [77]	12 power plants, Taiwan	Used the DEA approach and conducted the stability test to verify the DEA model. Heating values of the fuel were found to be the most important parameter for DEA model.
Nakano and Manage [78]	10 power generation companies, Japan	Used the DEA approach. Plants productivities were analyzed by comparing the various input costs (fuel, capital cost, number of employees) with the outputs in terms of the electricity produced.
Shrivastava et al. [79]	60 coal-fired thermal power plants, India	Evaluated the performance and concluded that the coal overuse is one of the major reasons power plants inefficiency.

2.4. Literature gaps

It has been found that importance of developing mathematical models has increased since last two decades, as researchers are validating experimental results obtained during experimentation on fluidized bed combustors by comparing them with their mathematical

models. However, there is still a lot of work to be done and scope of improvement in the mathematical modeling of biomass-based fluidized bed combustors. Following observations have been made from the literature survey:

1. Work has been done on coal-based FBC mathematical modeling, but biomass-based mathematical modeling is still partially explored.
2. It has been found that most of the studies are based on lab-scale fluidized bed combustors and very few studies are available on real plant data. Out of studies available on real plant data, most of them are based on mono-fuel particle size
3. Limited work has been reported so far on the cotton stalk as a fuel in FBC systems. Limited literature is available on combustion, fluidization, and devolatization characteristics of the cotton stalk.
4. Most of the work has been done in fluidized bed reactors and very little work has been done in fluidized bed combustor.
5. Very limited number of thermo-economic models have been developed for biomass-based thermal power plants.

2.5. Problem formulation

The present work focuses on the study of cotton stalk combustion characteristics in an AFBC. A mathematical model consisting of three sub models viz., (i) a solid population balance model (ii) an oxygen mass balance model, and (iii) a thermo-economic model has been developed for the said plant. The outcomes of the model have been compared with real plant data. A 7.5 MW biomass-fired atmospheric fluidized bed combustor based thermal power plant located at village Gulabewala, Sri Muktsar Sahib, Punjab, India is selected for the study. Plant details and analysis of biomass fuel collected at plant site have been discussed in Chapter 3.

Chapter 3

PLANT DESCRIPTION AND EXPERIMENTAL INVESTIGATION

3.1. Plant description

Malwa Power Plant Limited (MPPL) is a biomass-based thermal plant established in Punjab and has been selected for the present study. The plant is owned by Dee Engineers Private Limited and is located at village Gulabewala in district Sri Muktsar Sahib, Punjab, India. This region is popularly known as Malwa region and is popularly known as the cotton belt. The land in this region is very conducive for cotton, mustard, wheat, pulses, oilseeds, etc. Malwa power plant is a mini thermal power plant using wide varieties of biomass as fuel. The electricity generated is supplied to the grid of Punjab State Power Corporation Limited (PSPCL) grid. The plant operates under sub-critical conditions and works on uniquely configured Rankine cycle. Biomass is made available at the plant site from surrounding villages in 50 km periphery and is also produced by plant authorities on land taken on lease. Biomass is stored in open sheds.

The water for boiler and other requirements is taken from the nearby canal. The boiler of the plant is designed mainly for burning paddy husk, but it also uses agricultural wastes, forestry wastes, and even cow dung as fuel. Annual fuel requirement of the plant at 100% capacity utilization is approximately 72,000 megatons. Almost 60% of the plant fuel requirement is fulfilled by the cotton stalk. The amount of various biomass fuels used in the plant is shown in Table 3.1.

3.1.1. Fuel processing and plant operation

Sun-dried biomass is chipped in the chipper machines and is loaded on the conveyor belts with the help of tractors. The chipped biomass is dropped on two compartments from the conveyor belt from where it is supplied to four number of screw feeders. The bed temperature is

controlled by changing the fuel feed rate through screw feeders. In turn, the bed temperature controls the pressure and temperature of the steam produced.

Table 3.1. Fuel consumption (Metric tons) at MPPL, Muktsar Sahib, Punjab, India

Biomass type	2009-2010	2010-2011	2011-2012
Mustard husk	1,965	4,330	604
Wheat straw	4,914	7,206	23,832
Paddy straw	24,763	19,922	19,536
Cotton stalk	38,745	37,598	25,664

Source: CMD reports 2009-10, 2010-11, 2011-12.

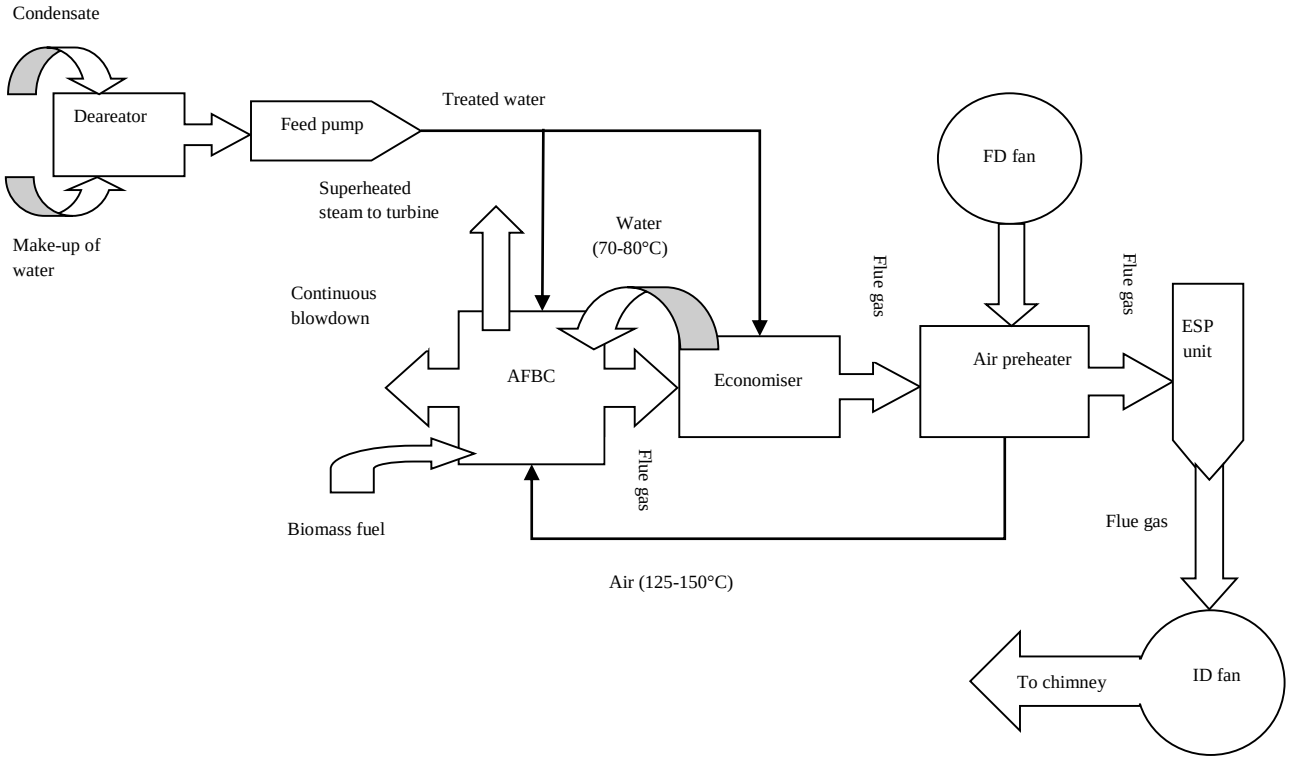

Figure 3.1. Plant flow diagram

Flow diagram of the plant is shown in Figure 3.1. Superheated steam produced in the AFBC at a pressure 66 bar and temperature 460 °C (± 5 °C) runs the steam turbine. Steam thus generated from the boiler, is used to run the steam turbine. The mechanical energy produced

at the output shaft of the turbine is converted into electricity by an electric generator. Steam from the turbine condenses in the condenser and is supplied back to the boiler drum. The make-up water from water treatment plant is also added to compensate the water losses during the cycle. Physico-chemical parameters of the MPPL are shown in Table 3.2.

Table 3.2. Physico-chemical parameters of the biomass-fired power plant

Physico-chemical parameter	**Value/ type**
Plant capacity	7.5 MW
Boiler	Bi-drum
Combustor type	AFBC
Distributor plate	Tuyre
Fluidized bed material	Silica sand
Collector type	Electrostatic precipitator
Bed cross-section type	Rectangular
Bed cross-section area	18.99 m^2
Combustor temperature	700 °C – 750 °C
Height of combustor	27.2 m
Steam pressure	66 bar
Fuel feed rate	2.75 kg/s
Steam temperature	460 **°C** (±5 **°C**)
Steam production rate	9.45 kg/s

Exhaust flue gases heat fluidizing air in an air pre-heater. A forced draught fan is used to supply heated fluidizing air to the combustion chamber. Fluidizing air is accelerated by passing it through a carbon steel tuyere type distributor plate fitted with cast iron nozzles. Bed material and fuel particles are fluidized by fluidizing air. Combustion of most of the volatiles and hence maximum heat release takes place in freeboard area of the combustor. The hot flue gases generated from the combustion of fuel passes over the water tubes, super-heater tubes, air pre-heater, and through

economizer. Flue gases are then passed through an electrostatic precipitator (ESP) unit which separates dust and ash particles from flue gases so that their amount exceed the maximum permissible limit set by pollution control board. The flue gases are left in the atmosphere through a chimney. The ash is produced as bottom ash (from furnace bottom), fly ash (from ESP unit), and its disposal is a big challenge. The ash is filled into the dumper trucks and is dumped in the empty land. Preventive measures are taken during ash disposal.

The high temperature in the combustor softens high alkali-containing ash which is deposited on the super-heater tubes. Soot blower is installed near the super-heater tubes to remove the ash deposited on the tube surfaces. The removed ash falls back into the bed and creates hindrance in fluidization. If this ash is allowed to stay in the combustor for long, it forms clinkers/ agglomerates leading to defluidization of the bed. Ash is removed continuously from the bottom of the combustor to minimize clinker formation.

3.2. Fuel analysis

At the time of study fuel samples of wheat straw, cotton stalk, rice husk, rice straw, and fly ash of cotton stalk were collected. The composition of various fuel samples and cotton stalk fly ash were estimated using proximate analysis and ultimate analysis tests. Table 3.3 and Table 3.4 shows the proximate analysis result (on air-dried basis) and the ultimate analysis result respectively for the collected samples. As cotton stalk contains lower ash amount in comparison to other fuel samples, thus reduces the solid pollutant amount in exhaust gases.

Cotton stalk (unlike rice husk) has wide particle size distribution (PSD). PSD of collected cotton stalk sample was conducted in a sieve shaker and results are shown in Table 3.5. Sieve analysis was done using mechanical sieve shaker at the material testing lab, Department of Civil Engineering, RIMT, Mandi Gobindgarh. Sieve analysis (details in section 3.4.3.) was conducted three times to minimize the uncertainty and error of experiment. Average mass retained was calculated by taking mean for each sieve.

Table 3.3. Proximate analysis of samples collected from the plant site

Biomass type	Proximate analysis (%) (on air dried basis)				
	Volatile matter	Fixed carbon	Ash	Moisture	Gross calorific value (MJ/kg)
Cotton Stalk	65.86	15.77	4.48	13.89	16.9
Rice husk	56.57	14.42	18.1	10.91	15.4
Rice straw	60.28	14.6	17.2	7.92	15.8
Wheat straw	64.10	17.80	8.90	9.20	17.1
Fly ash (CS)	-	9.8	90.2	-	-

Table 3.4. Ultimate analysis of samples collected from plant site

Biomass type	Ultimate analysis (%)				
	C	H	S	O	N
Cotton Stalk	41.3	6.8	0.5	39.7	0.7
Rice husk	34.6	4.2	0.1	31.7	0.5
Rice straw	35.2	4.8	0.2	33.9	0.8
Wheat straw	43.2	5.2	0.11	39.4	0.6

3.3. Agglomeration analysis

Coal and biomass-fired fluidized bed combustors face agglomeration as a very severe problem. It is more challenging to control or eliminate agglomeration with biomass as fuel as different biomass fuels contain different proportions of agglomeration causing elements. On bed material particles, ash deposition causes agglomeration/ sintering. Large size agglomerates lead to defluidization of the fluidized bed. The combustor is shut down, bed material is removed, and fresh bed material is reloaded in the bed. Removal and reloading of bed material takes 10

to 15 days, causing a loss of power output from the thermal power plant. The problems associated with agglomeration restrict the use of fluidized bed combustors at wide scale [80]. Preventing agglomeration in thermal power plants can avoid an emergency shutdown. The reasons for agglomeration and methods of its elimination are yet not clear.

Table 3.5. Particle size distribution of cotton stalk

Sieve Size (mm)	Mass retained in each experiment (%)			Cumulative mass		
	Set 1	Set 2	Set 3	Average mass retained (%)	Oversize (%)	Undersize (%)
+ 80	1.3	1.37	1.32	1.33	1.33	98.67
- 80 + 40	11.39	11.23	11.19	11.27	12.60	87.40
- 40 + 20	16.88	16.9	16.71	16.83	29.43	70.57
- 20 + 12.5	12.95	12.91	12.69	12.85	42.28	57.72
- 12.5 + 10	26.95	27.13	26.98	27.02	69.30	30.70
- 10 + 4.7	17.11	17.15	17.01	17.09	86.39	13.61
- 4.7 + 2.36	2.33	2.37	2.32	2.34	88.73	11.27
- 2.36 + 1.18	3.79	3.75	4.1	3.88	92.61	7.39
- 1.18 + 0.6	2.53	2.57	2.76	2.62	95.23	4.77
- 0.6 + 0.3	2.28	2.16	2.34	2.26	97.49	2.51
- 0.3 + 0.15	1.1	1.09	1.05	1.08	98.57	1.43
- 0.15 + 0.075	1.39	1.37	1.53	1.43	100	0

3.3.1. Mechanism of agglomeration

According to Mettanant et al. [81], agglomeration can be classified into defluidization induced agglomeration, melt induced agglomeration, and coating induced agglomeration discussed as follows:

Defluidization induced agglomeration

Biomass fuels have irregular shapes, rough surfaces, and large abrasive texture. During combustion of such fuel particles, fluidization may become non-uniform. Sometimes, defluidization may occur at some local points. The mobility of fuel and bed particles at these local points become restricted. Heat transfer to bed from these regions of local defluidization decreases, leading to an increase in local temperature. In case, the temperature becomes more than the melting or softening temperature of ash or bed material; small agglomerates may be formed in these regions. The increase in the size of these agglomerates is restricted if the drag force of fluidizing gas and surrounding particles is large enough to break these agglomerates. Alternatively, the agglomerate size may increase leading to defluidization of entire fluidized bed. Agglomerates formed by this mechanism are weak and can be broken if the fluidization velocity is increased beyond minimum fluidization velocity, else the entire bed may get defluidized. Defluidization induced agglomeration depends upon the chemical composition of ash, particle size and hydrostatic pressure exerted by the fluidizing gas on particles. Shallower beds are less susceptible to defluidization induced agglomeration than deeper beds.

Melt induced agglomeration

Although, biomass ash has varying compositions of potassium, calcium, sodium, and silicon as its major inorganic components, with a little amount of aluminum (in some biomass ashes) [82]. At higher bed temperatures, these inorganic biomass ash components react with bed material like sand and form a eutectic mixture [83]. Sodium-potassium eutectic mixture melts at 875°C and 754°C respectively, whereas the silica sand (SiO_2) melts at a temperature above 1450°C. Bed material is covered with the low melting eutectic mixture of inorganic silicates. At higher temperature, coating melts and bed material particles fuse with each other as shown in Figure 3.2 [85]. In a fluidized bed combustor remedial measures are taken to keep bed

temperature within limit, so that melt induced agglomeration does not take place. Bed temperature may increase due to local defluidization in certain regions leading to melt-induced defluidization.

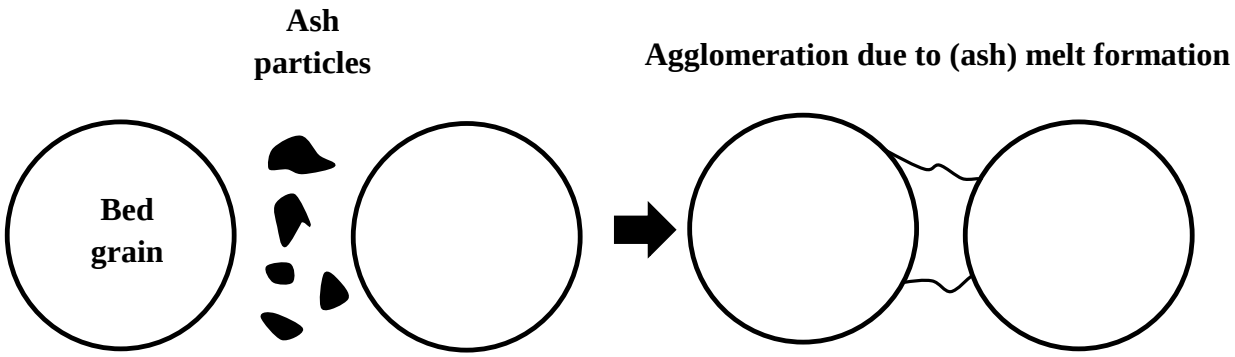

Figure 3.2. Mechanism of melt induced agglomeration (adapted from [85])

Coating induced agglomeration

Coating induced agglomeration is the most common agglomeration formation mechanism found in fluidized bed combustors. Bed particles are covered and are attached to each other with a very thin sticky layer (Figure 3.3). As described by Ohman et al. [86], the sticky layer is formed on the bed particles by three processes, viz. (i) fuel ash particles attached to bed particle surfaces, (ii) condensate formed during gaseous alkali compounds condensation such as KCl, K_2SO_4, KOH, and K and (iii) gaseous alkali compounds reacting with bed particle at its surface.

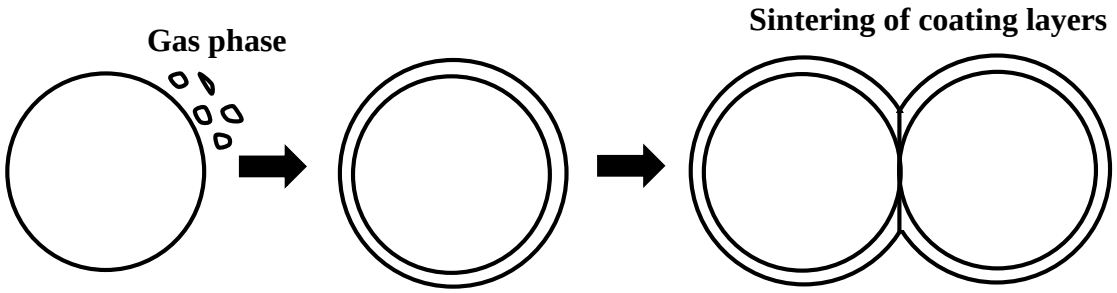

Figure 3.3. Mechanism of coating induced agglomeration (adapted from [85])

Sticky layer grows outward due to first two processes and it grows inward due to the third process. With the passage of time, contributions to sticky layer growth due to first two processes increases and due to the third process decrease, as the already developed layer acts as a barrier between gaseous alkali compounds and bed material surface.

Sodium (Na) and potassium (K) are alkali elements which mainly contribute towards agglomeration, whereas the presence of calcium (Ca) reduces the tendency of agglomeration. Sometimes [Ca/(Na+K)] ratio of fuel is used to predict the agglomeration behavior of biomass. A higher value means lower agglomerate formation probability. Holkkonen et al. [87] proposed that agglomeration tendency is higher under the following condition:

$$\frac{(K_2O+Na_2O)}{SiO_2} > 1 \qquad (3.1)$$

3.3.2. Methods of reducing agglomeration

In the fluidized bed combustor, bed material is under vigorous movement due to fluidizing gas. This can break apart the agglomerates. The fluidized bed will defluidize due to agglomeration when the rate of formation of agglomerates is more than the rate at which agglomerates break apart. Agglomeration can be avoided to a certain extent by using the followings:

- *Agglomeration resistant bed materials*: Bed materials such as silica, alumina (Al_2O_3), feldspar, limestone ($CaCO_3$), ferric oxide (Fe_2O_3), dolomite ($CaCO_3.MgCO_3$), and magnesite ($MgCO_3$) reduces the tendency to agglomeration [87-89]. Brus et al. [90] found that using blast furnace slag instead of silica sand as bed material with reed canary grass, olive residues, and bark as fuel reduces the agglomeration tendency.
- *Additives*: Additives such as limestone ($CaCO_3$), dolomite ($CaCO_3.MgCO_3$), calcium oxide (CaO), magnesium oxide (MgO), and kaolin ($Al_2Si_2O_5(OH)_4$) reduces the agglomeration tendency. It has been found that adding 10% of kaolin in a fluidized bed using quartz as bed material, burning bark, and wheat straw increased agglomeration temperatures from 988°C

to 1000°C for bark and from 739°C to 885°C for wheat straw [91]. Agglomeration temperature increases from 830°C to 890°C with dolomite as an additive and from 830°C to 905°C with kaolin as an additive while burning mixture of bone meal, meat and refuse-derived fuel in a fluidized bed combustor [92].

- *Coarse bed material:* Large size bed material particles have more inertia in comparison to small size bed particles and their collisions are more energetic making the low probability of agglomerate formation. Chirone et al. [84] found that sand particles of size 600-850 µm take twice the time to defluidize as taken by sand particles of size 212-400 µm. In another investigation, it has been reported that adding 30% of coarse bed particles is the optimum ratio for avoiding agglomeration [93].
- *Fuels with high agglomeration temperature:* Fuels with a high amount of calcium have high agglomeration temperature and fuels with a high amount of potassium have low agglomeration temperature [86]. Out of olive flesh, cane trash, rice husk, and bagasse - cane trash and bagasse are found to have higher agglomeration temperatures (> 1000°C) and are more suitable as fuel for fluidized bed combustors [94].
- *Co-combustion:* Biomass fuel co-combustion with high ash containing fossil fuels can reduce the formation of agglomerates in the fluidized bed combustors. Fossil fuels have kaolinites and alumino-silicates which acts as sorbents and reduces the concentration of sodium or potassium in the biomass ash. Using 20% coal (containing 40% ash) with coffee husk reduces concentration of potassium to 13.5% from 43.8% [89].

3.3.3. Agglomeration study of cotton stalk

Reasons of agglomeration for a particular fuel are estimated by studying the coating over the agglomerates using SEM/EDX analysis. The agglomerate sample collected from MPPL, Muktsar Sahib, is shown in Figure 3.4. The size of agglomerates formed at plant site was very

huge and agglomerates were also too hard to be broken by hand. To study the agglomerate behavior of cotton stalk at 7.5 MW FBC plant at MPPL, cotton stalk and bed material (silica sand) samples were collected from the plant site at the time of agglomeration.

Figure 3.4. Agglomerate collected from MPPL, Sri Muktsar Sahib

Figure 3.5. Steel bowl with holes

A steel bowl (Figure 3.5) of 6 cm diameter with 1mm diameter holes (50 in numbers) at the bottom was used for the analysis. Holes were provided to achieve the conditions similar to that in fluidized bed combustor with distributor plate at the bottom of the combustor. 50 gram of cotton stalk was taken in the steel bowl and was heated in a muffle furnace at 800°C for 20 minutes. Cotton stalk ash was mixed with silica sand (Figure 3.6(a)). Samples of cotton stalk ash and silica sand mixture were heated for 15 minutes in the steel bowl with holes at three different temperatures viz. 700°C, 800°C, and 900°C and the bowl was allowed to cool. Results obtained from combustion test at 700°C, 800°C, and 900°C are shown in Figure

3.6(b), Figure 3.6(c), and Figure 3.6(d) respectively. Chemical analysis results of the ash sample collected from the plant site at the time of agglomeration are given in Table 3.6. Ash fusion temperature is 860˚C.

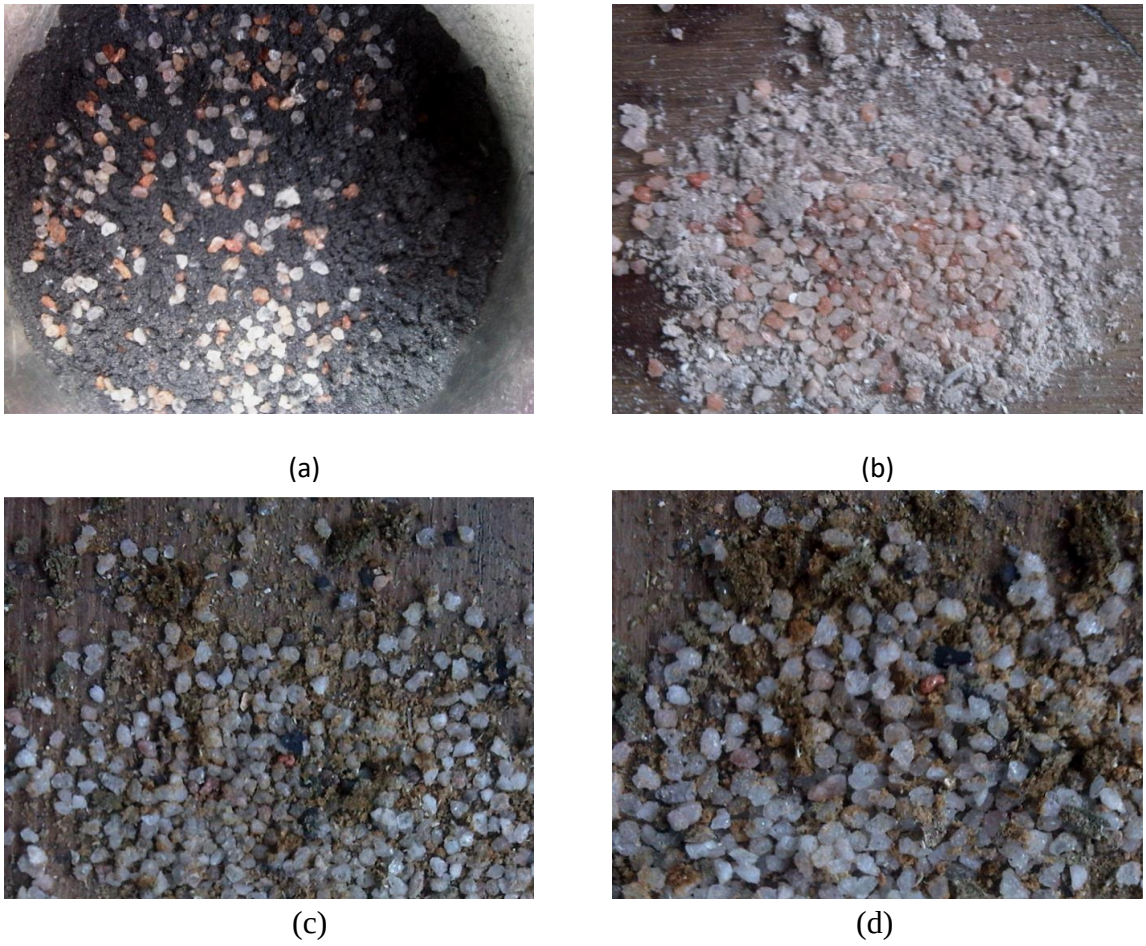

Figure 3.6. Cotton stalk ash and silica sand mixture at room temperature and elevated temperatures. (a) room temperature (b) 700°C (c) 800°C (d) 900°C

3.4. Testing procedures

The fuel is tested for determining its composition and particle size distribution. Fuel properties are the input parameters for mathematical model development. Various tests conducted for collected fuel samples and ash are discussed below:

3.4.1. Proximate analysis

The proximate analysis determines the amount of fixed carbon, volatile, moisture and ash in a fuel. The proximate analysis was carried out as per ASTM D 3172-13 standards at Chemistry

lab, Chitkara University, Rajpura, Punjab. An air oven, weighing machine, silica crucible with lid and a muffle furnace are required for proximate analysis. The temperature inside the ventilated air oven must be uniformly maintained at 110˚C. Silica crucible with lid is used for heating the fuel sample in the muffle furnace and the muffle furnace must provide a uniform temperature of 900˚C. Procedure of determination of fixed carbon, volatile, moisture and ash for cotton stalk are explained below. Same proximate analysis procedure was used for samples of rice husk, rice straw, wheat straw, and cotton stalk fly ash collected from plant site.

Table 3.6. Chemical analysis of ash sample collected from plant

Components	**%**
Silica (as SiO_2)	6.42
Alumina (as Al_2O_3)	18.72
Iron oxide (as Fe_2O_3)	0.37
Titanium Oxide (as TiO_2)	0.04
Calcium Oxide (as CaO)	26.64
Magnesium Oxide (as MgO)	1.84
Sodium Oxide(as Na_2O)	4.52
Potassium Oxide (as K_2O)	23.21
Manganese Oxide(as MnO)	0.05
Sulphate (as SO_3)	7.80
Phosphorus (as P_2O_5)	4.23
Chloride (as Cl)	6.11

Moisture content

A cleaned silica crucible with lid was dried for an hour in air oven at 110˚C. It was then allowed to cool for 20 minutes. Silica crucible was weighed on weighing machine and one gram (approximately) of the cotton stalk was put in the crucible. The silica crucible with cotton stalk was put in the air oven at 110˚C for an hour. The crucible was removed from the air oven and put in a desiccator. The crucible was weighed again. Moisture content is determined as follows:

Weight of moisture, X_1 = Weight of cotton stalk before heating - Weight of cotton stalk after heating $=\{(Y_2 - Y_1) - (Y_3 - Y_1)\} = Y_2 - Y_3$

Weight of moisture in cotton stalk (%), $XW = \left\{{X_1}/{(Y_2 - Y_1)}\right\} \times 100$ (3.2)

Volatile matter

Amount of volatile matter in a fuel sample is the loss in its weight when it is heated at 900˚C for 9 minutes in the absence of air. Silica crucible with lid was weighed on weighing machine. Cotton stalk sample after moisture removal was put in the crucible and was weighed on the weighing machine. Crucible with cotton stalk was kept in a muffle furnace at 900˚C for 9 minutes. The crucible was removed, cooled first on a cooled iron plate and then in a desiccator. The crucible was weighed on the weighing machine. Volatile matter is determined as follows:

Weight of volatile matter, X_2= Weight of cotton stalk before heating - Weight of cotton stalk after heating = $\{(Y_4 - Y_1) - (Y_5 - Y_1)\} = Y_4 - Y_5$

Weight of volatile matter in cotton stalk (%), $XV = \left\{{X_2}/{(Y_4 - Y_1)}\right\} \times 100$ (3.3)

Ash content

Ash content is the weight of the residue left after heating cotton stalk at 800˚C for one hour under controlled conditions. Cleaned silica crucible was heated at 800˚C in a muffle furnace

for one hour and allowing it to cool for 20 minutes. Silica crucible was weighed on weighing machine. One gram (approximately) of the cotton stalk was put in the crucible and was uniformly spread in the crucible. Cotton stalk containing crucible was put in the muffle furnace at 450˚C for thirty minutes and then at 800˚C for next thirty minutes. The crucible was removed and cooled. The crucible was weighed on the weighing machine. Ash content is determined as follows:

Weight of ash = Weight of ash and silica crucible after heating - Weight of empty silica crucible and lid = $X_3 = Y_6 - Y_1$

Weight of ash in cotton stalk (%), $XA = \left\{ {}^{X_3}/_{(Y_2 - Y_1)} \right\} \times 100$ (3.4)

Fixed carbon

Fixed carbon percentage is determined as follows:

Weight of fixed carbon (%), $XC = 100 - (XW + XV + XA)$ (3.5)

3.4.2. Ultimate analysis of cotton stalk

The ultimate analysis is used to determine hydrogen, carbon, nitrogen, sulphur, and oxygen content of the fuel. The ultimate analysis was conducted as per ASTM D 3176-15 standards in CHNSO analyzer at Bali laboratories, Ludhiana.

3.4.3. Sieve analysis test of cotton stalk

Sieve analysis test of the cotton stalk was conducted at RIMT, Mandi Gobindgarh. For conducting the sieve analysis, cotton stalk sample collected from plant site was oven dried to remove moisture. Oven dried sample was weighed. Sieves were cleaned with a brush and were placed with the largest sieve (80 mm) at the top. A pan was placed at the bottom. Oven dried weighed sample of the cotton stalk was put on the top sieve and stack of sieves was placed in

the sieve shaker. Clamps were fixed after putting the cover on the top sieve. Time was set for 10 minutes and sieve shaker was switched on. The mass of cotton stalk retained in each sieve was weighed and the values are shown in Table 3.5.

3.4.4. Emission gas concentration measurement

Emission gas concentration measurement was done using IMR 1400-IR combustion gas analyzer (accuracy ≤ -.3% and precision ≤ 0.2%).

It can measure the following parameters:

- Flue gas temperature
- Heat losses
- Combustion efficiency
- Carbon oxide (CO_2)
- Carbon monoxide (CO)
- Nitric oxide (NO)
- Nitrogen oxide (NO_2)
- Sulphur dioxide (SO_2)

Flue gas is drawn through a built-in sampling pump to a gas sampling probe into the analyzer. Then the gas flows to the condensation trap and after that to a particle filter where dust particles are removed. After this, the gas enters the sensor chamber where the concentrations of various gases are measured by the sensors.

3.4.5. Scanning Electron Microscope (SEM) analysis

Agglomerate studies were carried out by using SEM machine at Sophisticated analysis and instrumentation laboratory, Thapar Institute of Engineering and Technology, Patiala. SEM analysis is used to take high-resolution images of a sample. The sample is scanned by electron

beams. SEM has become a useful tool in the fields of engineering, microbiology, bakery, material science, and physics. The sample is placed in a vacuum enclosure and electron beam is focused on the specimen. The electrons hit the specimen surface and secondary emission of electrons take place. These electrons produce images which are seen on cathode ray tube.

Chapter 4

MODELING AND OPTIMIZATION

4.1. Introduction

The process of defining a system in terms of mathematical equations is called mathematical modeling. Mathematical modeling has become an essential component of research in natural science, social sciences and engineering. Researchers are now able to simulate complex problems related to fluid flow and heat transfer which they were not able to solve experimentally. Linear or non-linear, explicit or implicit, static or dynamic, deterministic or probabilistic, and continuous or discrete are the different classifications of mathematical models. The performance of the mathematical models can be enhanced by applying suitable optimization techniques.

In this chapter, a mathematical model for biomass-based bubbling atmospheric fluidized bed thermal power plant has been developed. The model consists of the followings:

- A solid population balance model: The solid population model has been developed for fuel with wide particle size distribution and applied on the cotton stalk with 0.075 mm to 80 mm particle size.
- An exit gas composition model: The model has considered bubble growth with bed height. Exit gas composition model estimates consumption of oxygen, oxygen conversion, and composition of exit gas.
- A thermodynamic model: The first law of thermodynamics (Energy) and the second law of thermodynamics (Exergy) based thermodynamic model for the plant under study for analyzing the energy-based performance of the thermal plant.

The developed mathematical model is suitable for AFBC using biomass fuel with

wide particle size distribution. Average fuel particle size, fuel density, fuel proximate analysis, ultimate analysis, fuel feeding rate, fluidized bed average temperature, fluidized bed cross-sectional area, and char surface temperature are the input data to the solid population model and exit gas composition model. Calculations for minimum fluidization velocity, bubble diameter, bubble velocity, gas viscosity, and gas density are performed on the basis of input parameters. Solid population model can predict fuel elutriation rate, fuel particle shrinkage rate, fuel carryover rate, carbon utilization efficiency, and bed carbon load. The solid population model is optimized for minimum elutriation rate and maximum carbon utilization efficiency using multi-response optimization method. The percentages of CO_2, N_2, and O_2 in the exhaust gas are calculated using exit gas composition model. Pressure, temperature, and flow rate are the input parameters to the thermodynamic model. First law of thermodynamics (energy) and the second law of thermodynamics (exergy) based thermodynamic model is used to predict the sources of irreversibility and exergy destruction in the plant under study. The thermodynamic model has been optimized for minimum exergy destruction and maximum exergy efficiency using multi-response optimization method. In addition, economic assessment of the plant using break-even analysis has also been conducted.

The present model is different from the models developed so far on the following points:

- Limited work has been done in three phase modeling considering bubble growth along bed height.
- No work has been reported on the cotton stalk as a fuel in FBC systems. Limited literature is available on combustion, fluidization, and devolatization characteristics of the cotton stalk.
- Most of the work has been done on fluidized bed reactors and very little work has been done on fluidized bed combustor.

4.2. Hydrodynamic parameters

Average particle diameter

The average diameter of the fuel particle is one of the parameters used for a solid population model formulation. There are different techniques available in the literature [95–99] for determination of particle size distribution. In the developed model, Rosin-Rammler (R-R) equation explained by Vesilind [95] has been used for determining cotton stalk average particle diameter. R-R distribution function $F(d_p)$ and R-R density function $f(d_p)$ are as follows:

$$F\left(d_p\right)=1-\exp\left[-\left(\frac{d_p}{d_{p_{mean}}}\right)^m\right] \tag{4.1}$$

$$f\left(d_p\right)=\frac{m}{d_{p_{mean}}^m}d_p^{(m-1)}\exp\left[-\left(\frac{d_p}{d_{p_{mean}}}\right)^m\right] \tag{4.2}$$

Particle size distribution is described in terms of size modulus ($d_{p_{mean}}$) and distribution modulus (m). Size modulus ($d_{p_{mean}}$) represents sample's relative size only and it has no direct relation to the sample average particle size.

Minimum fluidization velocity

The velocity of the fluidizing gas at which the bed particles mass is balanced by the drag force produced by the fluidizing gas is known as minimum fluidization velocity. It is one of the important parameters responsible for the efficient performance of any FBC. The fluidized bed is supposed to be completely fluidized when fluidizing gas velocity is at least equal to or more than the minimum velocity of fluidization. Fuel and bed material particles may begin to escape out of bed with further increase in fluidizing gas velocity. Different correlations for calculation of the minimum fluidization velocity are available in the literature, but the following

correlation by Chitester et al. [100] has been found suitable for particles with wide size distribution:

$$U_{mf} = \left(\frac{\mu_g}{d_{p\,mean}\rho_g} \right) \left[\left\{ (28.7)^2 + \frac{0.0494 l \rho_g (\rho_p - \rho_g) g}{\mu_g^2} \right\}^{0.5} - 28.7 \right] \tag{4.3}$$

Superficial gas velocity through the bed

The chemically correct molar feed rate of fluidizing air ($\dot{F}_{MTH}$) required to burn a particular fuel (in this case cotton stalk), is calculated using actual fuel feed rate ($\dot{W}_{cotton\ stalk}$) along with carbon (*XC*), hydrogen (*XH*), sulphur (*XS*), oxygen (*XO*), and moisture content (*XW*) (as determined from ultimate analysis of fuel) by using the following correlation:

$$\dot{F}_{MTH} = \dot{W}_{cotton\ \ stalk} (1 - XW) \left[\frac{XC/12 + XH/4 + XS/32 - XO/32}{0.21} \right] \tag{4.4}$$

In fluidized bed combustor, excess air (E_{xair}) is supplied for confirming the complete combustion of fuel. Hence, the actual molar feed rate of fluidizing air ($\dot{F}_{ME}$) depends upon excess air, which is as follows:

$$\dot{F}_{ME} = \dot{F}_{MTH} (1 + E_{xair}) \tag{4.5}$$

The superficial gas velocity is calculated using following correlation:

$$U_o = \frac{\dot{F}_{ME}\, RT_b}{P_{av} A_o} \tag{4.6}$$

Gas viscosity

Fluidization behavior of a fluidized bed depends upon fluidizing gas viscosity. The gas viscosity is a sole function of fluidized bed temperature. The following relation for fluidizing gas viscosity in terms of fluidized bed temperature [101] is used in the present work:

$$\mu_g = 1.4\times10^{-5}\left(T_b\right)^{1/2} \tag{4.7}$$

Gas density

The density of fluidization gas is calculated using the relation suggested by Bird et al. [101].

$$\rho_g = 353.2\times10^{-3}\times T_b^{-1} \tag{4.8}$$

Average bubble diameter

It is important to calculate average bubble diameter correctly. Out of the different correlations available in the literature, the correlation suggested by Stubington et al. [102] has been used in the present model.

$$d_b = 0.54\left(U_o - U_{mf}\right)^{0.4}\left(Z + 4\sqrt{A_o}\right)^{0.8} g^{-0.2} \tag{4.9}$$

Single bubble velocity

Single bubble rise velocity is estimated using relation suggested by Davidson and Harrison [39].

$$u_{br} = 0.711\sqrt{gd_b} \tag{4.10}$$

Absolute velocity of crowd of bubbles

The absolute velocity of the crowd of bubbles is also calculated using correlation suggested by Davidson and Harrison [39].

$$u_b = \left(U_o - U_{mf}\right) + u_{br} \tag{4.11}$$

4.3. Solid population balance model

Solid population balance model is developed by using following assumptions.:

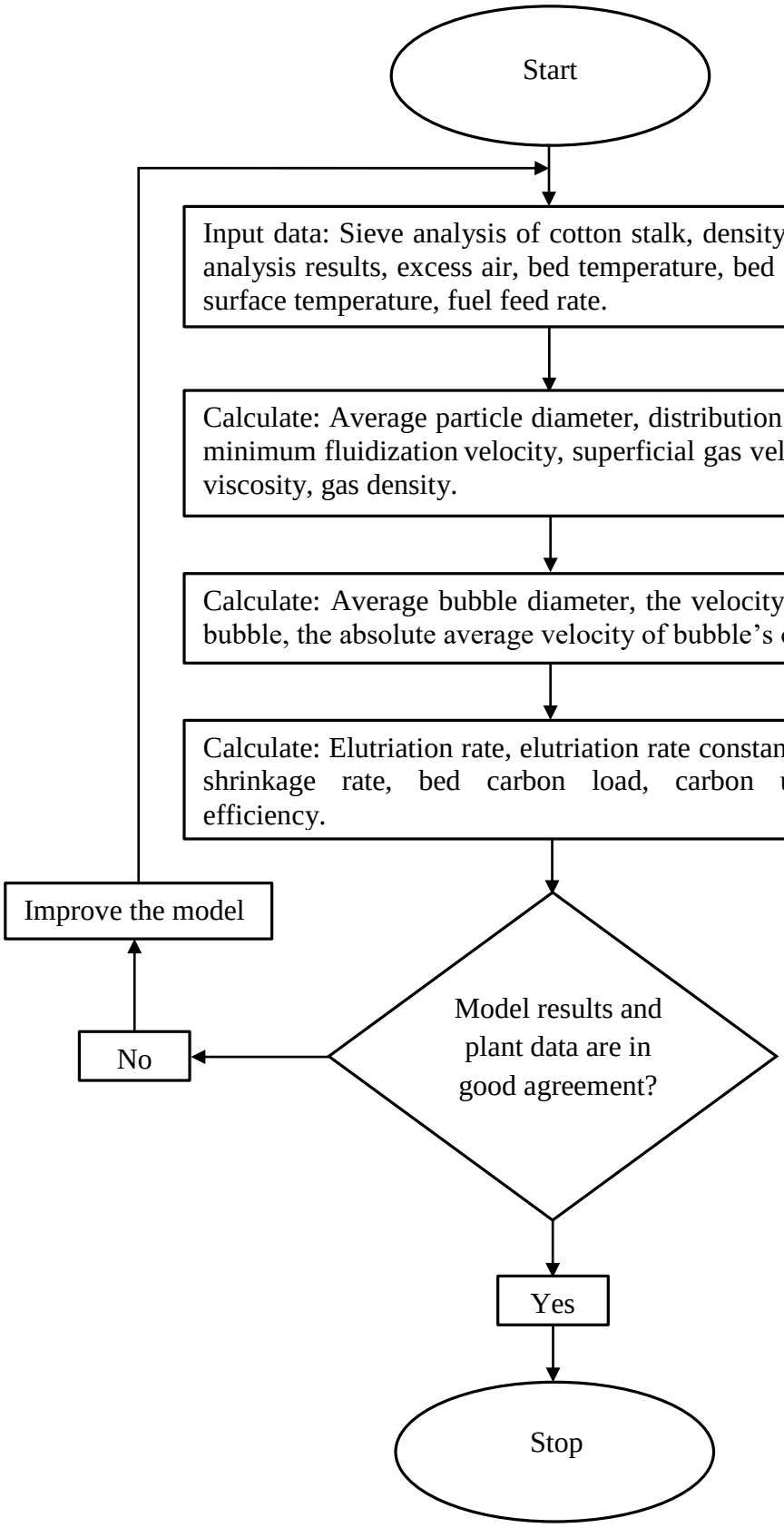

Figure 4.1. The flow chart of solid population balance model

- Combustible particles shrink in size during the process of combustion.
- Combustibles are sufficiently rounded.
- Fragmentation of char particles due to thermal and mechanical shocks are not considered.

Flowchart of Solid population balance model of an AFBC using wide particle size distribution is shown in Figure 4.1.

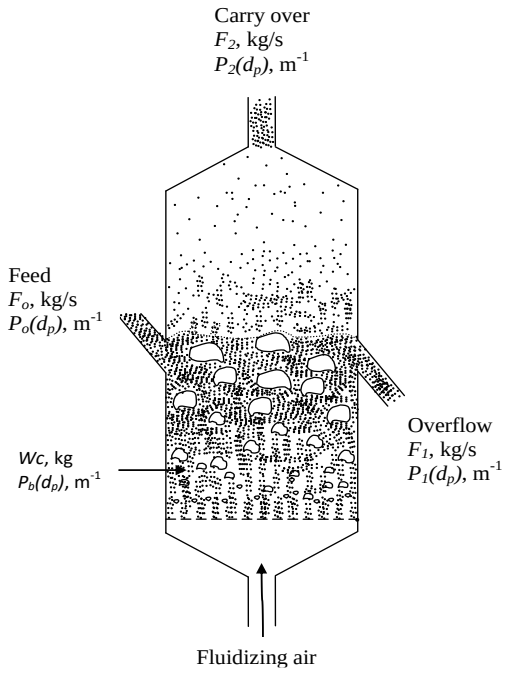

Figure 4.2. Atmospheric fluidized bed combustor under steady state

Figure 4.2 represents an atmospheric fluidized bed combustor under steady state. There is a significant quantitative difference in char flow rates at entry and exit due to shrinking solid particles in FBC. An overall char mass balance for a unit time is shown as:

$$\dot{F}_o - \dot{F}_1 - \dot{F}_2 = (Total\ char\ shrinking\ in\ the\ bed) =$$

$$\sum_{all\ d_p} \left(Char\ shrinkage\ in\ d_p\ to\ d_p + d(d_p)\right) \tag{4.12}$$

Integrating equation (4.12) overall particle sizes gives

$$\dot{F}_o - \dot{F}_1 - \dot{F}_2 \quad = \int_{all\ d_p} \frac{3W_c P_b(d_p)\frac{d(d_p)}{dt}}{d_p}\ d(d_p) \tag{4.13}$$

For size interval d_p to $d_p + d(d_p)$, equation for mass-balance for char is as follows:

(Char entered with the feed) – (Char left with overflow) – (Char left with the carryover) + (Larger size char shrunk into the interval) – (Smaller size char shrunk out of the interval) + (Char consumed during the combustion) = 0

Above is expressed mathematically as:

$$\dot{F}_o P_0(d_p) - \dot{F}_1 P_1(d_p) - W_c K(d_p) P_1(d_p) - W_c \frac{d}{dd_p}\left[\frac{d(d_p)}{dt} P_1(d_p)\right] + \frac{3W_c}{d_p} P_1(d_p) \frac{d(d_p)}{dt} = 0 \qquad (4.14)$$

For detailed derivation refer to Kunii and Levenspiel [9]. In equation (4.14), overflow has been neglected and overflow term has been removed.

4.3.1. Elutriation rate

The solids conversion in an FBC depends upon the residence time of solid particle in the fluidized bed. The residence time of particles is largely affected by elutriation rate. The short residence time of particles indicates larger elutriation rate. This results in low bed carbon load and low combustor efficiency. Elutriation of particles takes place when superficial velocity becomes more than the terminal velocity. Elutriation is complex for particles with wide size distribution than for monosize particles. For fuel particles of wide size distribution, initial shrinkage takes place due to moisture release followed by volatiles emission. Attrition of remaining char converts them into finer particles. Elutriation phenomenon becomes significant at this stage. Terminal velocity of fine char particles decreases and these particles are likely to get elutriated with fluidizing gas. At the same time, the chemical reaction of fine char particles with fluidizing gas (air) takes place. If the time taken for completion of the chemical reaction is lesser than elutriation time, combustion of char particle is complete before it gets elutriated. In this case, carbon utilization efficiency and bed carbon load will be high. If the time taken for completion of the chemical reaction is more than elutriation time, significant char elutriation takes place. Hence, determination of elutriation rate of particles from FBC is of great concern for plant authorities. Available correlations for elutriation rate constant [$K^*(d_p)$] are shown in Table 4.1.

Table 4.1. Elutriation rate constant correlations

References	Correlations and remarks
Yagi and Aochi [103]	$\frac{K^*(d_p) g d_p^2}{\mu_g (U_o - U_T)} = 0.0015 R_{et}^{0.6} + 0.01 R_{et}^{1.2}$ Suggested elutriation rate correlation for small particles from bubbling fluidized bed.
Wen and Hashinger [104]	$\frac{K^*(d_p)}{\rho_g (U_o - U_T)} = 1.52 \times 10^{-5} \frac{(U_o - U_T)}{(g d_p)^{0.5}} \times R_{et}^{0.725} \left(\frac{\rho_s - \rho_g}{\rho_g}\right)^{1.15}$ Suggested elutriation rate constant correlation for two and multi-particle systems.
Tanaka et al. [105]	$\frac{K^*(d_p)}{\rho_g (U_o - U_T)} = 0.046 \frac{(U_o - U_T)}{(g d_p)^{0.5}} \times R_{et}^{0.3} \left(\frac{\rho_s - \rho_g}{\rho_g}\right)^{0.15}$ Correlated elutriation rate with the dimensionless groups derived from momentum and material balance equations.
Merrick and Highley [106]	$\frac{K^*(d_p)}{\rho_g U_o} = 0.0001 + 130 exp\left[-10.4 \left(\frac{U_T}{U_o}\right)^{0.5} \left(\frac{U_{mf}}{U_o - U_{mf}}\right)^{0.25}\right]$ Suggested elutriation rate constant correlation for particle size below 63 µm and high gas velocity.
Geldart et al. [107]	$\frac{K^*(d_p)}{\rho_g U_o} = 23.7\, e^{\left(-5.4 \frac{U_T}{U_o}\right)}$ Developed an empirical correlation and examined the particle size effect on elutriation.
Colakyan and Levenspiel [108]	$\frac{K^*(d_p)}{\rho_s} = 0.011 \left(1 - \frac{U_T}{U_o}\right)^2, for\ U_T < U_o$ $K^*(d_p) = 0, for\ U_T \geq U_o$ Developed elutriation rate correlation for coarse particles with high gas velocity.
Kota el al. [109]	$\frac{K^*(d_p)}{\rho_g (U_o - U_T)} = 2.07 \times 10^{-4} Fr^{\alpha} R_{et}^{1.6} \left(\frac{\rho_s - \rho_g}{\rho_g}\right)^{0.61}$ $\alpha = R_{et}^{-0.6}$ and $Fr = \frac{(U_o - U_T)^2}{g d_p}$ Correlated elutriation rate constant with Reynold's number and Froud's number.

Many empirical correlations [103, 104, 107] are applicable only to elutriation of fine particles. These correlations are used for calculating elutriation rate constant of small particles from bubbling FBC. Correlation given by Merrick and Highley's [106] has been found to be suitable for elutriation rate constant of fine particles with particle size lesser than 63 μm fluidized with high gas velocities. Colakyan and Levenspiel's [108] correlation is found best suited for coarse fuel particles subjected to higher fluidization velocities. In the present work, the most suitable correlation for elutriation rate constant has been identified by calculating the coefficient of correlation *(r)*, for all available correlations (Table 4.1).

Using elutriation rate constant, particle elutriation rate is calculated as follows:

$$\dot{K}(d_p) = \frac{K^*(d_p)}{H_{mf}(1-\varepsilon_{mf})\rho_s} \tag{4.15}$$

4.3.2. Particle shrinkage rate

In this study, particle shrinkage rate in FBC has been calculated using shrinking core model. The approach suggested by Saxena and Rehmat [110] has been followed. It is one out of most comprehensive models available for calculating particle shrinkage rate. In this model, an ash film has been assumed to cover unburnt char particle. During the chemical reaction of char with surrounding air, oxygen diffusion takes place through ash layer and it reaches the core of char particle. Saxena and Rehmat [110] tested their model for a char particles batch to determine char burn out time. Results of the model showed good qualitative agreement with Avedesian and Davidson [111] model.

There may exist a difference between reality and model assumptions. For example, the chemical reaction may not take place along a sharp interface between fresh solids and ash but may occur along the diffused front. The shrinking behavior exists between the continuous model and shrinking core model. Wen and Ishida [112] have addressed this problem. Also, because of the high rate of heat release, temperature gradients may exist between different

particles or between bulk and particle. Wen and Wang [113] have treated this problem very well. Despite these issues, shrinking core model has been found to represent chemically reacting gas-solid systems in simple and best manner [112]. Overall particle shrinkage rate is as given:

$$\left(\frac{dd_p}{dt}\right)_{overall} = \left(\frac{dd_p}{dt}\right)_{combustion} + \left(\frac{dd_p}{dt}\right)_{attrition} \tag{4.16}$$

Particle shrinkage rate due to attrition is calculated by correlation suggested by Chirone et al. [114] as follows:

$$\left(\frac{dd_p}{dt}\right)_{attrition} = A_{att}\left[U_o - U_{mf}\right] \tag{4.17}$$

Here, A_{att} is attrition constant (dimensionless) and in the present work mean value of $A_{att} = 4.0 \times 10^{-7}$, has been used [114].

Particle shrinkage rate due to combustion is calculated using correlation suggested by Turnbull et al. [115] as follows:

$$\left(\frac{dd_p}{dt}\right)_{combustion} = \frac{2M_c}{\rho_c}\left[\frac{1}{K_s} + \frac{d_p}{S_H D_g}\right]^{-1} C_p \tag{4.18}$$

K_s is called surface reaction rate constant. In the present work, the following correlation has been used [116] for K_s:

$$K_s = 4.32 \times 10^{11} T_p^{-0.5} \exp\left(\frac{-44000}{RT_p}\right) \tag{4.19}$$

D_g, is called gas diffusivity and its value is calculated as follows [101]:

$$D_g = 5.14 \times 10^{5} \left(T_b\right)^{1.5} \tag{4.20}$$

The 7.5 MW FBC at MPPL while using cotton stalk is found to work at an average combustor temperature of 1023 K. It has been suggested in the literature that maximum temperature difference between FBC bed and char particle surface cannot exceed beyond 200

K [117]. In the present study, shrinking char particle combustion is assumed to follow single film theory of combustion as the char particle temperature is below 1373 K [118]. Char particle single film theory suggests that for char particle's direct oxidation, oxygen must diffuse across ash film to reach char surface. Oxygen reacts with char to produce CO_2 and CO. CO is further oxidized to form CO_2 by a homogeneous reaction. Oxidation of CO to form CO_2 takes place in the gaseous phase or the boundary layer around char.

4.3.3. Bed carbon load

For shrinking particles with wide particle size distribution, bed carbon load (W_c) is calculated using following correlation:

$$W_c = \dot{F}_0 \int_{d_{p\min}}^{d_{p\max}} \frac{d_p}{\left|\frac{d(d_p)}{dt}\right|} I(d_p, d_{p\max}) d(dp) \times \int_{d_p=d_p}^{d_p=d_{p\max}} \frac{P_o(d_p) d(d_p)}{d_p^3 I(d_p, d_{p\max})} \tag{4.21}$$

4.3.4. Carbon utilization efficiency

The following correlation is used to calculate carbon utilization efficiency:

$$\eta_c = \frac{(\dot{W}_{cotton\ stalk}\, XC) - \dot{F}_2}{\dot{W}_{cotton\ stalk}\, XC} \times 100 \tag{4.22}$$

4.3.5. Optimization of solid population balance model

Solid population balance model optimization has been done using multi-response optimization method [119]. Fuel particle diameter, fuel feed rate, and fractional excess air supplied has been taken as the input parameters. Selected input parameter levels are shown in Table 4.2. Carbon utilization efficiency and elutriation rate are selected as responses. Maximum carbon utilization efficiency and minimum elutriation rate are the objectives as both lead better combustor performance. Orthogonal array arrangement is as shown in Table 4.3.

Table 4.2. Input parameters and their levels

Factors		Levels		
		1	**2**	**3**
A	Fuel particle diameter (mm)	8	10	12
B	Fuel feed rate (kg/s)	2.0	2.75	3.5
C	Fractional excess air	0.1	0.3	0.5

Table 4.3. Orthogonal array arrangement [119]

Trial Nos.	Factors		
	A	**B**	**C**
1	1	1	1
2	1	2	2
3	1	3	3
4	2	1	2
5	2	2	3
6	2	3	1
7	3	1	3
8	3	2	1
9	3	3	2

4.4. Exit gas composition model

In this part, an exit gas composition model for an FBC using fuel particles with wide size distribution (such as cotton stalk) has been developed. The following assumptions have been used:

- The bed consists of three phases viz. bubble, cloud-wake, and emulsion phases.
- The bubble grows along bed height.
- The thermal energy balance would be based upon heat generated by the combustion reaction and lost via convection and radiation.
- The bed operates isothermally under steady state condition.

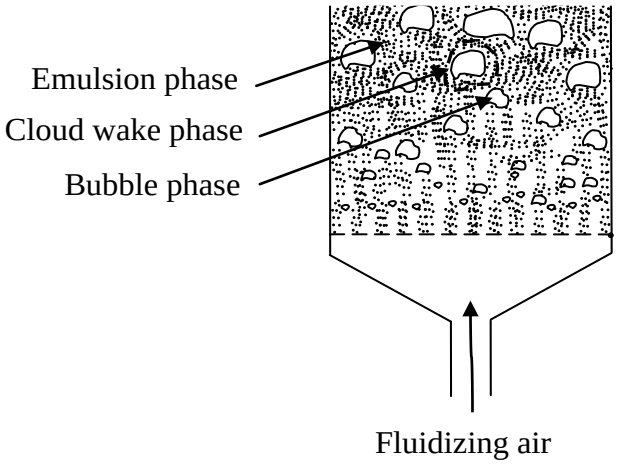

Figure 4.3. Three-phase fluidized bed

The present model is inspired by the model developed by Mohapatra [120] for an FBC using wide size coal washery rejects. It is assumed that (i) gas exchange between phases takes place in following stages viz. (a) bubble phase to cloud-wake phase (b) cloud-wake phase to the emulsion phase (refer Figure 4.3), (ii) in gas first order isothermal reaction takes place and the number of moles does not change. Figure 4.4 shows basic features of three-phase exit gas composition model.

The mass balance equations for reactant gas and each phase over a differential element of height *dZ* is given as follows:

Bubble phase

$$U_b C_b - U_b(C_b + dC_b) - (K_{bc})_b \epsilon_b (C_b - C_{cw}) dZ = 0 \tag{4.23}$$

After rearranging equation (4.23):

$$\frac{dC_b}{dZ} = \frac{(K_{bc})_b \epsilon_b}{U_b} (C_{cw} - C_b) \tag{4.24}$$

Cloud wake phase

$$U_{cw} C_{cw} - U_{cw}(C_{cw} + dC_{cw}) + (K_{bc})_b \epsilon_b (C_b - C_{cw}) dZ - (K_{ce})_b \epsilon_b (C_{cw} - C_e) dZ - Kf_{cw} \epsilon_b C_{cw} dZ = 0 \tag{4.25}$$

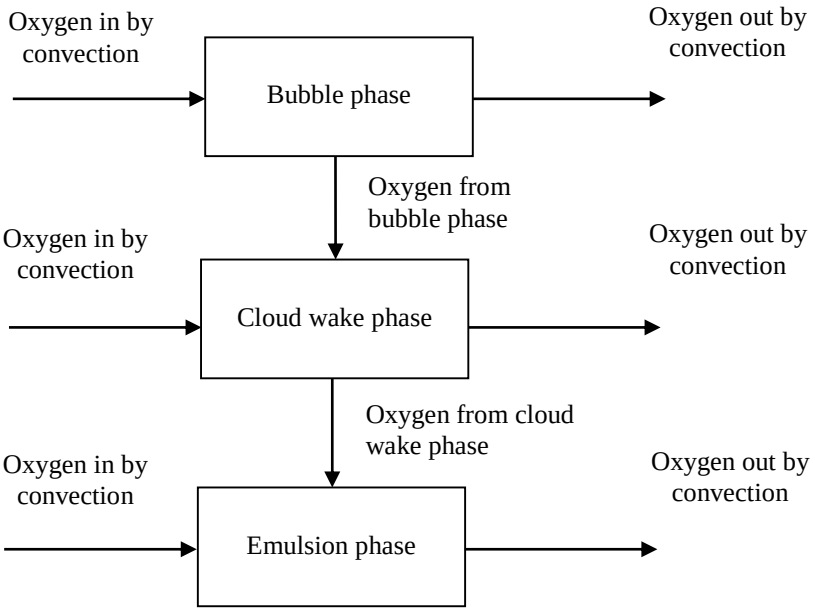

Figure 4.4. Basic features of three-phase exit gas composition model

Here, *K* is the reaction rate constant per unit dense phase volume (i.e., Cloud wake phase and emulsion phase).

After rearranging Equation (4.25):

$$\frac{dC_w}{dZ} = \frac{(K_{bc})_b \epsilon_b}{U_{cw}} C_b + \frac{(K_{ce})_b}{U_{cw}} C_e - \frac{[(K_{bc})_b + (K_{ce})_b + K f_{cw}]}{U_{cw}} C_{cw} \quad (4.26)$$

Emulsion phase

$$U_{mf} C_e - U_{mf}(C_e + dC_e) + (K_{ce})_b \epsilon_b (C_{cw} - C_e) dZ - K[1 - \epsilon_b(1 + f_{cw})] C_e dZ = 0 \quad (4.27)$$

After rearranging Equation (4.27), we get:

$$\frac{dC_e}{dZ} = \frac{(K_{ce})_b}{U_{mf}} C_{cw} - \frac{(K_{ce})_b \epsilon_b + K[1 - \epsilon_b(1 + f_{cw})]}{U_{mf}} C_e \quad (4.28)$$

Gas concentration fed to each phase at the bed bottom is equal to the incoming gas concentration.

i.e. at $Z = 0$; $\quad C_b = C_{cw} = C_e = C_o \quad (4.29)$

Equations (4.23–4.28) is solved for boundary condition specified in equation (4.29) for calculating the concentration of reactant gas for each phase. 4th order Runga-Kutta method

of has been used for solving the equations. The reactant gas concentration for every phase is calculated as:

$$C_b = C_o + \left[\frac{\alpha_1+2\alpha_2+2\alpha_3+\alpha_4}{6}\right] dZ \tag{4.30}$$

$$C_{cw} = C_o + \left[\frac{\beta_1+2\beta_2+2\beta_3+\beta_4}{6}\right] dZ \tag{4.31}$$

$$C_e = C_o + \left[\frac{\gamma_1+2\beta_2+2\beta_3+\beta_4}{6}\right] dZ \tag{4.32}$$

For detailed derivation of $\alpha_i, \beta_i,$ and γ_i $(i = 1 - 4),$ refer to the work by Mohapatra [120].

Average composition of exit gas coming at height *dZ* is calculated as:

Oxygen:

$$C_{avg} = \frac{\left(U_b C_b + U_{cw} C_{cw} + U_{mf} C_e\right)}{U_o} \tag{4.33}$$

Carbon dioxide:

$$CO_2 = C_o - C_{avg} \tag{4.34}$$

Nitrogen:

$$N_2 = \left(\frac{0.79}{22{,}400}\right)\left(\frac{273}{T_b}\right) + \frac{[XN(1-XW)]}{(28U_o A_o)} \tag{4.35}$$

Equations (4.33 – 4.35) are used to estimate flue gas composition using exit gas composition model. Overall fractional oxygen consumption (*X*) is given by:

$$X = 1 - \frac{C_{avg}}{C_o} \tag{4.36}$$

Correlations for hydrodynamic parameters used in the present model are shown in Table 4.4.

4.5. Thermodynamic model

The importance of the energy-exergy analysis for improving the system's thermodynamic of performance has been well understood. In this section, a comprehensive thermodynamic

model of 7.5 MW biomass based Malwa Power Private Limited (MPPL) power plant has been developed. The energy-exergy models have been formulated for a biomass-based power plant. By using this model, the source of maximum energy destruction and exergy destruction in the plant can be located.

Table 4.4. Hydrodynamic parameters

Parameters	**Theoretical/empirical correlation**
Minimum velocity of fluidization [100]	$U_{mf} = \left(\frac{\mu_g}{d_{p_{mean}}\rho_g}\right)\left[\left\{(28.7)^2 + \frac{0.0494 d_p^3 \rho_g (\rho_p - \rho_g) g}{\mu_g^2}\right\}^{0.5} - 28.7\right]$
Gas viscosity [101]	$\mu_g = 1.4 \times 10^{-5}(T_b)^{\frac{1}{2}}$
Gas density [101]	$\rho_g = 353.2 \times 10^{-3} \times T_b^{-1}$
Average bubble diameter [102]	$d_b = 0.54(U_o - U_{mf})^{0.4}(Z + 4\sqrt{A_o})^{0.8} g^{-0.2}$
Single bubble velocity [39]	$u_{br} = 0.711\sqrt{g d_b}$
Bubble's crowd average absolute velocity [39]	$u_b = (U_0 - U_{mf}) - u_{br}$
Superficial gas velocity [121]	$U_o = \frac{\dot{F}_{ME} . R . T_b}{P_{av} A_o}$ where $\dot{F}_{ME} = \dot{F}_{MTH}(1 + E_{xair})$ $\dot{F}_{MTH} = \dot{W}_{cotton\ \ stalk}(1 - XW)\left[\frac{XC/12 + XH/4 + XS/32 - XO/32}{0.21}\right]$
Reynold's number [121]	$R_{e_p} = \frac{\rho_g U_o d_p}{\mu_g}$
Voidage at minimum fluidization [122]	$\epsilon_{mf} = 0.3507\left(\frac{d_p^3 \rho_g (\rho_s - \rho_g)}{\mu_g^2}\right)^{0.0387}\left(\frac{\rho_g U_{mf} d_p}{\mu_g}\right)^{-0.0704}$
Transport disengagement height [63]	$TDH = 4.47 d_{bed}{}^{0.5}$

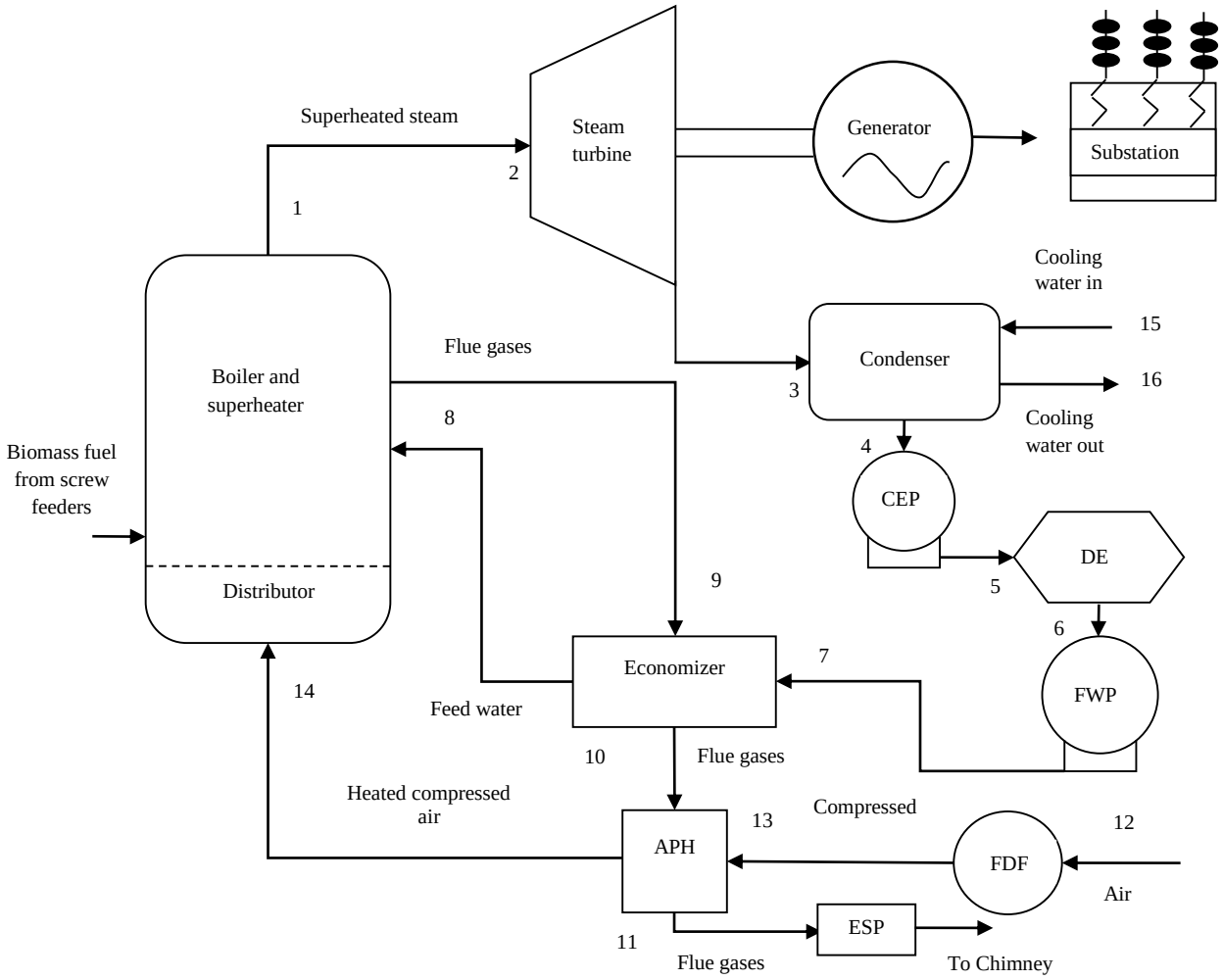

Figure 4.5. Flow diagram of the plant for energy and exergy performance model

Figure 4.5 shows the flow diagram of biomass-based MPPL power plant. The fundamental equations for mass, energy, and exergy balance are the base of the thermodynamic model. The energy term and exergy term calculations at every node point become possible by using these equations. The energy terms include boiler heat requirement, turbine work output, and pump power consumption. The exergy terms include component's exergy at each node point, exergy destruction, and exergy efficiencies. The thermodynamic model is based on the following assumptions:

- Each component is a control volume and works under steady state condition.
- All the gas components follow the ideal gas laws.
- Dead state pressure and dead state temperature are 1.013 bar and 25^{o}C, respectively.

4.5.1. Energy model

The energy performance model is based on the first law of thermodynamics. Using first law of thermodynamics, the desired input/output values of the thermodynamic variables can be calculated or measured. The main thermodynamic variables are pressure (*p*), temperature (*T*), steam mass flow rate ($\dot{m}$), and enthalpy (*H*).

Boiler

The boiler is the main component of any thermal power plant. Fuel combustion takes place in the presence of air in the combustion chamber. The heat generated by the combustion of fuel converts water in the boiler drum into steam at high pressure and temperature. Performance evaluation of the boiler is necessary to maintain a record of heat produced by the fuel combustion. Boiler performance is evaluated on the basis of energy consumption, evaporative capacity, and heat balance sheet. The heat required to evaporate 1 kg water from and at 100˚C is called evaporative unit. Boiler's performance is evaluated on the basis of following parameters [123]

(i) Evaporative capacity: Evaporation capacity is the ratio of steam mass generated per hour to the mass of fuel burnt per hour.

$$m_a = \frac{mass\ of\ steam\ generated\ per\ hour}{mass\ of\ fuel\ burnt\ per\ hour} = \frac{\dot{m}_1}{\dot{m}_{fuel}} \tag{4.37}$$

(ii) Equivalent evaporation: It is the amount of steam (dry and saturated) generated from water at 100˚C at normal pressure.

$$m_e = \frac{\dot{m}_1(h_1 - h_8)}{\dot{m}_{fuel} h_{fg_{@100^\circ C}}} = \frac{m_a(h_1 - h_8)}{2257} \tag{4.38}$$

(iii) Evaporation factor: It is the ratio of heat absorbed per kg of water under operating conditions to the heat absorbed per kg of water from and at 100˚C.

$$F_e = \frac{(h_1 - h_8)}{h_{fg_{@100^\circ C}}} = \frac{(h_1 - h_8)}{2257} \tag{4.39}$$

(iv) Economizer efficiency: It is the ratio of heat absorbed by the feed water in the economizer to the heat available with the flue gases.

$$\eta_{economizer} = \frac{\dot{m}_7(h_8 - h_7)}{\dot{m}_9(h_9 - h_{10})} \tag{4.40}$$

Many times, calculating the amount of heat utilized in economizer is more informative in comparison to the economizer efficiency. Percentage heat utilized in the economizer is given by the relation:

$$heat\ utilized\ in\ economizer = \left[\frac{\dot{m}_7(h_8 - h_7)}{\dot{m}_{fuel} LHV}\right] \times 100 \tag{4.41}$$

(v) Boiler efficiency: The boiler efficiency is measured in terms of the steam efficiency, given as the ratio of steam energy (the energy carried away by the water in its conversion to steam) to the total heat energy generated by the fuel.

$$\eta_{steam} = \frac{\dot{Q}}{\dot{Q}_1} \tag{4.42}$$

Here, $\dot{Q} = \dot{m}_1(h_1 - h_8)$ (4.43)

and $\dot{Q}_1 = \dot{m}_{fuel} \times LHV$ (4.44)

(vi) Overall efficiency of boiler: It is the ratio of heat utilized in the boiler plant to the heat produced by the combustion of fuel.

$$\eta_{boiler(overall)} = \frac{\dot{m}_8[(h_1 - h_8) + (h_8 - h_7)]}{(\dot{m}_{fuel} \times LHV)} \tag{4.45}$$

(vii) Heat balance sheet: A portion of the heat generated by the combustion of fuel is utilized to produce steam from water and rest of the heat is released into the surroundings with flue gases. Assuming superheater to be part of the boiler, the heat balance for the boiler is shown in Figure 4.6.

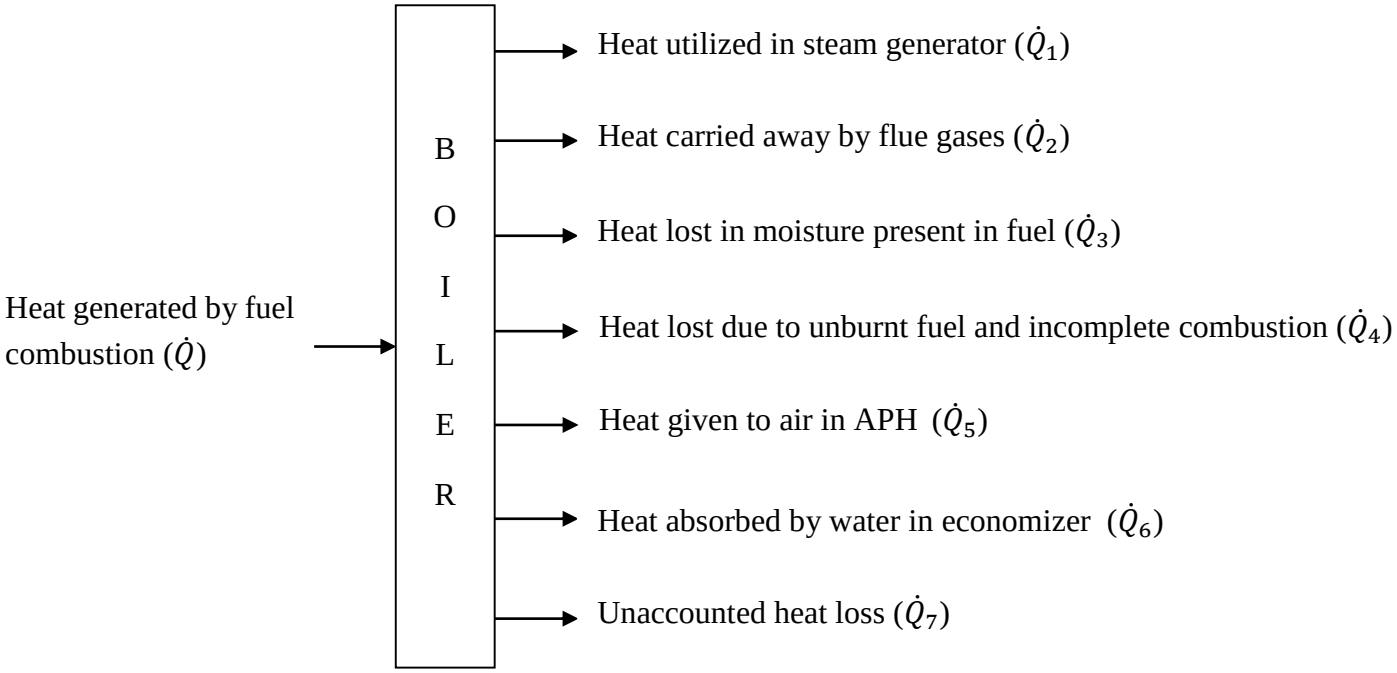

Figure 4.6. Heat balance for the boiler

Various heat quantities are calculated as follows:

Heat generated by fuel combustion $\left(\dot{\mathrm{Q}}\right) = \dot{m}_f \times LCV$ (4.46)

Heat utilized in steam generator $\left(\dot{Q}_1\right) = \dot{m}_1(h_1 - h_8)$ (4.47)

Heat carried away by flue gases $\left(\dot{Q}_2\right) = m_g \times \dot{m}_{fuel} \times c_{p_g}(T_{11} - T_o)$ (4.48)

Where, $m_g =$ mass of gases produced per kg of fuel (4.49)

Heat lost in moisture in fuel $\left(\dot{Q}_3\right) = \dot{m}_{fuel} \times \dot{m}_{moisture} \times \left(h_{fg_o} + c_{p_s}T_g\right)$ (4.50)

where,$\dot{m}_{moisture} =$ (moisture formed + moisture present) per kg fuel

Heat lost due to unburnt fuel and incomplete combustion $\left(\dot{Q}_4\right)$

$$= \dot{m}_{fuel} \times 23680 \times \left[\frac{(C \times CO)}{(CO + CO_2)}\right] \quad (4.51)$$

Heat given to air in APH$\left(\dot{Q}_5\right) = \dot{m}_{10} \times c_{p_g}(T_{10} - T_{11})$ (4.52)

Heat given to water in economizer$\left(\dot{Q}_6\right) = \dot{m}_9 \times c_{p_g}(T_9 - T_{10})$ (4.53)

Unaccounted heat loss$\left(\dot{Q}_7\right) = \dot{\mathrm{Q}} - \left(\dot{Q}_1 + \dot{Q}_2 + \dot{Q}_3 + \dot{Q}_4 + \dot{Q}_5 + \dot{Q}_6\right)$ (4.54)

Steam turbine

Steam turbine converts heat energy of the steam into mechanical power. Superheated steam at high pressure and high temperature expands in the steam turbine. The mechanical power output of the steam turbine is calculated as follows:

$$\dot{W}_{turbine} = \dot{m}_2(h_2 - h_3) - Energy\ loss \tag{4.55}$$

$$where \quad Energy\ loss = \dot{W}_{turbine} - \dot{m}_2(h_2 - h_3) \tag{4.56}$$

The first law efficiency of the turbine is given as:

$$\eta_{turbine} = \frac{\dot{W}_{turbine}}{\dot{m}_2(h_2 - h_3)} \tag{4.57}$$

Pump

The power consumed in the pumps (CEP and FWP) is taken as internal power consumption and the power consumed by the other equipment has been neglected. The pump power is calculated as follows:

$$\dot{W}_{pump} = \frac{\dot{m}(h_{out} - h_{in})}{\eta_{pump}} \tag{4.58}$$

Where η_{pump} is pump efficiency which is assumed to be equal to 80%.

Net power output is given by:

$$\dot{W}_{net} = \dot{W}_{turbine} - \sum \dot{W}_{pump} \tag{4.59}$$

The energy efficiency / the first law efficiency of the power plant is calculated as follows:

$$\eta_{energy} = \frac{\dot{W}_{net}}{(\dot{m}_{fuel} \times LHV)} \tag{4.60}$$

Hashem [76] has listed few more parameters which can be used to evaluate the performance of the plant. These parameters are as follow:

Electrical efficiency: It is the ratio of electrical energy generated to the total energy of the fuel.

$$\eta_{electrical} = \frac{E_{electrical}}{(\dot{m}_{fuel} \times LHV)} \quad (4.61)$$

Net Heat Ratio (NHR): It is the ratio of power generation potential of the fuel to the net electricity produced by the power plant. Power generation potential of the fuel is the total energy of fuel minus the energy amount required to produce the useful thermal energy by conventional means only. NHR is given as follows:

$$NHR = \frac{\left[\dot{m}_{fuel} \times LHV - \left(E_{steam}/\eta_{boiler}\right)\right]}{E_{electrical}} \quad (4.62)$$

Here, $\left(E_{steam}/\eta_{boiler}\right)$ is the energy required to produce the thermal energy by a boiler with boiler efficiency of η_{boiler} (for this study, the boiler efficiency value of 0.80 has been used).

Power to Heat Ratio (PHR): It is the ratio of net electricity produced by the power plant to useful steam energy produced.

$$PHR = \frac{E_{electrical}}{E_{steam}} \quad (4.63)$$

4.5.2. Exergy model

Power plant performance is the function of the performance of each of its component and the performance analysis on the basis of the first law of thermodynamics may sometimes be misleading. The exergy analysis is important as it gives different insight that the energy analysis is unable to do. The exergy analysis indicates the point of irreversibilities in the power plant and highlights the transformation potential of a component to maximum theoretical work under the given environmental conditions. In exergy model, the exergy destruction and the exergy efficiencies of all the major components of the thermal power plant have been assessed

and exergy losses per unit power output in the plant have been used as another exergy performance analysis parameter.

The exergy destruction rate for any component of the power plant can be derived from the exergy balance for that component. The component is assumed to be a control volume at steady state condition. Exergy destruction rate for a component can be calculated using following equation [124]:

$$\dot{E}x_D = \left[\sum \dot{E}x_{in} + \sum Q\left(1 - {}^{T_o}/_{T}\right)_{in}\right] - \left[\sum \dot{E}x_{out} + \sum Q\left(1 - {}^{T_o}/_{T}\right)_{out}\right] \pm \dot{W} \quad (4.64)$$

Where, exergy rate of a stream is given as [90]:

$$\dot{E}_x = \dot{E}_x^{tm} + \dot{E}_x^{ch} \quad (4.65)$$

In this analysis the thermo-mechanical exergy due to mass flows crossing the control volume is calculated by using following expression [75]:

$$\dot{E}_x^{tm} = \dot{m}[(h - h_o) - T_o(s - s_o)] \quad (4.66)$$

Biomass during combustion forms carbon dioxide, water vapor, and other products. The reaction for the combustion of biomass used in the plant under consideration with chemically correct air amount is given as

$$41C + 6.76H_2 + 44.38(O_2 + 3.76N_2) \rightarrow 41CO_2 + 6.76H_2O + 166.87N_2 \quad (4.67)$$

Assuming that combustor is operating with 30% excess air supply, the combustion reaction becomes:

$$53.3C + 8.788H_2 + 57.69(O_2 + 3.76N_2) \rightarrow 53.3CO_2 + 8.788H_2O + 216.93N_2 \quad (4.68)$$

For one mole of carbon, the equation becomes:

$$C + 0.16H_2 + 1.08(O_2 + 3.76N_2) \rightarrow CO_2 + 0.16H_2O + 4.07N_2 \quad (4.69)$$

The exergies of the reactants and the products are given as follows [124]:

$$\dot{E}_{x,R} = \sum N_R\left(\overline{h_{fo}} - h - \overline{h_0} - T_o s\right) \quad (4.70)$$

$$\dot{E}_{x,P} = \sum N_P\left(\overline{h_{fo}} - h - \overline{h_0} - T_o s\right) \quad (4.71)$$

Table 4.5. Exergy efficiencies and exergy destructions of the main components

Name of the component	Figure	Exergy destruction rate ($\dot{E}x_D$)	Exergy efficiency (η_{E_x})
Boiler	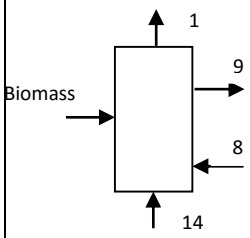	$\dot{E}_{x_{fuel}} + \dot{E}_{x_{14}} + \dot{E}_{x_7} - \dot{E}_{x_1} - \dot{E}_{x_9}$	$\frac{(\dot{E}_{x_1} - \dot{E}_{x_7})}{(\dot{E}_{x_{fuel}} + \dot{E}_{x_{14}}) - \dot{E}_{x_9}}$
Turbine	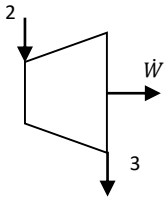	$\dot{E}_{x_2} - \dot{E}_{x_3} - \dot{W}$	$\frac{\dot{W}}{\dot{E}_{x_2} - \dot{E}_{x_3}}$
Water Cooled Condenser (WCC)	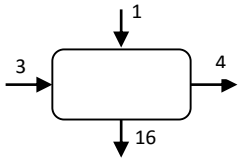	$\dot{E}_{x_3} + \dot{E}_{x_{15}} - \dot{E}_{x_4} - \dot{E}_{x_{16}}$	$\frac{(\dot{E}_{x_{16}} - \dot{E}_{x_{15}})}{(\dot{E}_{x_3} - \dot{E}_{x_4})}$
Economizer	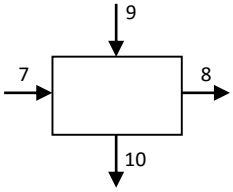	$\dot{E}_{x_7} + \dot{E}_{x_9} - \dot{E}_{x_8} - \dot{E}_{x_{10}}$	$\frac{(\dot{E}_{x_8} - \dot{E}_{x_7})}{(\dot{E}_{x_9} - \dot{E}_{x_{10}})}$
Air Pre-Heater (APH)	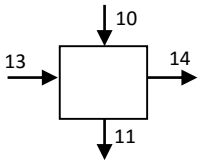	$\dot{E}_{x_{10}} + \dot{E}_{x_{13}} - \dot{E}_{x_{14}} - \dot{E}_{x_{11}}$	$\frac{(\dot{E}_{x_{14}} - \dot{E}_{x_{13}})}{(\dot{E}_{x_{10}} - \dot{E}_{x_{11}})}$
CEP	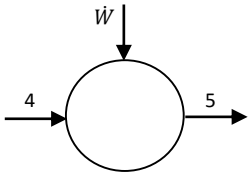	$\dot{E}_{x_4} - \dot{E}_{x_5} + \dot{W}$	$\frac{\dot{E}_{x_5} - \dot{E}_{x_4}}{\dot{W}}$
FWP	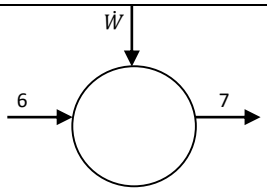	$\dot{E}_{x_6} - \dot{E}_{x_7} + \dot{W}$	$\frac{\dot{E}_{x_7} - \dot{E}_{x_6}}{\dot{W}}$

The exergy efficiencies and the exergy destructions of the main components of the biomass-fired power plant are given in Table 4.5.

Total exergy destruction will be the sum of exergy destruction of each component of the power plant. For the power plant, exergy efficiency will be given as:

$$\eta_{exergy} = \frac{\dot{W}_{net}}{\dot{m}_{fuel} \times Ex_{fuel}} \tag{4.72}$$

where, Ex_{fuel} is the specific exergy of the biomass fuel used at the power plant.

By the exergy and energy analysis, useful information required for performance improvement of the plant can be obtained.

4.5.3. Optimization of thermodynamic model

The thermodynamic model is optimized for exergy analysis. Optimization is done using multi-response optimization method [119]. The steam pressure at turbine inlet, steam temperature at turbine inlet, and fuel feed rate have been taken as the input parameters. Input parameter levels selected for the study are shown in Table 4.6. Exergy efficiency and total exergy destruction are selected as responses. Maximum exergy efficiency and minimum total exergy destruction are the objectives as both lead better plant performance. Orthogonal array arrangement is shown in Table 4.7.

Table 4.6. Input parameters and levels

Factors		Levels		
		1	**2**	**3**
X	Turbine inlet steam pressure (bar)	60	65	70
Y	Turbine inlet steam temperature (˚C)	430	450	470
Z	Fuel feed rate (kg/s)	1.5	2.75	4

Table 4.7. Orthogonal array arrangement [119]

Trial No.	Factors		
	X	Y	Z
1	1	1	1
2	1	2	2
3	1	3	3
4	2	1	2
5	2	2	3
6	2	3	1
7	3	1	3
8	3	2	1
9	3	3	2

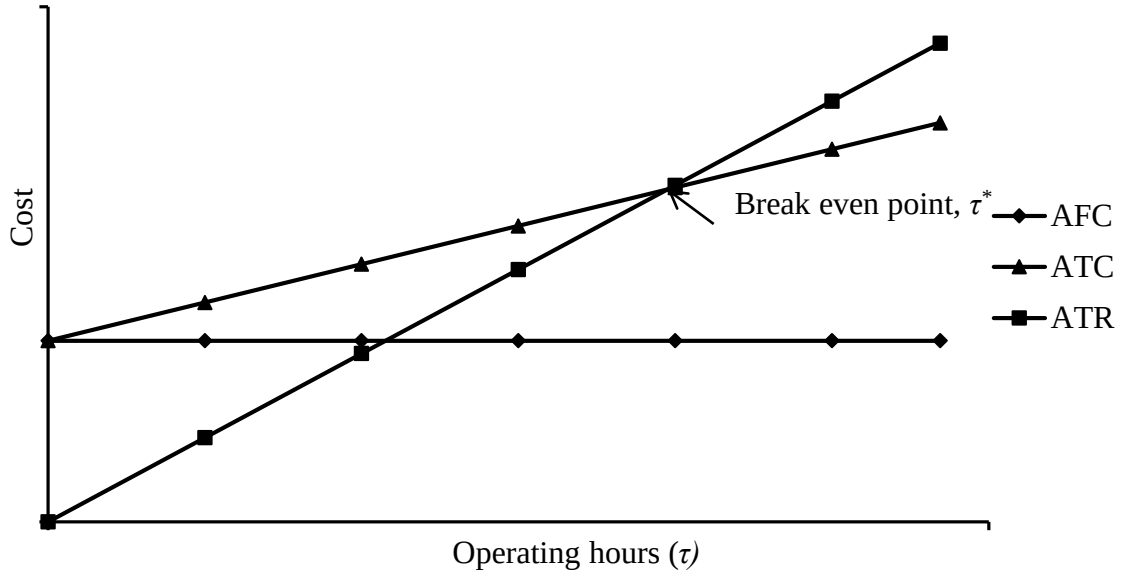

Figure 4.7. Break-even analysis

4.6. Economic analysis

For the economic study of the plant, the break-even analysis method has been followed. In this method, the Annual Total Variable Cost (ATVC), Annual Total Revenue (ATR), Annual Fixed Cost (AFC), and total operating hours (τ) in a year are noted. ATC of running is the sum of ATVC and AFC. ATC and ATR are plotted against the operating hours (τ) for a year, as shown

in Figure 4.7. ATR line starts from the origin, whereas ATC line starts from the AFC point on the cost axis. The break-even in terms of hours of operation (τ^*) is the point where ATR line intersects ATC line. Below τ^* the plant is in the loss and above τ^* the plant is in profit. It can be expressed as:

$$\text{Annual Net Profit (ANP)} = \text{ATR} - (\text{ATVC} + \text{AFC}) = \text{ATR} - \text{ATC} \quad (4.73)$$

Improvement in exergy efficiency of the plant has a significant effect on ANP. For the same network output, a slight increase in the exergy efficiency leads to decrease in fuel requirement (refer equation 4.72). This results in an increase in ANP.

4.7. Input Data

The following is the input data for the mathematical model:

Proximate analysis of cotton stalk	
Enter the value of volatile matter (%)	65.86
Enter the value of fixed carbon (%)	15.77
Enter the value of ash (%)	4.48
Enter the value of moisture (%)	13.89
Ultimate analysis of cotton stalk	
Enter the value of carbon (%)	41.3
Enter the value of hydrogen (%)	6.8
Enter the value of Sulphur (%)	0.5
Enter the value of oxygen (%)	39.7
Enter the value of nitrogen (%)	0.7
Physico-chemical parameters	
Enter fuel feed rate (g/s)	2.75
Enter density of fuel (g/m^3)	460×10^3
Enter fuel gross calorific value (J/kg)	16.9×10^6
Enter fractional excess air	0.3
Enter bed temperature (K)	1023
Enter bed cross-section area (m^2)	18.99
Enter char surface temperature (K)	1223
Enter size modulus (m)	10.28×10^{-3}
Enter distribution modulus	1.22

Chapter 5

RESULTS AND DISCUSSION

In this chapter, the results obtained from sub-models have been shown and discussed. The data collected from 7.5 MW biomass based Malwa Power Plant Limited, Sri Muktsar Sahib, Punjab, India has been used as input to the model developed. At the time of the study, the samples of cotton stalk, wheat straw, rice straw, and rice husk, were collected from the plant site. Table 3.4 and Table 3.5 showed the proximate analysis and the ultimate analysis results of the fuel samples, respectively. It was observed that only cotton stalk or mixture of different biomass fuels were used in the combustor at the plant site. Temperature and pressure at different state points were also recorded from the monitor placed in the control room. The model predictions have been validated with experimental data obtained from the plant site. Multi-response optimization method has been used for optimizing solid population balance model and thermodynamic model. Solid population balance model has been optimized for maximum carbon utilization efficiency and minimum elutriation rate. The thermodynamic model has been optimized for maximum overall exergy efficiency and minimum total exergy destruction.

5.1. Solid population balance model

Figure 5.1 shows cotton stalk's particle size distribution. The Rosin-Rammler (R-R) distribution of cotton stalk has been shown in Figure 5.2. Distribution modulus (m) and size modulus ($d_{p_{mean}}$) values obtained from R-R equation are 1.22 and 10.82 mm respectively. Size modulus ($d_{p_{mean}}$) is one of the model input parameters. For a specific size modulus, higher distribution modulus indicates narrower size distribution of fuel particle and vice-versa. The proximate and ultimate analysis results along with particle size distribution results and physico-chemical parameters of the plant become input parameters to the solid population balance and exit gas composition model.

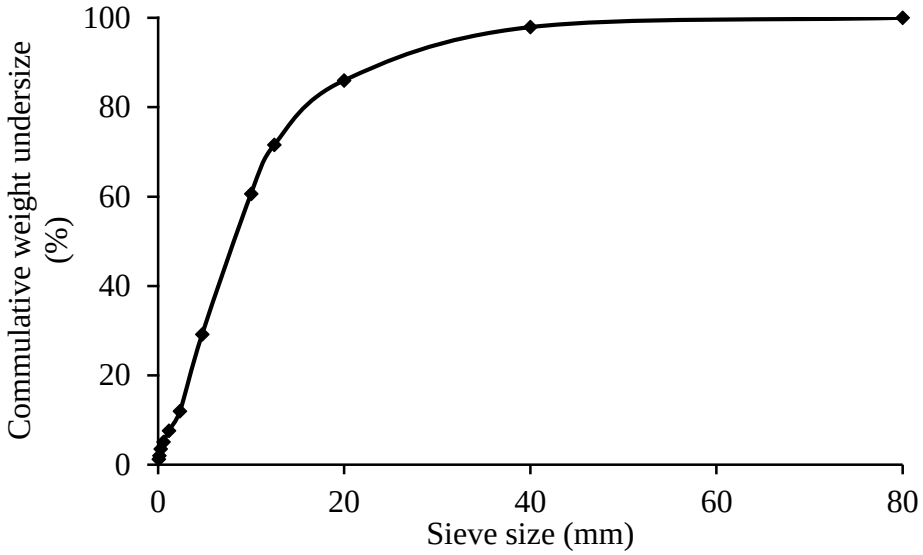

Figure 5.1. Particle size distribution of cotton stalk

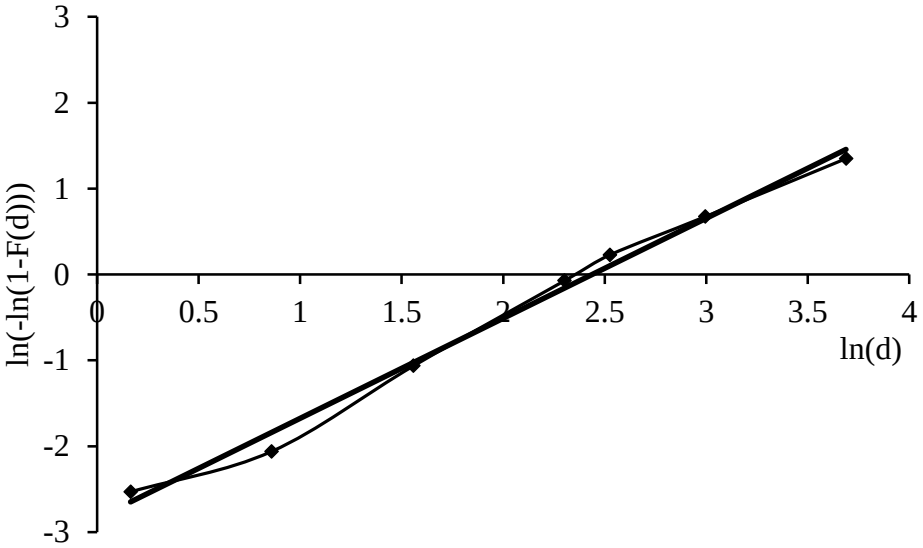

Figure 5.2. Rosin-Rammler distribution

Distribution modulus effect on carryover rate is shown in Figure 5.3. It can be observed that for larger distribution modulus carryover rate is lower. This is because large distribution modulus value is an indication of narrow particle size distribution. It means that fewer particles are available for elutriation resulting in lower carryover rate. The residence time of particles increases resulting an increased combustor efficiency.

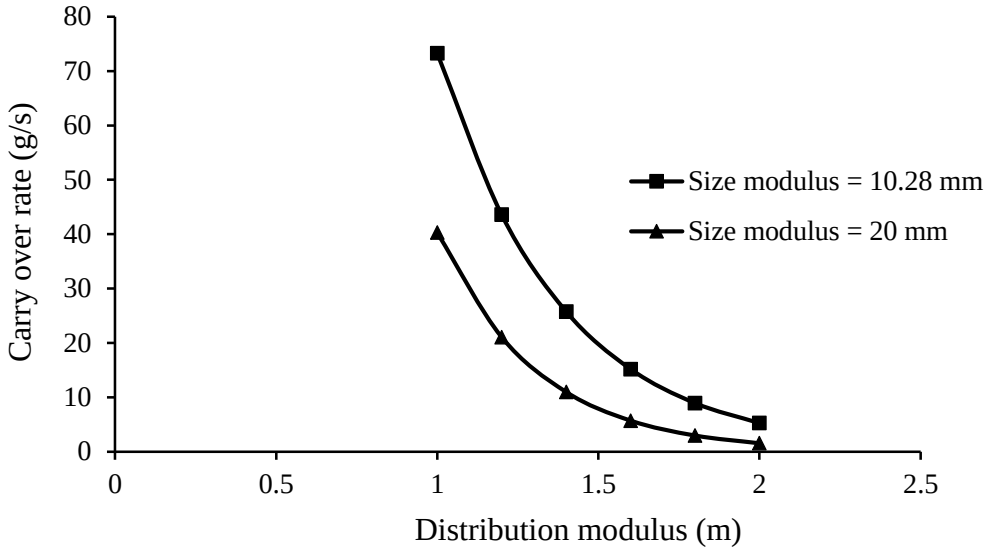

Figure 5.3. Carryover rate variation with distribution modulus

Table 5.1. Goodness fit for elutriation rate correlations

References	**Correlation coefficient, *r***	***r*²**
Tanaka et al. [105]	-0.893	0.797
Merrick and Highley [106]	-0.752	0.566
Colakyan and Levenspiel [108]	-0.901	0.812
Kato el al. [109]	-0.335	0.112

The goodness fit for different elutriation rate correlations is shown in Table 5.1. Correlations for wider particles have been only considered. It can be concluded from Table 5.1 that Colakyan and Levenspiel correlation [108] is applicable for the cotton stalk, as it has r^2 value nearest to unity and in this work, same correlation is used.

The effect of particle diameter on elutriation rate is shown in Figure 5.4. Larger particles are heavy and are difficult to get elutriated. Combustion takes place under the steady state in combustor due to the presence of large particles. Lighter particles are subjected to easy elutriation. Elutriation of fuel particles with diameter greater than 0.6 mm become negligible (Figure 5.4). This is attributed to the fact that the terminal velocity of fuel particles having the diameter more than 0.6 mm exceeds their corresponding superficial velocity. Colakyan and

Levenspiel [108] have reported same observation in their work. Figure 5.4 also shows an increase in elutriation rate for constant particle diameter when fractional excess air amount increases from 0.2 to 0.3. Bed temperature increases with increase in excess air. Overall reaction rate increases with increase in bed temperature. This leads to increased number of fines generated which result increase in elutriation rate.

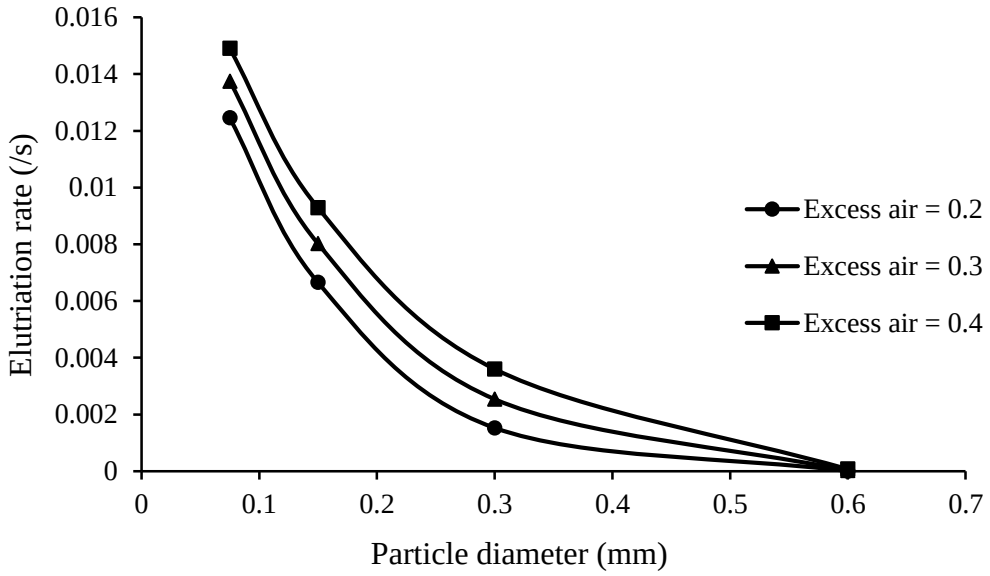

Figure 5.4. Effect of particle size on elutriation rate

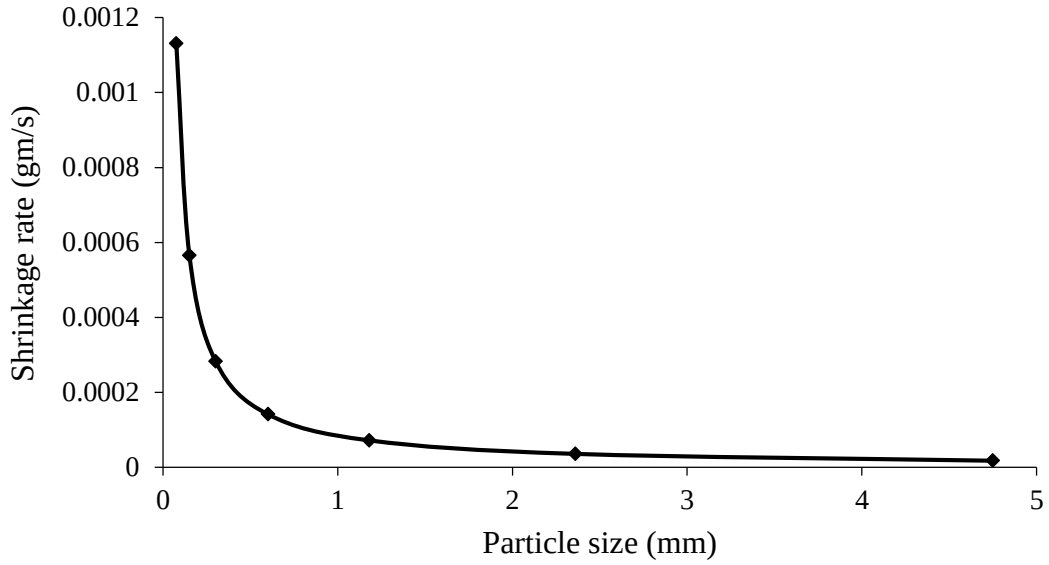

Figure 5.5. Shrinkage rate variation with particle size

Figure 5.5 shows the effect of fuel particle size on particle shrinkage rate. It can be observed from figure 5.5 that there is a sharp fall in particle shrinkage rate up to 1 mm. It is nearly constant for particle size more than 1 mm. The influence of shrinkage due to combustion is more in comparison to attrition.

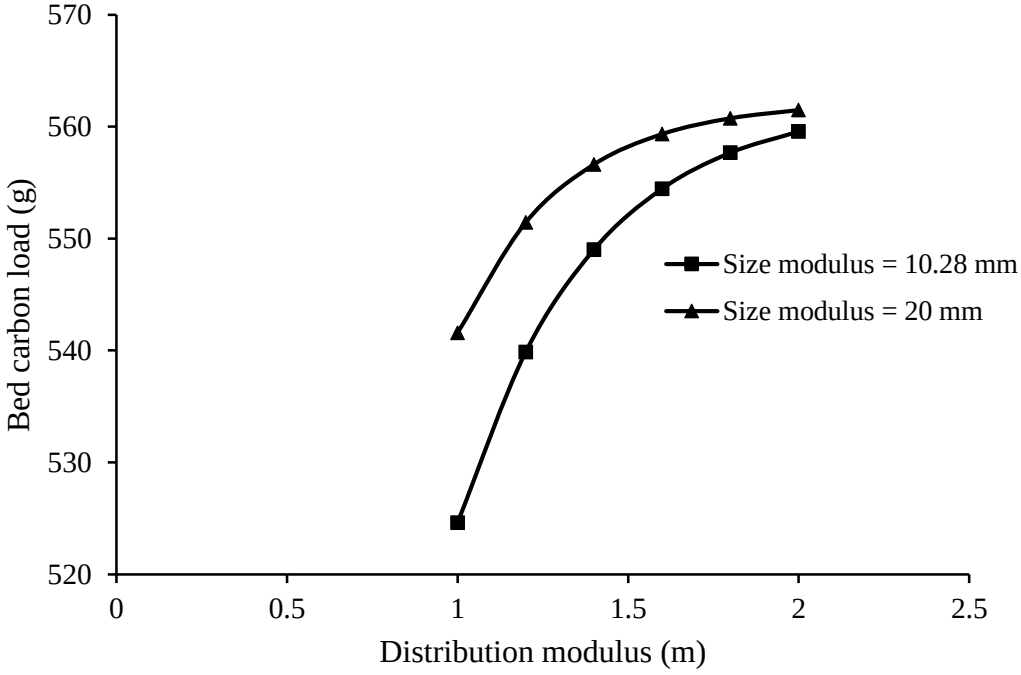

Figure 5.6. Distribution modulus versus bed carbon load

Figure 5.6 shows the effect of distribution modulus on bed carbon load. Bed carbon load is directly related to distribution modulus. Bed carbon load indicates the amount of carbon surface required to maintain combustion under steady state. With increase in the distribution modulus, the particle size distribution gets narrower. The elutriation rate increases leading to elutriation of fine particles. An increased bed carbon load compensates loss in surface area.

Table 5.2 shows carbon utilization efficiency calculations corresponding to plant data. Carbon from the proximate analysis is taken as carbon inlet to the combustor. Amount of unburnt carbon in the fly ash, bed ash, and unburnt cotton stalk are calculated. The plant carbon utilization efficiency is found to be 97.44%. Carbon utilization efficiency values from plant's

data and model are shown in Table 5.3. The model predictions and plant values are showing good agreement with an error of 1.25%.

Table 5.2. Carbon Utilization Efficiency (CUE) calculation

Parameters	Value
$\dot{m}_{fuel}$	2.75
Carbon in fuel (%)	15.77
$X_o = \dot{m}_{fuel} \times \frac{\text{Carbon in fuel (\%)}}{100}$	433.67
$\dot{m}_{ash}$	99.80
Carbon in fly ash (%)	9.80
$X_1 = \dot{m}_{ash} \times \frac{\text{Carbon in fly ash (\%)}}{100}$	9.78
Bed ash (g/s)	15.4
Carbon in bed ash (%)	Nil
$\dot{m}_{unburnt\ fuel}$	8.20
$X_2 = \dot{m}_{unburnt\ fuel} \times \frac{\text{Carbon in fuel (\%)}}{100}$	1.29
$CUE = \frac{\{X_o - (X_1 + X_2)\}}{X_o} \times 100$	97.44

Table 5.3. Measured and model predicted carbon utilization efficiency

Excess air	Carbon utilization efficiency (%)	
	Measured	Model predicted
0.3	97.44	96.22

Distribution and size modulus effect on carbon utilization efficiency is shown in Figure 5.7. For a specific size modulus, distribution modulus is showing inverse effect on the carbon utilization efficiency. It shows inefficient combustion of the cotton stalk with wider

feed size distribution in an FBC. It is attributed to the fact that for wider feed size distribution of the cotton stalk the number of fines increases. These fine fuel particles escape with carryover. It results loss in bed carbon load as well as carbon utilization efficiency. The carbon utilization efficiency is also affected by the size modulus of the fuel sample.

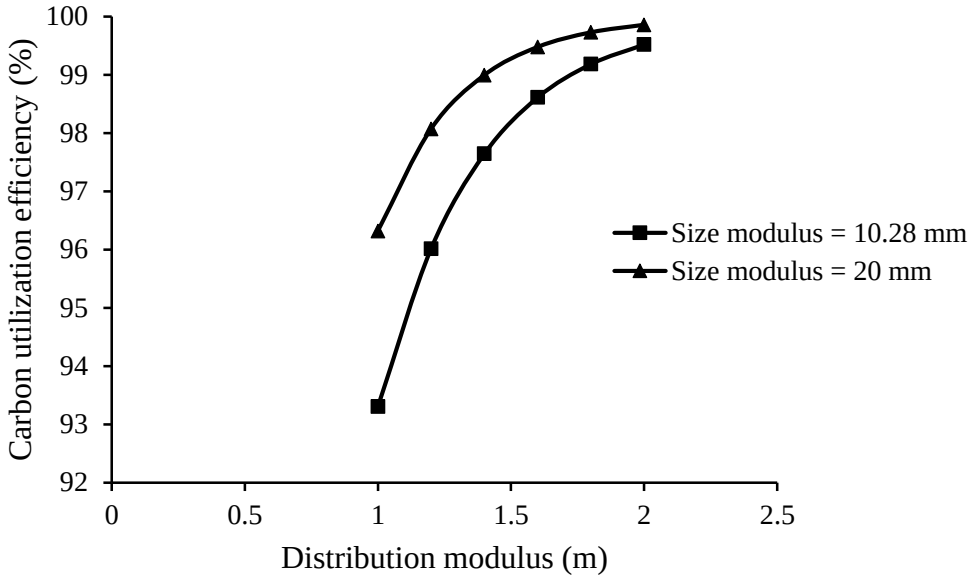

Figure 5.7. Carbon utilization efficiency variation with distribution modulus

For a given distribution modulus value, size modulus is directly linked to the carbon utilization efficiency. With decrease in size modulus, the number of fines increases and vice versa. So, for the low value of size modulus number of fines is more. The fines below critical size escape with carryover leading to fall in combustion efficiency. In an FBC, the combustion is less efficient if the cotton stalk with wide particle distribution and small particle size is used. It is also to be noted that the range of particle size must be kept below normal range accepted for FBC.

5.1.1. Optimization of solid population model

Multi-response optimization method has been used to optimize solid population balance model [119]. Fuel particle diameter (factor A), fuel feed rate (factor B), and fractional excess air supplied (factor C) has been taken as the input parameters. Carbon Utilization Efficiency

(CUE) and elutriation rate (ER) are selected as responses. Maximum carbon utilization efficiency and minimum elutriation rate are the objectives as both lead better combustor performance. Calculations for CUE and ER at different orthogonal array arrangements are shown in Table 5.4.

Table 5.4. CUE and ER at different orthogonal array arrangements

Trial no.	Factors			CUE	ER
	A	B	C		
1	5	1.5	0.1	0.999988	0.00001700
2	5	2.75	0.3	0.999732	0.000674407
3	5	4	0.5	0.997833	0.007931001
4	10	1.5	0.3	0.999993	0.000010232
5	10	2.75	0.5	0.999856	0.000362084
6	10	4	0.1	0.999865	0.000492296
7	15	1.5	0.3	0.999997	0.000004776
8	15	2.75	0.5	0.999933	0.00016895
9	15	4	0.1	0.999937	0.000229707

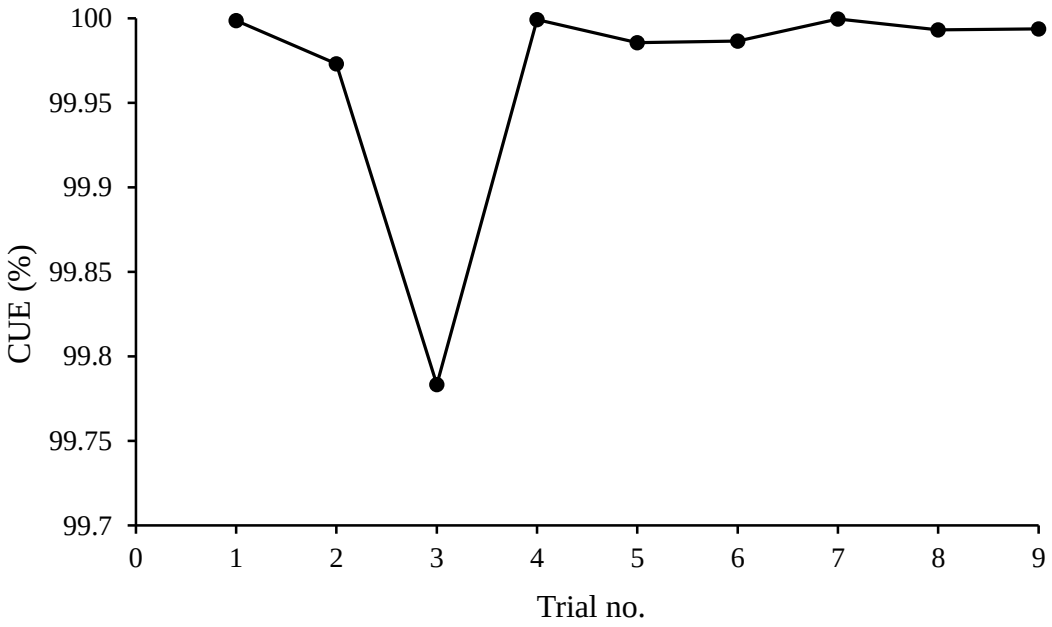

Figure 5.8. CUE variation with different orthogonal array arrangements

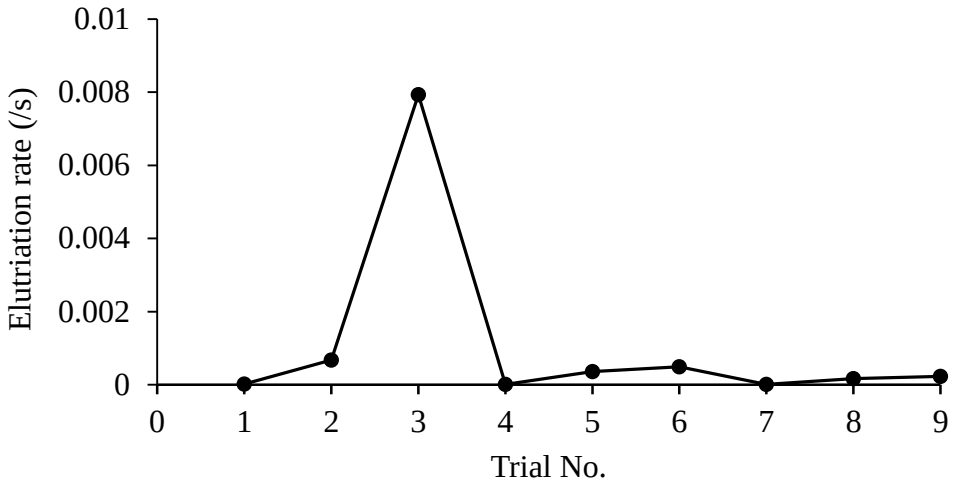

Figure 5.9. Elutriation rate variation with different orthogonal array arrangements

Variation of Carbon utilization efficiency (CUE) and elutriation rate (ER) with each trail is shown in Figure 5.8 and Figure 5.9 respectively. It can be observed that CUE is minimum and ER is maximum at trial number 3 (fuel particle diameter = 5 mm, fuel feed rate = 4 kg/s, and excess air = 0.5). Minimum CUE indicates incomplete combustion due to high fuel feed rate. The smaller particle size of 5 mm at trial number 3 leads to increase in ER. Elutriation of fuel particles is further increased due to high excess air supplied.

The weights are calculated for CUE and ER. For CUE (Larger – the better), CUE value corresponding to each trial number is divided by total CUE value (Σ CUE). For ER (smaller – the better), reverse normalization has been used. For each ER response, 1/ER is calculated and then the weight of ER (W_{ER}) is obtained. From Table 5.5, Σ CUE = 8.997133 and Σ 1/ER = 382674.5.

Here, $W_{CUE_i} = \frac{CUE_i}{\sum CUE}$ and $W_{ER_i} = \frac{\left({}^{1}/_{ER_i}\right)}{\sum\left({}^{1}/_{ER}\right)}$ (5.1)

Multi-Response Performance Index (MRPI) for i^{th} trial is calculated using following formula:

$$(MRPI)_i = W_{CUE_i} \times CUE_i + W_{ER_i} \times ER_i \quad (5.2)$$

The weight and MRPI for each trial are given in Table 5.5.

Table 5.5. Weights and MRPI values

Trial no.	CUE	W_{CUE}	ER	W_{ER}	MRPI
1	0.999988	0.111145	0.00001700	0.153681	0.111146
2	0.999732	0.111117	0.000674407	0.003875	0.11109
3	0.997833	0.110906	0.007931001	0.000329	0.110668
4	0.999993	0.111146	0.000010232	0.255396	0.111147
5	0.999856	0.111131	0.000362084	0.007217	0.111117
6	0.999865	0.111132	0.000492296	0.005308	0.111119
7	0.999997	0.111146	0.000004776	0.547351	0.111148
8	0.999933	0.111139	0.00016895	0.015467	0.111134
9	0.999937	0.11114	0.000229707	0.011376	0.111135

Table 5.6. MRPI as response to the optimization problem

Trial no.	Factors			MRPI
	A	B	C	
1	5	1.5	0.1	0.111146
2	5	2.75	0.3	0.11109
3	5	4	0.5	0.110668
4	10	1.5	0.3	0.111147
5	10	2.75	0.5	0.111117
6	10	4	0.1	0.111119
7	15	1.5	0.3	0.111148
8	15	2.75	0.5	0.111134
9	15	4	0.1	0.111135

Table 5.7. Level totals of MRPI

Input parameters	LEVEL 1	LEVEL 2	LEVEL 3
A	0.332907	0.333374	0.333421
B	0.333444	0.333369	0.332889
C	0.333367	0.333374	0.332961

MRPI is considered as a single response to the problem and as it is weighed score, optimal levels are identified based on maximum MRPI value. Table 5.6 shows optimization problem with MRPI scores. The level totals of MRPI are given in Table 5.7. The optimal levels are selected based on maximum MPRI. The optimal levels are A-3 (fuel particle diameter = 15 mm), B-1 (fuel feed rate = 1.5 kg/s), and C-2 (excess air = 0.3). At optimal levels of input parameters, maximum carbon utilization efficiency of 99.9997% and minimum elutriation rate of 4.776×10^{-7} /s is achieved.

5.2. Exit gas composition model

This model predicts the composition of the exhaust flue gas from the plant. The model variation is within 6%. This may be due to the simplified assumptions. Exit gas composition results obtained from the model are compared with real plant data in Table 5.8. Table 5.9 shows the actual composition of exit flue gas from MPPL at various fractional excess air supplied.

Table 5.8. Model predictions validation with the real plant data

Exit gas components	UPP (14.5 MW) village Lambi	JPP (10 MW) village Jalkheri [48]		MPPL (7.5 MW) village Gulabewala	
Volume (%)	**Plant**	**Plant**	**Model**	**Plant**	**Model**
N_2	74-78	76-79	79.41	75-78	77.6
CO_2	11-14	10-14	13.87	9-12	11.35
O_2	7-11	6-9	7.12	7-10	7.92

Table 5.9. Exit flue gas composition at various fractional excess air

Fractional excess air	Bed temperature (°C)	NO_X (%)	CO_2 (%)	O_2 (%)
0.1	735	77.7	10.8	7.2
0.2	744	77.1	10.6	7.5
0.3	751	76.5	10.3	8.1
0.4	759	75.8	9.5	8.6
0.5	768	75.3	9.1	8.9

Oxygen conversion and exit flue gas composition change with fractional excess air supplied are shown in Figure 5.10. Plant values and model predictions are in good agreement with an error of 10-16% for carbon dioxide and 4-9 % for oxygen. Since the combustibles amount in the FBC remain unchanged, the amount of carbon dioxide in the exhaust gases decreases with increase in fractional excess air supply. Simultaneously, amount of oxygen increases with the increase in the excess air leading to increase in heat loss along with exhaust gases. However, with increase in fractional excess air the oxygen conversion decreases.

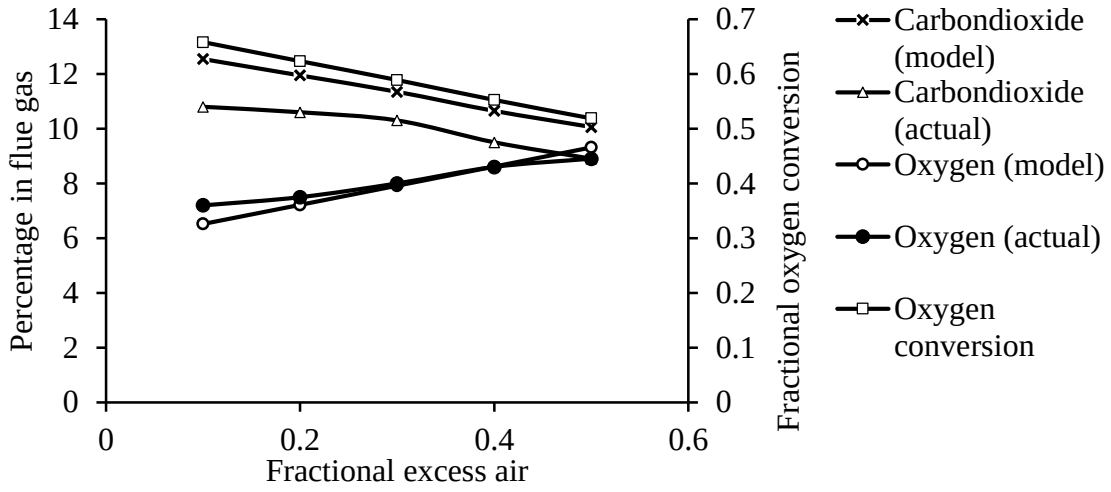

Figure 5.10. Fractional oxygen conversion and exit gas composition variation with excess air

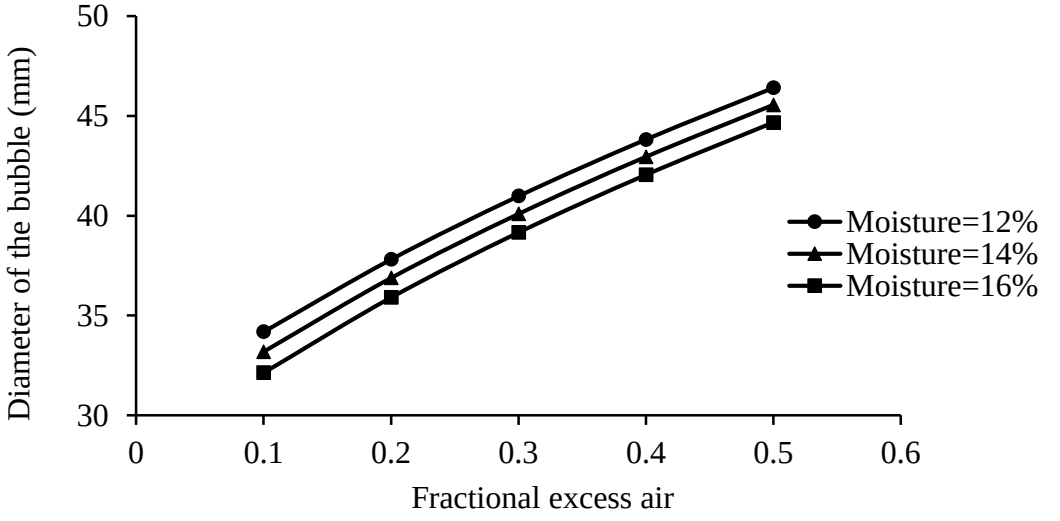

Figure 5.11. Bubble diameter variation with moisture content and excess air

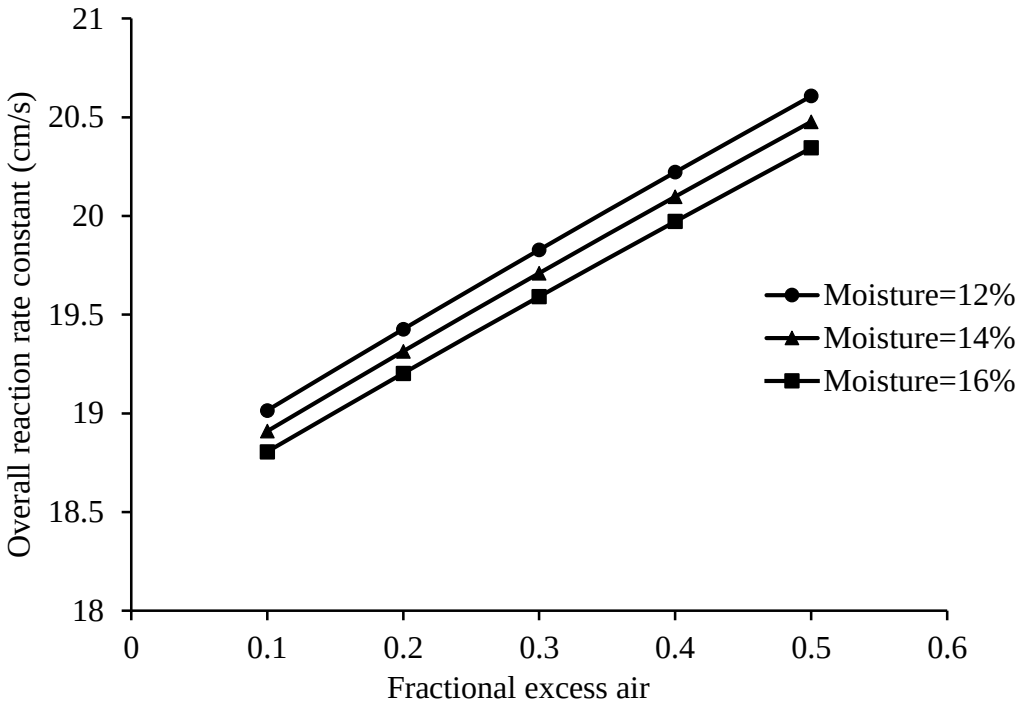

Figure 5.12. variation of overall reaction rate constant with moisture content and fractional excess air

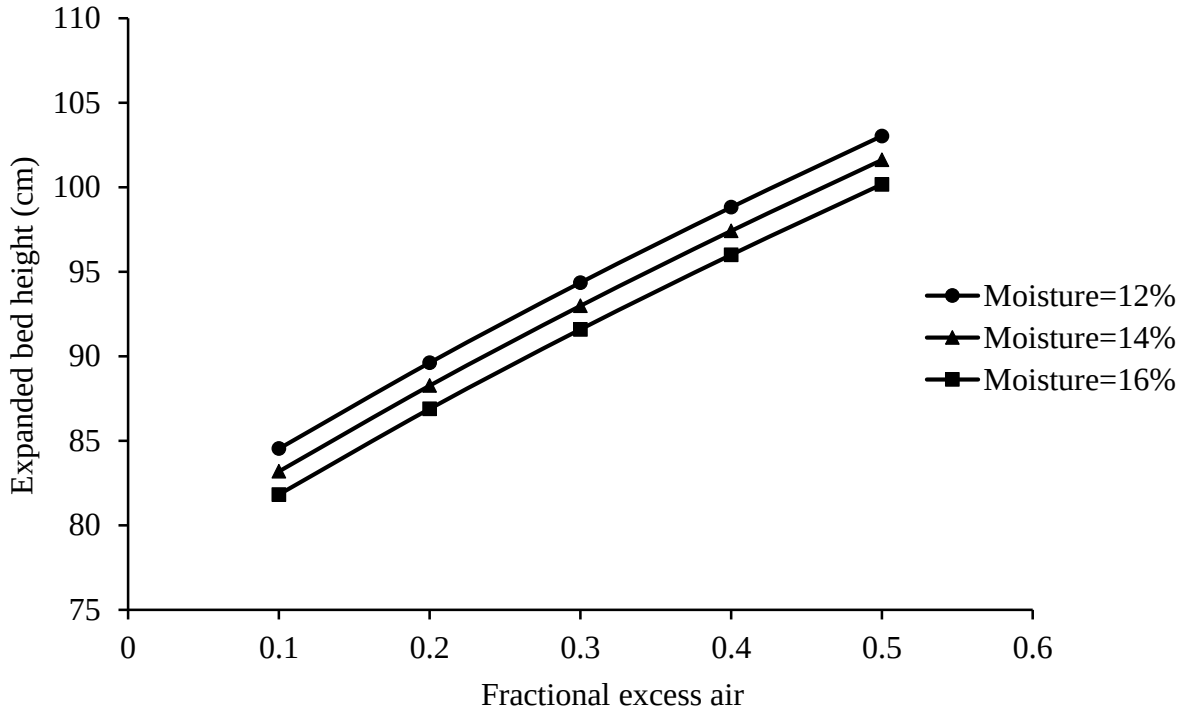

Figure 5.13. Variation of expanded bed height with moisture content and fractional excess air

Figure 5.11 shows that diameter of the bubble increases as excess air increases and moisture in the fuel decreases. With an increase in excess air, the superficial velocity increases leading to a gradual increase in bubble diameter. This results decreased coefficient of gas interchange leading to dropped oxygen conversion.

Excess air has a direct impact on the overall reaction rate, as shown in Figure 5.12. Increase in excess air leads to increase in bed temperature promoting overall reaction rate. From Figure 5.12, it can be observed that fuel moisture content has an inverse impact on overall in reaction rate. With rise of moisture in fuel, the bed temperature decreases leading to a decrease in overall reaction rate. Figure 5.13 shows the impact of fuel moisture content and excess air on expanded bed height. The bed height is directly proportional to excess air and is inversely related to fuel moisture content. Bed height is a function of bubble diameter. With decreasing moisture content and increasing excess air, the bubble diameter increases. This is also reflected in the expanded bed variation.

5.3. Thermodynamic model

A mixture of three different biomass fuels was used in the 7.5 MW biomass-based thermal power plant at the time of the observations. Proximate analysis and ultimate analysis of these biomass fuels are given in Table 3.3 and Table 3.4. In the model, following average values of the fuel compositions are used: carbon = 41%, hydrogen = 6.76%, nitrogen = 0.83%, Sulphur = 0.55%, oxygen = 38.85%, moisture = 9.40%, ash = 10.59%, volatiles = 64.45%, and LCV = 3,050 kcal/kg. Process parameters like enthalpy, entropy, and exergy calculations at various state points are shown in Table 5.10.

5.3.1. Energy model

In this section, results from the first law of thermodynamics based energy model have been shown and discussed. First law based detailed analysis of the boiler is presented below.

Table 5.10. Enthalpy, entropy, and exergy at various state points

State point	Pressure (kPa)	Temperature (°C)	Mass flow rate (kg/s)	Specific enthalpy (kJ/kg)	Specific entropy (kJ/kg-K)	Exergy (kW)
0	100	25	-------	104.83	0.3672	0
1	6700	455	8.75	3301.1	6.6774	11239.01
2	6500	450	8.75	3295.6	6.6786	11187.7
3	20	60.2	8.45	2393.34	7.9262	1742.15
4	20	60.06	8.45	251.42	0.832	50.146
5	1010	65	8.45	272.1	0.894	87.8
6	355	103.8	8.75	436.06	1.3522	288.34
7	7050	105	8.75	441.28	1.3615	309.36
8	7050	174	8.75	740.09	2.0802	1018.5
9	104	375	15.05	3636.28	7.3494	1953.64
10	102	228	15.05	3460.24	7.1168	347.429
11	100	143	15.05	3354.82	6.829	51.61
12	100	30	13.67	606.26	6.898	18.1
13	1043	40	13.67	625.39	6.936	124.8
14	1035	143	13.67	721.24	7.225	257.78
15	100	25	820	125.74	0.4368	0
16	100	39	820	169.9	0.582	858.2

Boiler energy analysis

Steam is produced from the water using heat produced by combustion of fuel in the combustor of the boiler. Values of various performance parameters (based on higher heating value, HHV) calculated for the fluidized bed combustor installed at 7.5 MW biomass based Malwa Power Private Limited (MPPL) thermal power plant are shown in Table 5.11. The overall efficiency of the boiler is found to be 71.36%. The effect of the change in boiler overall efficiency on fuel consumption is shown in Figure 5.14. It can be observed from the Figure 5.14 that for each 1%

improvement in the boiler efficiency fuel consumption decreases by 1.43%. This makes it necessary to consider all the measures to improve the boiler's overall efficiency.

Table 5.11. Performance parameters for the combustor

Parameters	Value
Evaporative capacity (kg of steam/ kg of fuel)	3.18
Equivalent evaporation (kg of steam/ kg of fuel)	3.61
Evaporation factor	1.135
Heat utilized in the economizer (%)	7.46
Boiler efficiency (%)	74.2
Boiler overall efficiency (%)	71.36

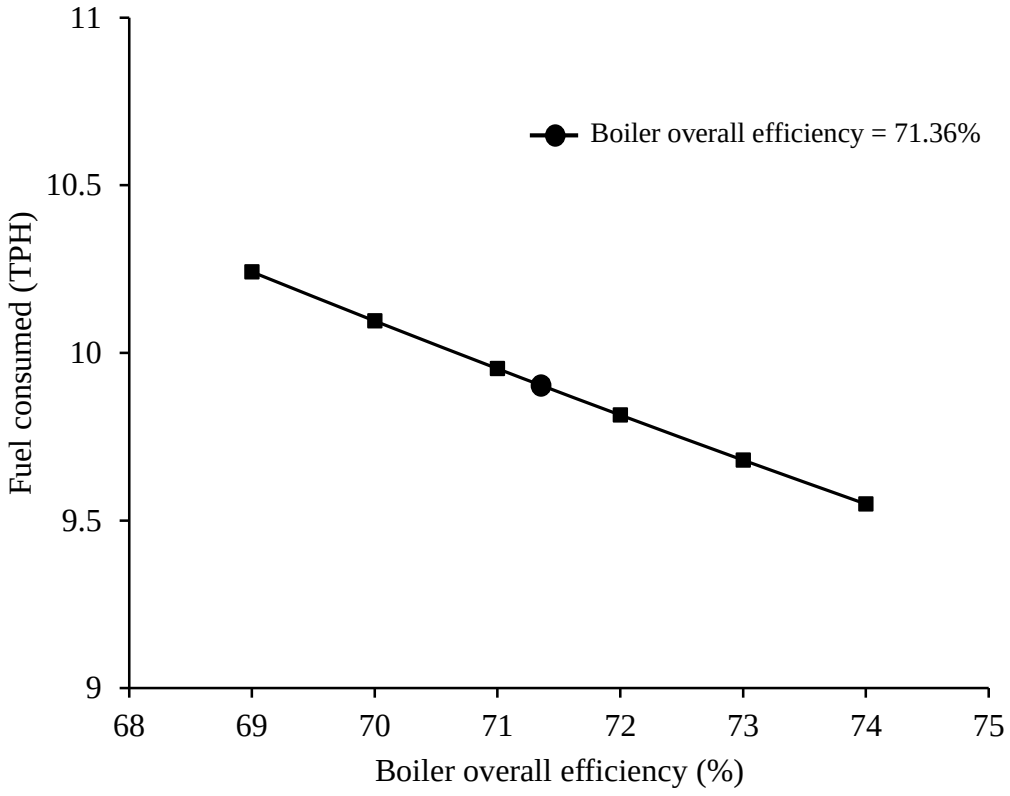

Figure 5.14. Effect of fuel consumption on overall boiler efficiency

Heat balance sheet for the boiler is shown in Figure 5.15 and percentage-wise heat utilized in different components of the combustor is shown in Figure 5.16**.** It can be observed that 63.91% of the heat produced by fuel combustion is utilized in the steam generator. The

maximum amount of heat is lost to the moisture present in the fuel (16.32%). Heat loss due to moisture present in the fuel can be reduced by sun drying the biomass before feeding it to the combustor.

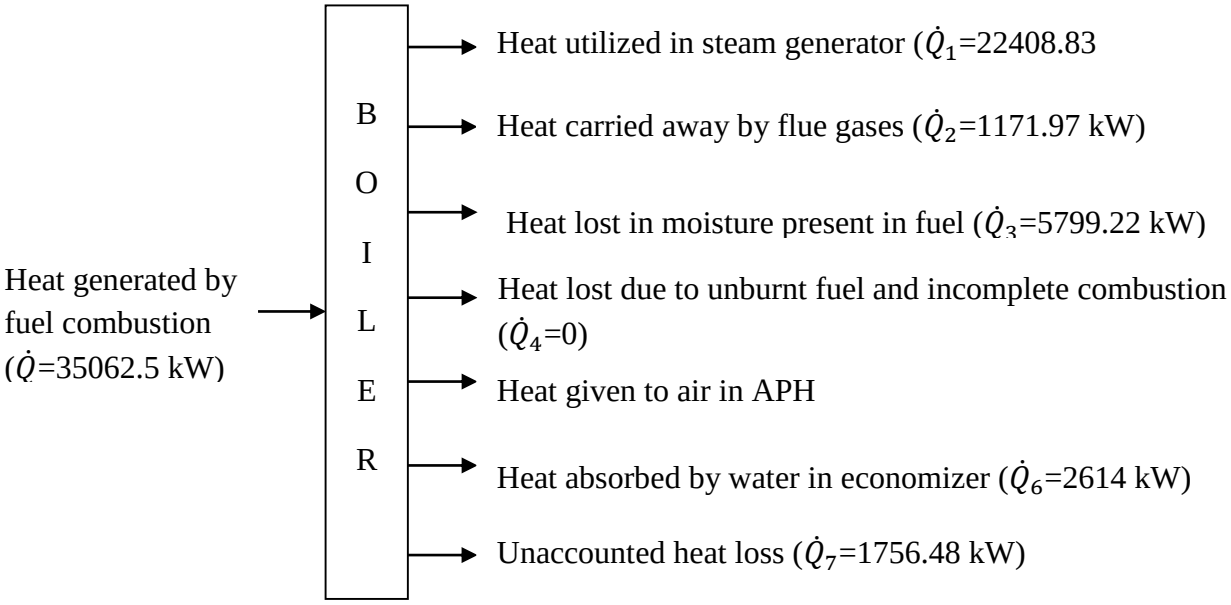

Figure 5.15. Heat balance for boiler

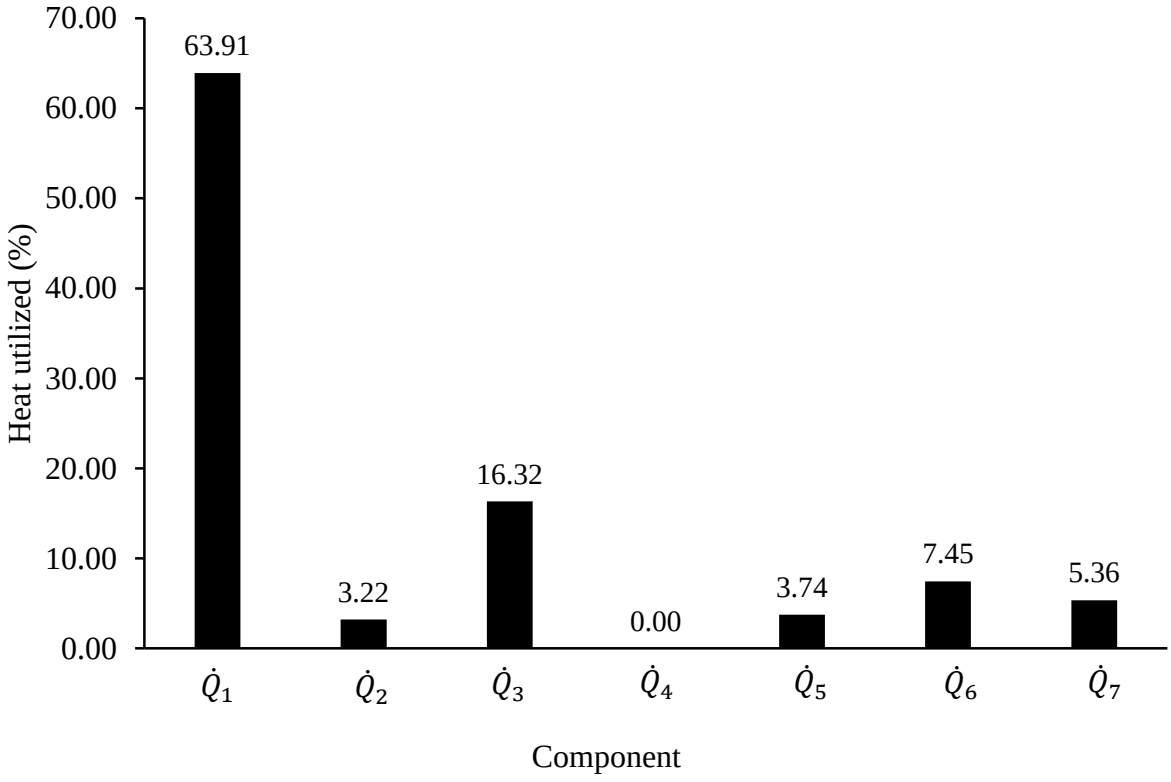

Figure 5.16. Percentage-wise heat utilized in different components of the combustor

Table 5.12. Energy performance results

Parameters	Value
Heat supplied to boiler (kW)	29,840
Power output from turbine(kW)	7,394
Power consumption in CEP (kW)	220
Power consumption in FWP (kW)	60
Heat transfer rate in economizer (kW)	2614
Heat transfer rate in air preheater-APH (kW)	1,312
Heat rejection rate in the condenser (kW)	18,099
Energy efficiency (%)	26.7
Steam efficiency (%)	74.2
Electrical efficiency (%)	23.8
Net heat ratio (NHR)	1.34
Power to heat ratio (PHR)	0.2528

Plant energy analysis

Energy analysis results of the plant (based on lower heating value, LHV) are shown in Table 5.12. The energy efficiency of the plant is found to be 26.7%. It can be observed from Table 5.12 that about 60% of the heat added in the boiler is released to the surroundings by the condenser. Due to condensation of steam in the condenser, the back pressure decreases resulting in a reduction in steam consumption. It reduces the fuel consumption and increases the power output from the turbine leading to an increase in cooling water amount requirement. The amount of heat released in the condenser increases with a decrease in condenser pressure. It is due to increase in enthalpy of condensation with the decrease in condenser pressure. Although this amount of energy loss cannot be neglected, thermodynamically it is insignificant as it is of low quality [125].

Table 5.13. Exergy performance results

Components	Exergy destruction $\dot{Ex}_D(kW)$	Exergy efficiency η_{Ex} (%)
Boiler	21,422	33.8
Turbine	1,550	83.8
CEP	182	17.5
FWP	39.1	35
Economizer	898	44.2
APH	162	44.1
Condenser	834	26.24
Complete cycle	*25,087.1*	*22.8*

5.3.2. Exergy model

Exergy analysis results of each component under consideration are shown in Table 5.13 and Figure 5.17. The exergy efficiency of the plant is 22.8% and exergy destruction in the condenser is 3.3% of the total exergy destruction. From Figure 5.18, it is observed that as per energy analysis largest heat losses occur in the condenser and its design need a revision. But exergy analysis of the plant suggests (refer Figure 5.19) that exergy losses in the condenser are significantly low and largest exergy losses occur in the boiler (≈85%). Energy analysis suggests that one needs to focus on improving the performance of the water-cooled condenser, whereas exergy analysis indicates that slight improvement in the boiler's performance will lead to positive changes in the output of the plant. This highlights the importance of exergy analysis over energy analysis and strengthens the fact that decision based on the energy performance analysis is insufficient and are not reliable. The plant efficiency can be improved by reducing the condenser pressure as this can give the higher expansion of steam in the turbine. Since this

plant has a water-cooled condenser; the temperature of the cooling water can be controlled. Reducing the temperature of cooling water below ambient at condenser entry can increase the performance of the plant.

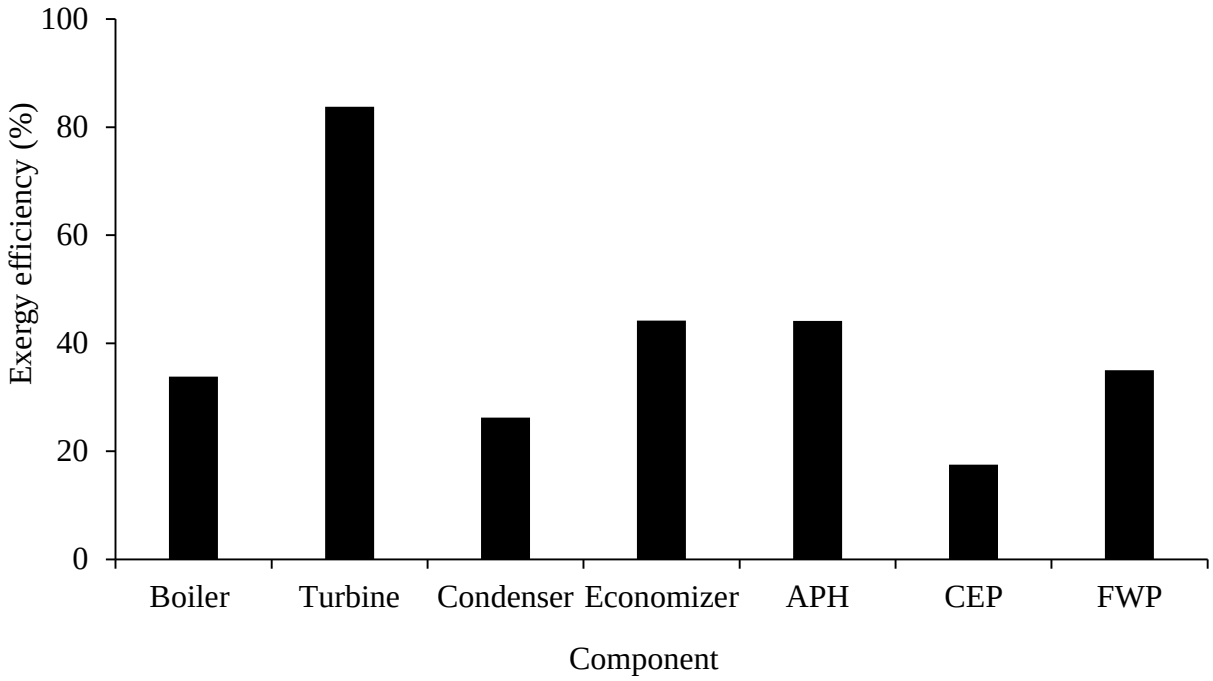

Figure 5.17. Component-wise exergy efficiency

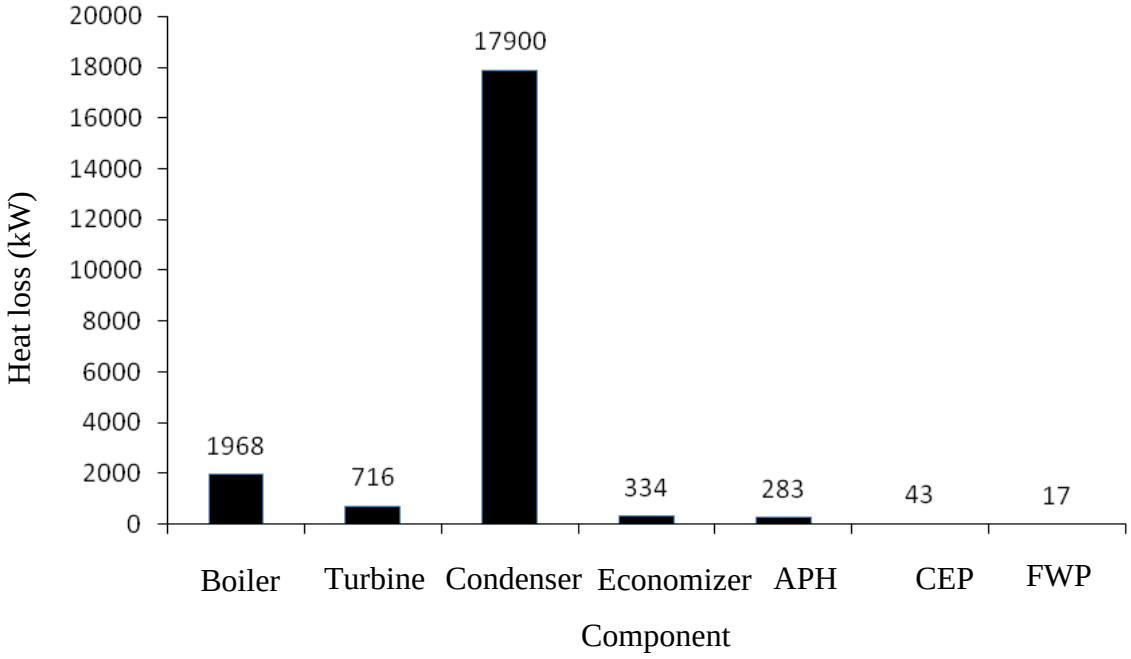

Figure 5.18. Energy analyses of various components of MPPL power plant

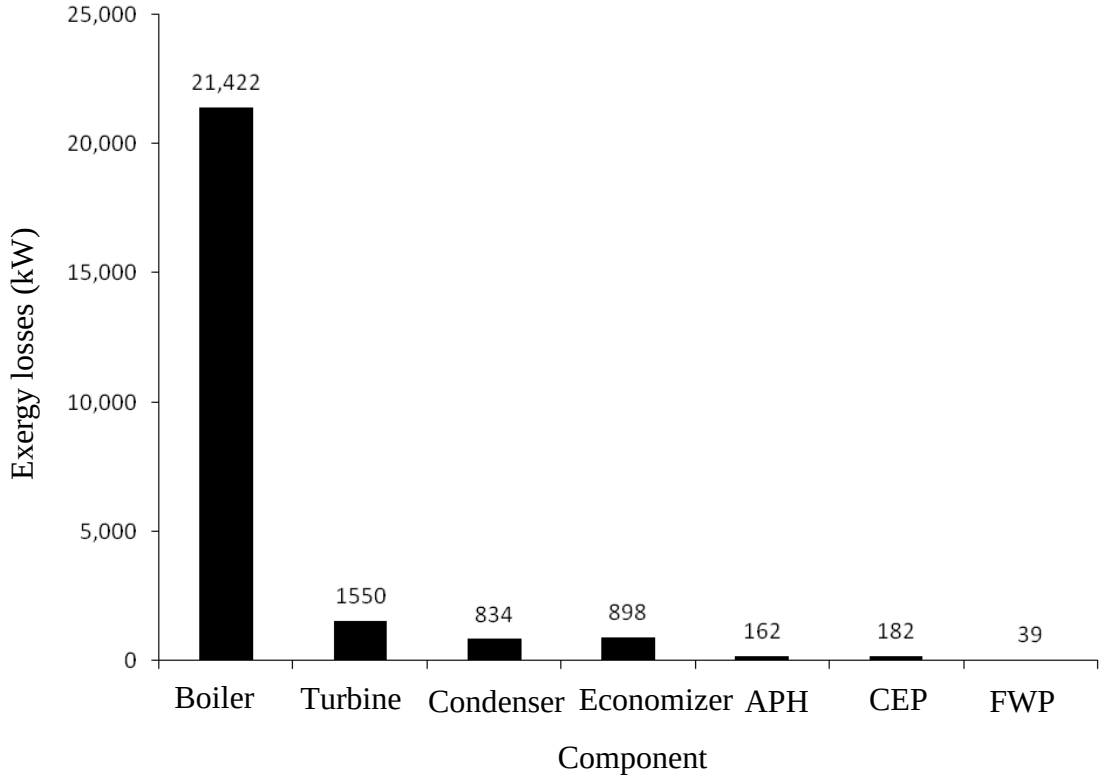

Figure 5.19. Exergy destructions in various components of MPPL power plant

5.3.3. Optimization of exergy model

Exergy model has been optimized using Multi-response optimization method. Turbine inlet pressure (factor X), turbine inlet steam temperature (factor Y), and fuel feed rate (factor Z) has been taken as the input parameters. Overall plant exergy efficiency (η_{E_x}) and complete cycle exergy destruction (Ex_D) are selected as responses. Maximum overall plant exergy efficiency and minimum complete cycle exergy destruction are the objectives as both lead better combustor performance. The optimization calculations are shown in Table 5.14. Variation of overall plant exergy efficiency and complete cycle exergy destruction with each trail is shown in Figure 5.20 and Figure 5.21 respectively. It can be observed that overall plant exergy efficiency is minimum and complete cycle exergy destruction is maximum at trial number 7 (turbine inlet pressure = 70 bar, turbine inlet steam temperature = 430˚C, and fuel feed rate = 4 kg/s).

Table 5.14. Overall plant exergy efficiency and complete cycle exergy destruction at different orthogonal array arrangements

Trial Nos.	Factors			$\eta_{Ex}(\%)$	$Ex_D(kW)$
	X	Y	Z		
1	60	430	1.5	39.33	9953.551
2	60	450	2.75	22.72	25250.28
3	60	470	4	16.45	40571.00
4	65	430	2.75	21.22	25564.74
5	65	450	4	15.49	40838.53
6	65	470	1.5	43.53	9733.999
7	70	430	4	14.44	41152.99
8	70	450	1.5	40.85	10022.13
9	70	470	2.75	23.56	25318.34

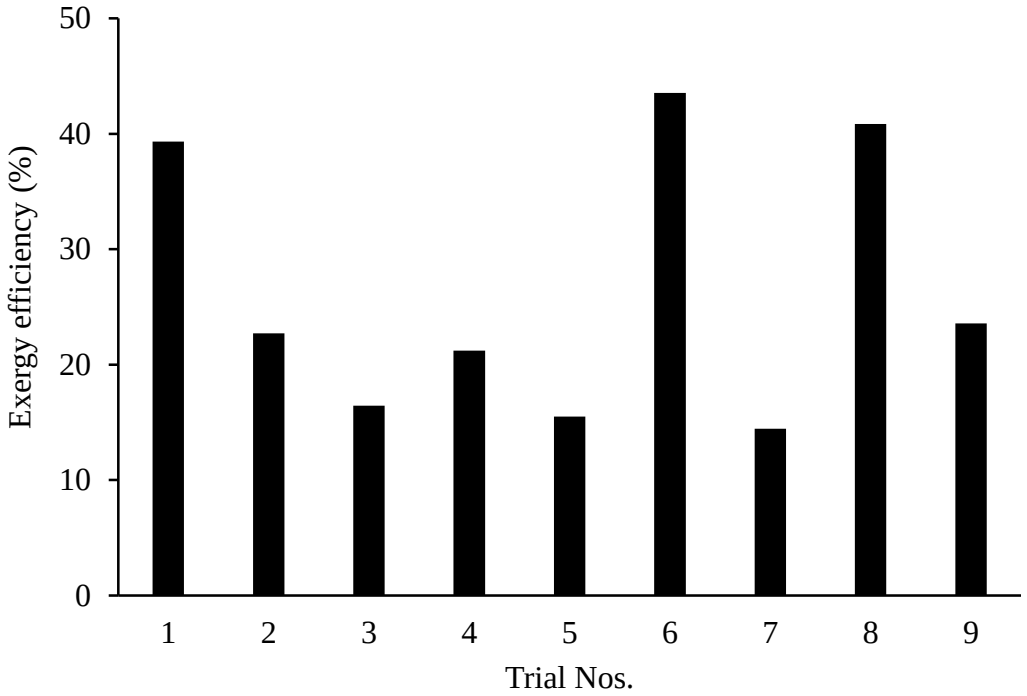

Figure 5.20. Overall plant exergy efficiency variation with different orthogonal array arrangements

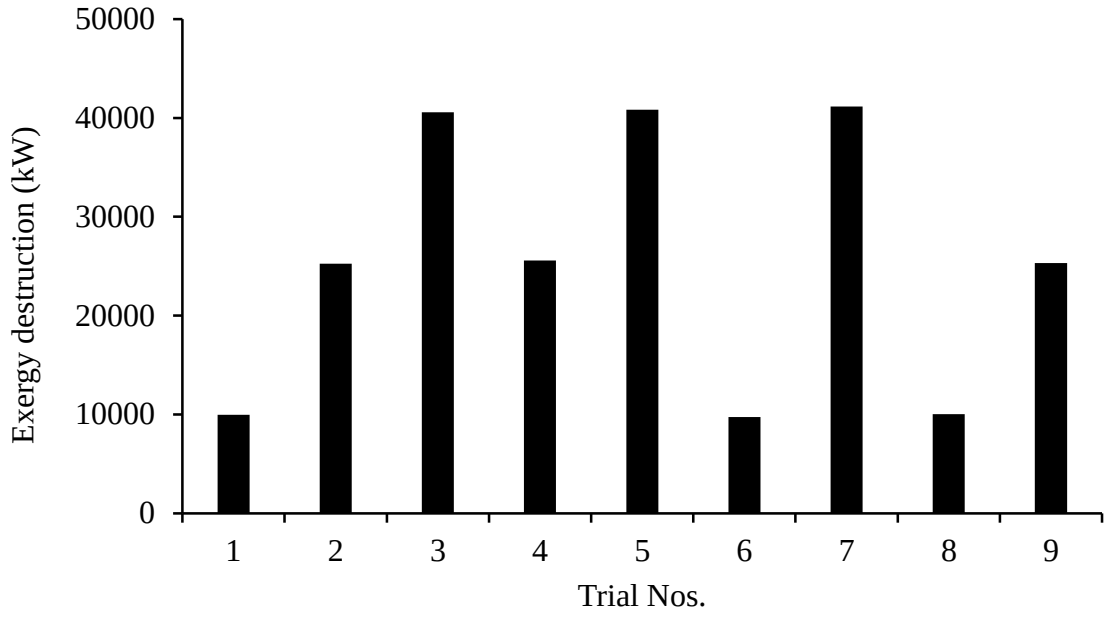

Figure 5.21. Complete cycle exergy destruction variation with different orthogonal array arrangements

The weights are calculated for overall plant exergy efficiency (η_{E_x}) and complete cycle exergy destruction (Ex_D). For overall plant exergy efficiency (larger – the better), overall plant exergy efficiency value corresponding to each trial number is divided by total overall plant exergy efficiency value ($\sum \eta_{E_x}$). For Ex_D (smaller – the better), reverse normalization has been used. For each Ex_D response, $1/Ex_D$ is calculated and then the weight of Ex_D (W_{Ex_D}) is obtained. From Table 5.15 $\sum \eta_{E_x} = 237.59$ and $\sum(1/Ex_D) = 0.004197$.

Here, $W_{\eta_{E_x}} = \dfrac{\eta_{Ex_i}}{\Sigma \eta_{E_x}}$ and $W_{Ex_D} = \dfrac{(1/Ex_{D_i})}{\Sigma(1/\mathrm{Ex}_D)}$ (5.3)

Multi-response performance index (*MRPI*) for i^{th} trial is calculated using following formula:

$$(MRPI)_i = W_{\eta_{E_{x_i}}} \times \eta_{E_{x_i}} + W_{Ex_{D_i}} \times Ex_{D_i} \quad (5.4)$$

The weight and MRPI for each trial are given in Table 5.15.

MRPI is considered as a single response to the problem and as it is weighted score, optimal levels are identified based on maximum MRPI value. The optimization is shown with MRPI in Table 5.16. The level totals of MRPI are given in Table 5.17.

Table 5.15. Weight and MRPI for each trial

Trial Nos.	η_{Ex}	$W_{\eta_{Ex}}$	Ex_D	W_{Ex_D}	MRPI
1	39.33	0.165548	9953.551	0.110507	244.7563
2	22.72	0.09561	25250.28	0.1113	240.4167
3	16.45	0.069234	40571.00	0.111561	239.3836
4	21.22	0.089306	25564.74	0.111378	240.1397
5	15.49	0.0652	40838.53	0.111611	239.2548
6	43.53	0.183209	9733.999	0.110292	246.2197
7	14.44	0.060769	41152.99	0.111667	239.1222
8	40.85	0.171942	10022.13	0.110429	245.2689
9	23.56	0.099182	25318.34	0.111256	240.582

Table 5.16. MRPI as response to the optimization problem

Trial Nos.	Factors			MRPI
	X	Y	Z	
1	60	430	1.5	244.7563
2	60	450	2.75	240.4167
3	60	470	4	239.3836
4	65	430	2.75	240.1397
5	65	450	4	239.2548
6	65	470	1.5	246.2197
7	70	430	4	239.1222
8	70	450	1.5	245.2689
9	70	470	2.75	240.582

Table 5.17. Level totals of MRPI

Factors	Level 1	Level 2	Level 3
X	724.5566	725.6142	724.9731
Y	724.0181	724.9404	726.1853
Z	736.2449	721.1383	719.2203

The optimal levels are selected based on maximum MPRI. The optimal levels are X-2 (turbine inlet pressure = 65 bar), Y-3 (turbine inlet steam temperature = 470˚C), and Z-1 (fuel feed rate = 1.5 kg/s). At optimal levels of input parameters, maximum overall plant exergy efficiency (η_{E_x}) of 43.53% and minimum complete cycle exergy destruction (Ex_D) of 9733.999 kW can be achieved. It is worth noting here that solid population balance model and exergy analysis model both optimized for fuel feed rate of 1.5 kg/s.

5.4. Economic analysis

Economic analysis of the plant is based on the statistics for the year 2014. In this particular year, the plant was functional for 5690 hours and 45,011 MWh of electricity was found to be salable. Biomass fuel burnt in the combustor was purchased from outside and was also generated from the land taken on the lease in the surrounding areas. The land taken on lease is the biggest contributor to maintain the ATC below annual total revenue at the end of the year 2014. Fuel consumptions and fuel cost for the year 2014 are given in Table 5.18. AFC, ATVC, and net revenue generated by the plant are shown in Table 5.19, Table 5.20, and Table 5.21 respectively. Generally, it is found that biomass-based thermal power plants are economically costlier in comparison to coal-fired thermal power plants. But for the plant under consideration, the generation cost per kWh is Rs 2.91(refer Table 5.21), whereas the generation cost per kWh for coal-fired thermal power plants in India is Rs 3.05 [126]. This is due to the land taken on lease by plant authorities, which decreases AFC involved during plant operation and hence the generation cost per kWh also decreases. Profit analysis of the plant for the year 2014 is shown in Table 5.22. Figure 5.22 and Figure 5.23 shows the break-even analysis of the plant in terms of operating hours and net salable electricity respectively. The break-even points in terms of operating hours and net salable electricity for the plant are 3949.9 hours and 3124.57 MWh, respectively. Break-even analysis is helpful in estimating the relative effect of ATVC and AFC on the plant performance.

Table 5.18. Fuel consumptions and fuel cost (year 2014)

Fuel consumed (MT)	49011
Fuel purchased (MT)	19500
Fuel generated (MT)	29511
Average cost of fuel purchased (Rs/MT)	2,000
Average cost of fuel generated (Rs/MT)	821

Table 5.19. AFC calculations for the plant

Wages of the workers (Rs), N_1	36,60,000
Amount paid for land taken on lease (Rs), N_2	1,02,35,990
Salaries of the employees (Rs), N_3	1,22,24,400
Income of loading contractor (Rs), N_4	58,38,120
Diesel cost (Rs), N_5	1,02,20,035
$\boldsymbol{AFC\ (Rs) = N_1 + N_2 + N_3 + N_4 + N_5}$	***4,21,78,545***

Table 5.20. ATVC calculations for the plant

Maintenance and inspection cost (Rs), N_6	1,16,12,212
Fuel cost (Rs), N_7	3,90,00,000
Transportation of fuel (Rs), N_8	1,20,750
Machinery Purchase (Rs), N_9	0
$\boldsymbol{ATVC\ (Rs) = N_6 + N_7 + N_8 + N_9}$	***5,07,32,962***

Table 5.21. Net revenue generated

Net salable energy (kWh), N_{10}	3,19,46,500
Generation cost (Rs/kWh), N_{11}	2.91
Sale rate (Rs/kWh), N_{12}	3.49
Net revenue generated (Rs) $\boldsymbol{= N_{10} \times N_{12}}$	***11,14,93,285***

Table 5.22. Profit analysis of the plant

Net revenue generated	11,14,93,285
AFC	4,21,78,545
ATVC	5,07,32,962
Net profit *(Rs) = Net revenue generated- (AFC+ATVC)*	***1,85,81,778***
Net profit (%)	***16.66***

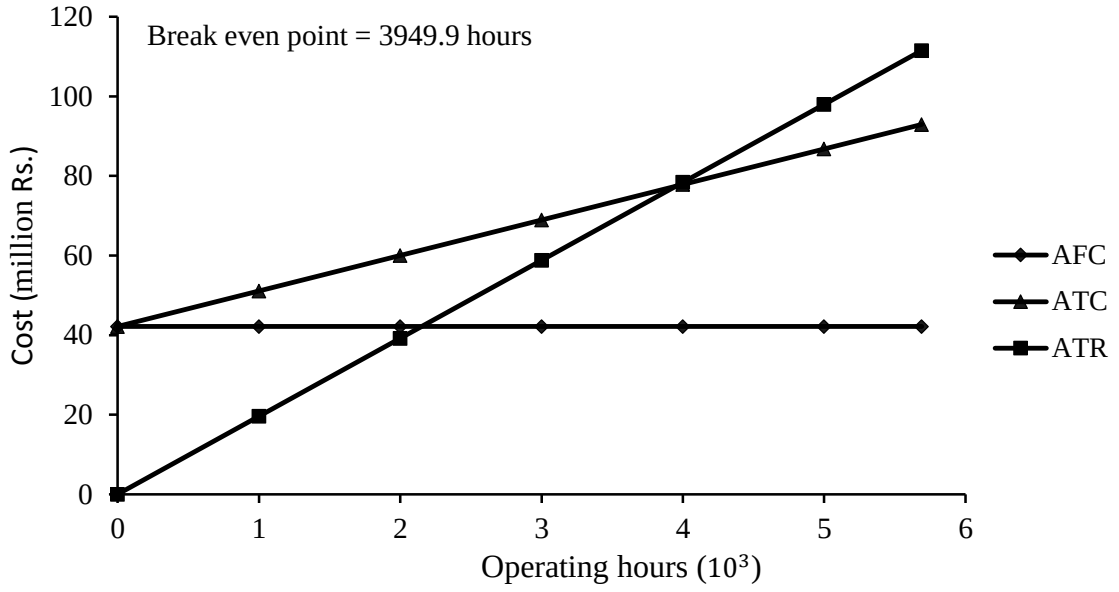

Figure 5.22. Break-even analyses in terms of operating hours

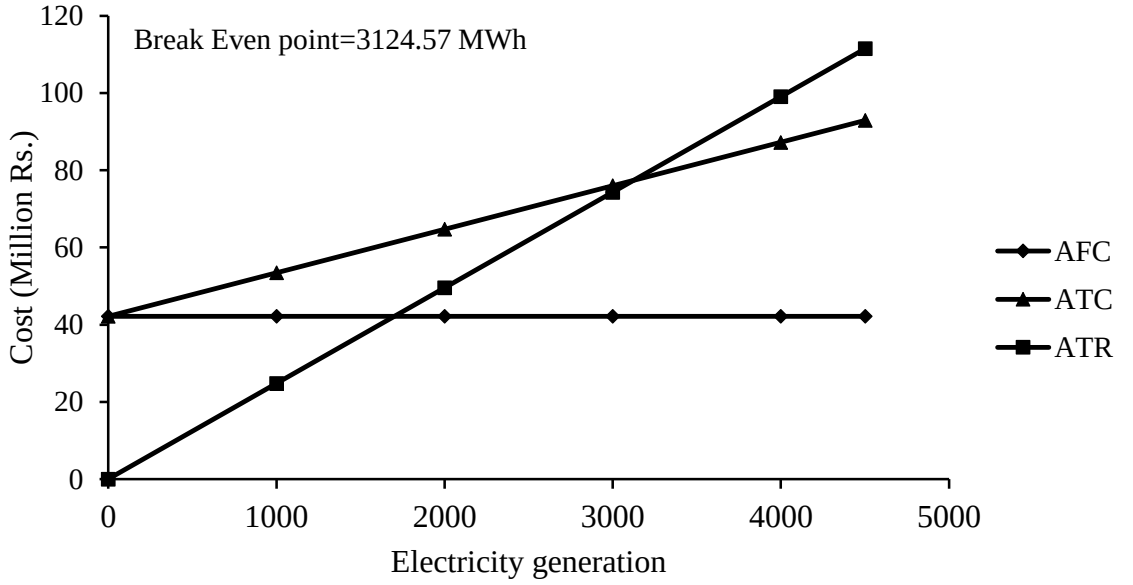

Figure 5.23. Break-even analyses in terms of electricity generation (MWh)

Reducing ATVC by 25% reduces the break-even in terms of operating hours to 3267.76 hours (Figure 5.24) and in terms of electricity generation is reduced to 2584.98 MWh (Figure 5.25). Net profit increases by Rs 1,26,83,241. Reducing AFC by 25% reduces break-even in terms of operating hours to 2962.4 hours (Figure 5.26) and in terms of net electricity generation, it is reduced to 2343.62 MWh (Figure 5.27).

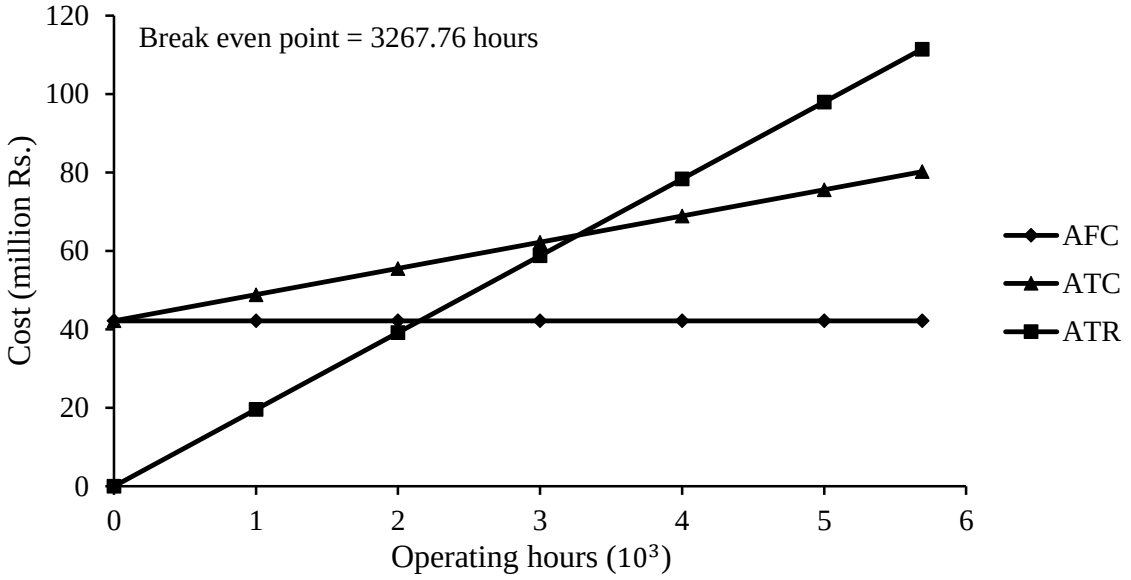

Figure 5.24. Break-even point for 25% less ATVC in terms of operating hours

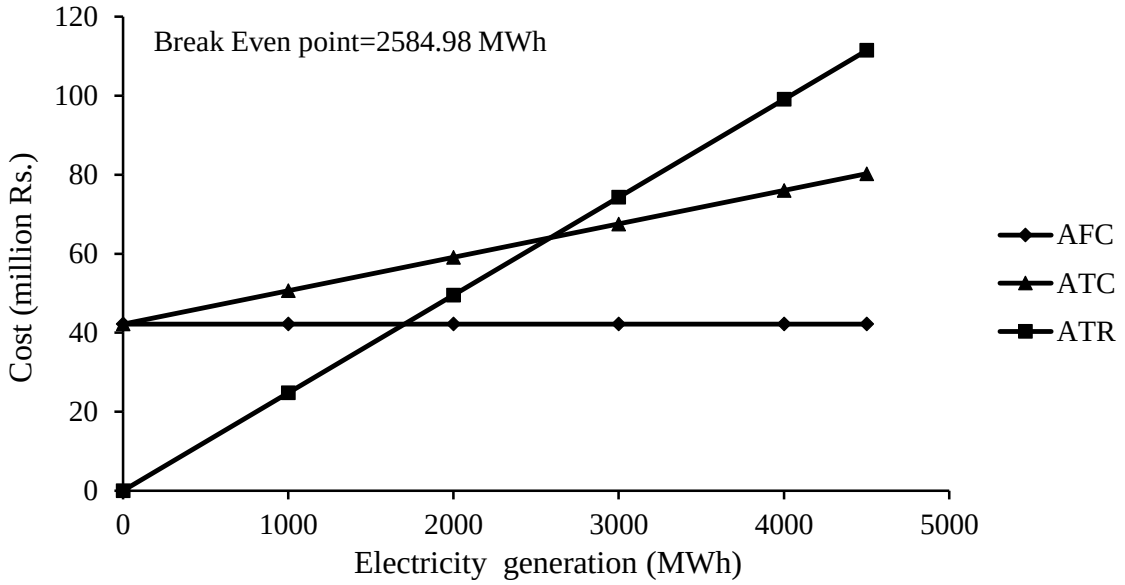

Figure 5.25. Break-even point for 25% less ATVC in terms of electricity generation

Net profit increases by Rs 1,05,44,637. The break-even point arrives earlier in terms of operating hours and electricity generated in reducing AFC by 25% than reducing ATVC by 25%. But the net profits earned are more in reducing ATVC by 25% than in reducing AFC by 25%. It is due to the fact that ATVC contributes more in comparison to AFC in ATC. Changing ATVC by 25% is recommended for this particular plant to earn maximum profit.

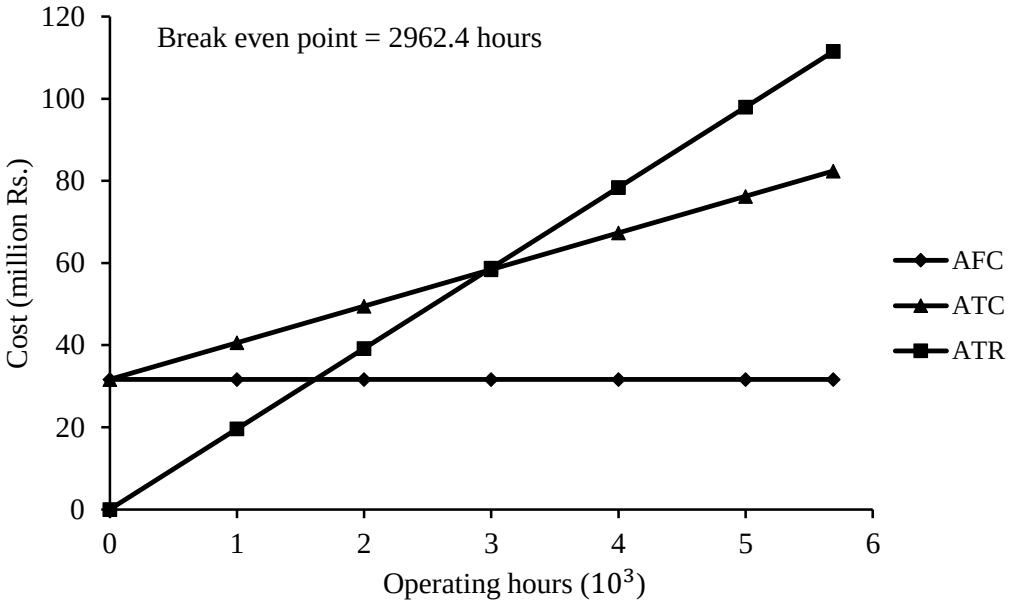

Figure 5.26. Break-even point for 25% less AFC in terms of operating hours

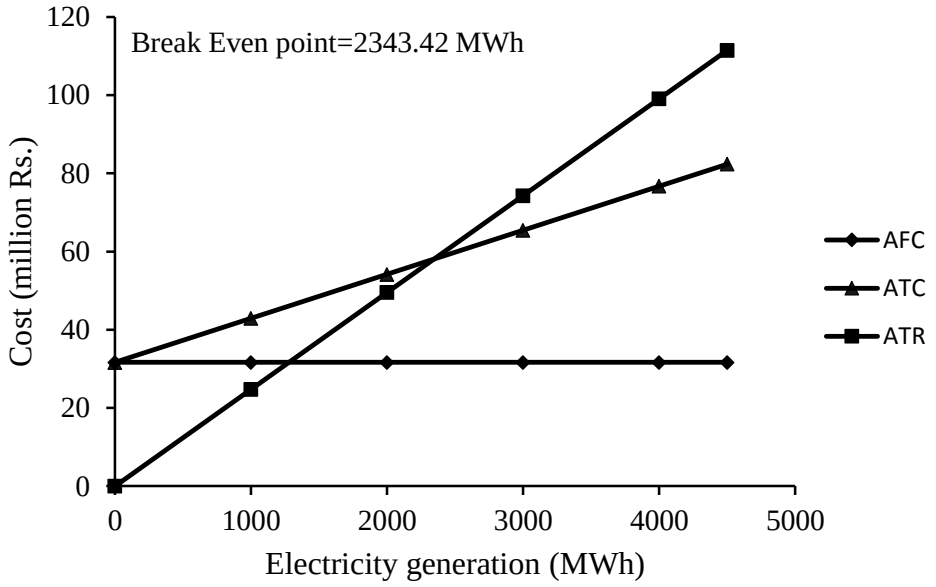

Figure 5.27. Break-even point for 25% less ATVC in terms of electricity generation

The exergo-economic analysis is a tool using which smooth operations and optimum design of a complex thermal system similar to one under consideration can be achieved. The demand for such analysis has increased in the recent past due to its ability to estimate the production cost required for optimizing the profits. Figure 5.28 shows the variation of net profit earned with the change in exergy efficiency. With slight decrease in exergy efficiency (22.8%

to 21.5%), net profit earned decreases sharply (16.7 % to 4.2%). This is due to the reason that for the same fuel feed rate, network output decreases with the decrease in exergy efficiency. This, in turn, decreases the net profit.

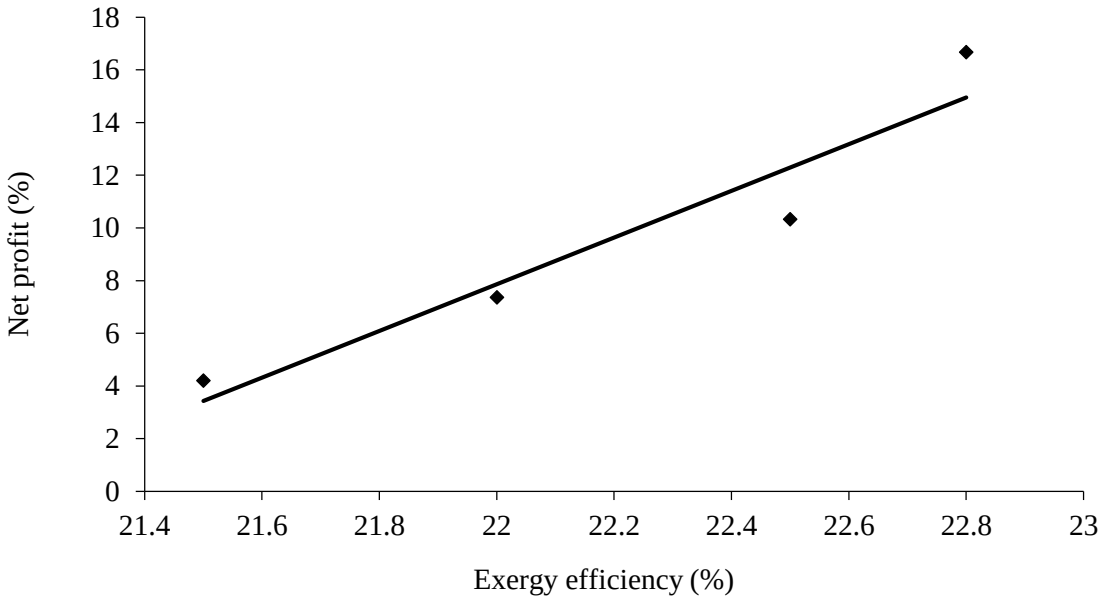

Figure 5.28. Net profit variations with exergy efficiency

5.5. Agglomeration study results

The Scanning Electronic Microscopy (SEM) test has been done on agglomeration samples collected from plant site and prepared from the combustion test. SEM test has been conducted at Sophisticated Analysis and Instrumentation laboratory, Thapar Institute of Engineering and Technology, Patiala. Much difference is not observed in SEM test results at 700°C and 800°C, but significant changes have been observed at 700°C and 900°C. SEM test results are shown in Figure 5.29, Figure 5.30 and Figure 5.31. It can be observed from Figure 5.30 that at 700˚C, burning cotton stalk particles stick to the sand surface. The melting rate of ash particles increases with increase in bed temperature to 900˚C. This leads to decrease in the ash viscosity. It increases the stickiness of the sand particle coated by the ash and accelerate the defluidization process.

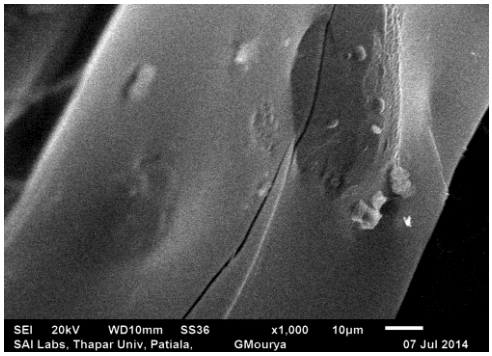

(a)

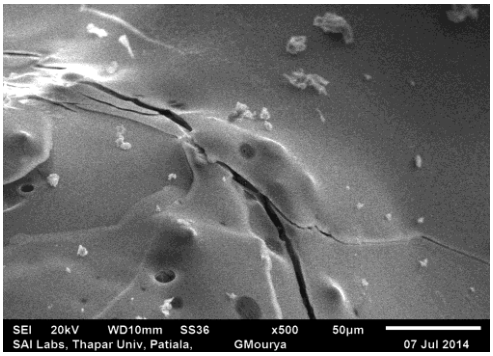

(b)

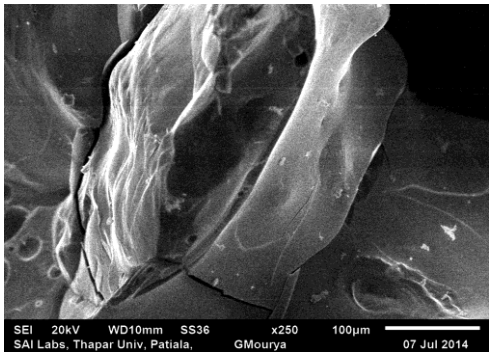

(c)

Figure 5.29. SEM images of the agglomerate sample collected from plant site

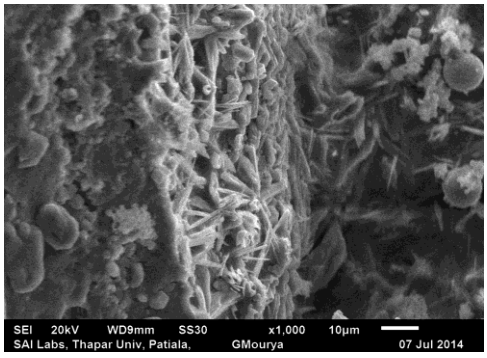

(a)

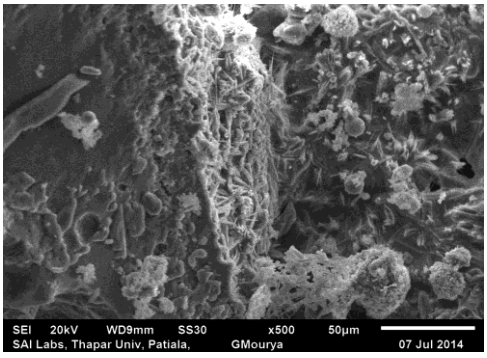

(b)

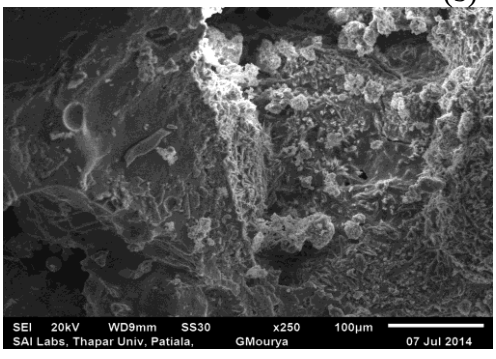

(c)

Figure 5.30. SEM images of the agglomerate produced during combustion test at 700°C

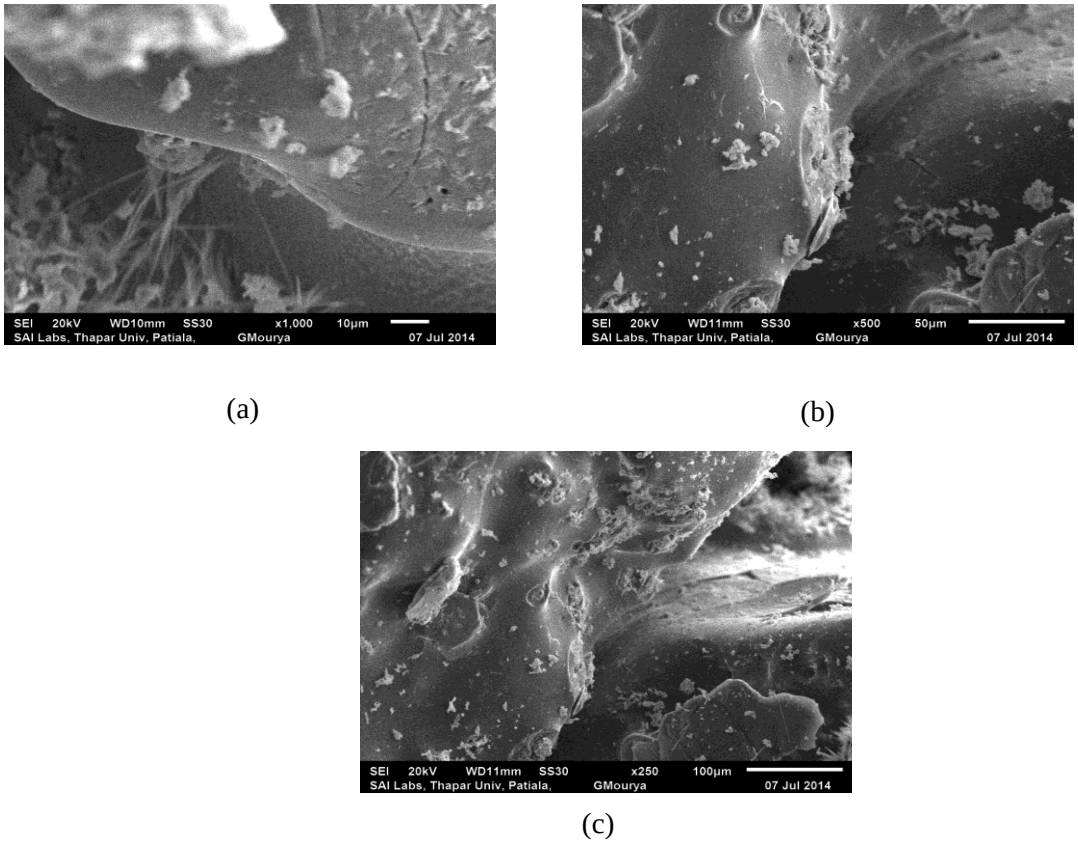

Figure 5.31. SEM images of the agglomerate produced during combustion test at 900°C

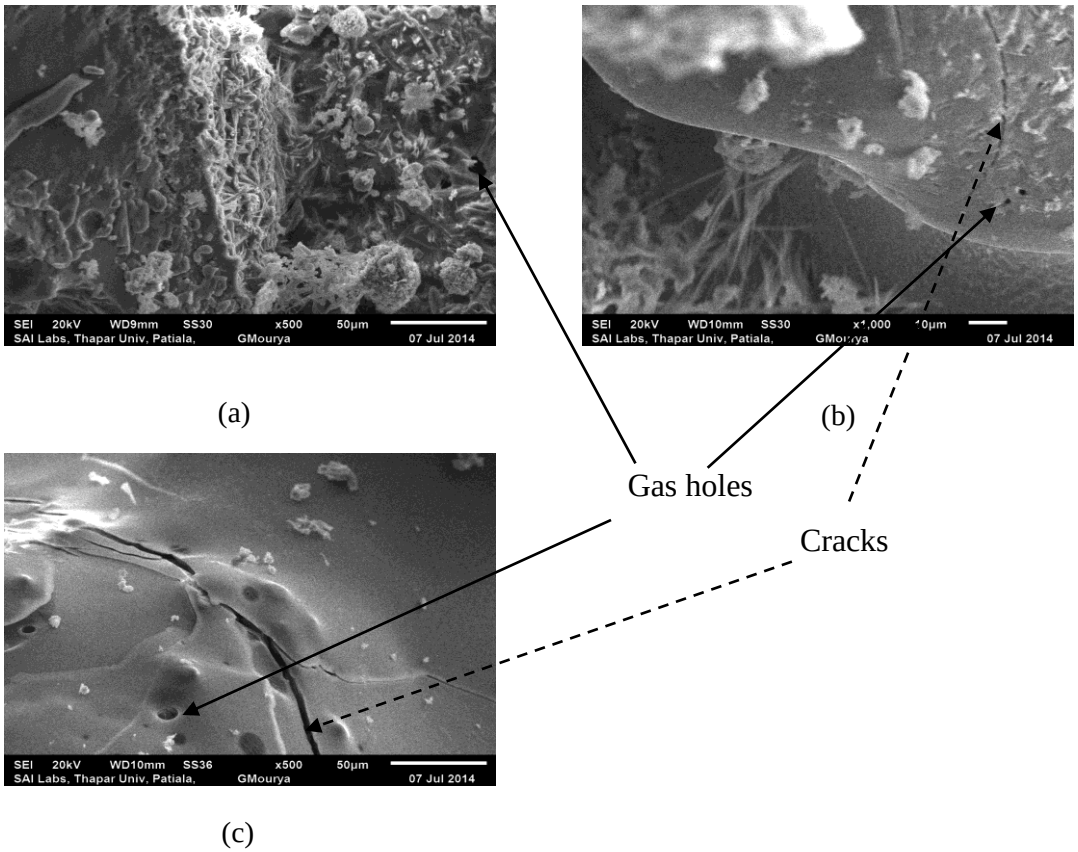

Figure 5.32. SEM images of the agglomerate (a) at 700°C (b) at 900°C (c) from plant site

The gaseous combustion products are released from the molten material in the fuel ash, which lead to the formation of gas holes and cracks on the surfaces (Figure 5.32). These molten materials should be low-melting point alkali silicates. In this case, agglomeration Index = 4.31; hence agglomeration tendency is high when cotton stalk is used as fuel. Based on this study, the following agglomeration mechanism is proposed:

The bed temperature is the major reason for agglomeration and defluidization of fluidized bed combustor using cotton stalk. With increase in the bed temperature, fuel particles burn and generate low-melting point alkali silicates. These low-melting alkali silicates stick to the sand particle surface. The burning cotton stalk particles adhere to sand surface. On completion of combustion, solidification of low melting point alkali silicates takes place leading to the formation of agglomerates.

5.6. Uncertainty analysis

Errors cannot be avoided in an experimental work and our attempt must be to keep these errors as minimum as possible. Errors can be systematic (same error by using an instrument in the same way) and random (due to inability to conduct measurements exactly in same way every time). Errors in experimental work lead to inaccuracy and uncertainty in results. Uncertainty can be due to apparatus calibration, condition, selection, reading, and observation. Errors and uncertainties can be due to inaccurate test procedures and inaccuracy in instruments. Every experimental study must be supported by uncertainty analysis. Uncertainty analysis is the only known basis for deciding whether data agrees with theory.

Uncertainty in the present study has been calculated using relations available in literature [127,128] as follows:

Let Y is the parameter calculated by using experimental measurements, such that

$$Y = Y(x_1, x_2, x_3, \ldots\ldots\ldots\ldots\ldots\ldots, x_n) \quad (5.5)$$

The absolute uncertainty in the measurement of Y is given as:

$$\delta Y = \sqrt{\left[\left(\frac{\partial Y}{\partial x_1}.\delta x_1\right)^2 + \left(\frac{\partial Y}{\partial x_2}.\delta x_2\right)^2 + \left(\frac{\partial Y}{\partial x_3}.\delta x_3\right)^2 + \ldots\ldots\ldots + \left(\frac{\partial Y}{\partial x_n}.\delta x_n\right)^2\right]} \quad (5.6)$$

Where, $\delta x_1, \delta x_2, \delta x_3, \ldots\ldots\ldots\ldots\ldots\ldots\ldots, \delta x_n$ are the errors in measurement of parameters $x_1,\ x_2,\ \ x_3, \ldots\ldots\ldots\ldots\ldots\ldots, x_n$.

Uncertainty in size modulus of cotton stalk is due to error in weighting balance machine and sieve shaker machine. Uncertainty in exit gas composition is due to error in gas analyzer.

$$Uncertainty\ in\ size\ modulus =$$

$$\sqrt{(error\ in\ weight\ measurement)^2 + (error\ in\ sieve\ analysis)^2} \quad (5.7)$$

Table 5.23. Uncertainty measurements

Parameter	**Uncertainty**
Size modulus	3.6
Carbon utilization efficiency	2.31
NO_x	5.0
CO_2	5.0
O_2	0.2

The uncertainty of the individual measurements has been taken from the manufacturer's data sheet. The uncertainty values in the present work are shown in Table 5.23.

5.7. Output data

The following is the output obtained from the mathematical model:

Minimum velocity of fluidization (cm/s)	140.55
Superficial gas velocity through the bed (cm/s)	257
Average bubble diameter (cm)	40.08
Terminal velocity (cm/s)	1121.5
Voidage at minimum fluidization	0.5365
Average bubble diameter (cm)	39.49
The average expanded bed height (cm)	92.94
fluidizing gas viscosity (g/cm.s)	4.29×10^{-5}
Overall reaction rate constant (cm/s)	19.70
The elutriation rate constant ($g/cm^2.s$)	2.15×10^{-6}
Carryover rate (g/s)	4.17
Shrinkage rate of cotton stalk (g/s)	0.00574
Bed carbon load (g)	636
Carbon utilization efficiency (%)	96.22
Amount of oxygen in exit gas (%)	7.92
Amount of carbon dioxide in exit gas (%)	11.35
Amount of nitrogen in exit gas (%)	77.6
The overall fractional oxygen consumption	0.589
Energy efficiency of the plant (%)	26,7
Steam efficiency (%)	74,2
Electrical efficiency (%)	23,8
Net heat ratio	1.34
power to heat ratio	0.2528
Exergy efficiency (%)	22,8
Net profit (%)	16.66

Chapter 6

CONCLUSIONS AND RECOMMENDATIONS

6.1. Conclusions

Following conclusions are drawn from the present work:

1. Solid population model predicted the performance of cotton stalk based 7.5 MW power plant with good accuracy. Distribution modulus and size modulus for the cotton stalk has been found to be 1.22 and 10.82 mm respectively.
2. The carbon utilization efficiency (97.44% with 30% excess air) and bed carbon load are increasing with increasing size modulus and distribution modulus. The particle elutriation rate falls as the feed particle size increases and as the excess air increases.
3. Solid population model has been optimized for maximum carbon utilization efficiency and minimum elutriation rate. Fuel particle diameter, fuel feed rate, and fractional excess air have been selected as input parameters and their optimal values are found to be 15 mm, 1.5 kg/s, and 0.3 respectively.
4. Exit gas composition model predicted exhaust gas composition for AFBC using cotton stalk with reasonable accuracy. The model variation is within 6%. Oxygen conversion falls with rise in excess air. The expanded bed height, overall reaction rate constant, bubble diameter, and rise with an increase in excess air and moisture content of the fuel.
5. Energy efficiency and exergy efficiency of the plant are found to be 26.7% and 22.8% respectively. The maximum exergy destruction takes place at the boiler and improving boiler’s performance result in an improvement in the power plant performance.
6. The thermodynamic model has been optimized for maximum overall plant exergy efficiency and minimum complete cycle exergy destruction rate. Optimal values of input parameters turbine inlet pressure, turbine inlet steam temperature, and fuel feed rate are found to be 65

bar, 470˚C, and 1.5 kg/s respectively. At optimal levels of input parameters, maximum overall plant exergy efficiency (η_{E_x}) of 43.53%, and minimum complete cycle exergy destruction (Ex_D) of 9733.999 kW can be achieved.

7. On comparing the effect of reducing AFC and ATVC, break-even point arrives earlier while reducing AFC by 25% and net profits are more in reducing ATVC by 25%. With the slight decrease in exergy efficiency (22.8% to 21.5%), net profit earned decreases sharply (16.7 % to 4.2%).
8. Ash melting rate increases and its viscosity decreases with an increase in bed temperature. As a result, ash particles stick to sand surfaces increasing the stickiness of the sand particles. This in turn accelerates the defluidization process. The gaseous combustion products release from the molten material is the fuel ash, which leads to the formation of gas holes and cracks on the surfaces.

6.2. Recommendations

1. Freeboard reactions in the model can be considered.
2. Experimental diffusion rate can be found for improvement in model predictions.
3. The model can be refined further by calculating the exact char surface temperature and by considering the fragmentation of char particles due to thermal and mechanical shocks.
4. Thermodynamic studies can be applied to other biomass-based thermal power plants and effect of parameters like ambient temperature, pressure, and humidity on plant performance can be studied.

REFERENCES

[1] Energy Statistics, 2015, Central Statistics Office, Ministry of Statistics and Programme Implementation, New Delhi, India.

[2] Parikka M, 2004, "Global biomass fuel resources", *Biomass and Bioenergy*, 27, 613-620.

[3] Chauhan S, 2012, "District wise agriculture biomass resource assessment for power generation: a case study from an Indian state, Punjab", *Biomass and Bioenergy*, 37, 205-212.

[4] Malik A and Mohapatra S K, 2013, "Biomass-based gasifiers for internal combustion (IC) engines – A review", *Sadhana*, 38, 461-476.

[5] Horio M, 2010, "Fluidization science, its development and future", *Particuology*, 8, 514-524.

[6] Wilhelm R H and Kwauk M, 1948, "Fluidization of solid particles", *Chemical Engineering Progress*, 44, 201-218.

[7] Davidson J F, 1961, "Symposium on fluidization- Discussion", *Transactions of the Institute of Chemical Engineering*, 39, 230-232.

[8] Row P N and Partridge B A, 1963, "Gas flow through bubbles in a fluidized bed -I Flow through an Ideal bubble", *Chemical Engineering Science*, 18, 511-524.

[9] Kunii D and Levenspiel O, 1991, "Fluidization engineering", New York – Wiley.

[10] Yue G, Lu J, Zhang H, Yang H, Zhang J, Liu Q, Li Z, Joos E and Jaud P, 2005, "Design theory of circulating fluidized bed boilers", *ASME 18th International Conference on Fluidized Bed Combustion*, Toronto, Ontario, Canada.

[11] http://www.britannica.com/technology/fluidized-bed-combustion

[12] http://www.jcoal.or.jp

[13] Sun Z, Jin B, Zhang M, Liu R and Zhang Y, 2008, "Experimental studies on cotton stalk combustion in a fluidized bed", *Energy,* 33, 1224-1232.

[14] Sun Z, Shen J, Jin B and Wei L, 2010, "Combustion characteristics of cotton stalk in FBC", *Biomass and Bioenergy*, 34, 761-770.

[15] Geldart D, 1986, "Gas fluidization theory", Wiley International Publisher.

[16] Kalita P, Saha U K and Mahanta P, 2013, "Effect of biomass blending on hydrodynamics and heat transfer behavior in a pressurized circulating fluidized bed unit", *International Journal of Heat and Mass Transfer,* 60, 531-541.

[17] Biswal K C, Bhowmik T G and Roy G K, 1985, "Prediction of minimum fluidization velocity for gas solid fluidization of regular particles in conical vessels", *Chemical Engineering Journal*, 30, 57–62.

[18] Sau D C, Mohanty S and Biswal K C, 2007, "Minimum fluidization velocities and maximum bed pressure drops for gas–solid tapered fluidized beds", *Chemical Engineering Journal,* 132, 151-157.

[19] Wang X, Lu J, Zhang J, Yang H, Zhang H, Yue G, Suda T and Sato J, 2005, "Experimental measurement of bubble parameters during fluidized bed scaling", *ASME 18th International Conference on Fluidized Bed Combustion*, Toronto, Ontario, Canada.

[20] Armstrong L M, Gu S, Luo K H and Mahanta P, 2013, "Multifluid modeling of the desulfurization process within a bubbling fluidized bed coal gasifier", *AIChE*, 59, 1952-1963.

[21] Papadikis K, Gu S and Bridgwater A V, 2010, "Geometrical optimization of a fast pyrolysis bubbling fluidized bed reactor using computational fluid dynamics" *Energy and fuels*, 24, 5634-5651.

[22] Yagi S and Kunii D, 1955, "Studies on combustion of carbon particles in flames and fluidized beds", *Proceedings of 5th Symposium on Combustion*, The Combustion Institute, 231-244.

[23] Toomey R D and Johnstone H F, 1952, "Gas fluidization of solid particles", *Chemical Engineering Progress,* 48, 220-226.

[24] Davidson J F and Harrison D, 1963, "Fluidized Particles", *Cambridge University Press*, United Kingdom.

[25] Grace J R and Clift R, 1974, "On the two-phase theory of fluidization", *Chemical Engineering Science*, 29, 327-334.

[26] Pyle D L and Harrison D, 1967, "An experimental investigation of two-phase theory of fluidization", *Chemical Engineering Science*, 22, 1199-1207.

[27] Godard K E and Richardson J F, 1968, "Distribution of gas flow in a fluidized bed", *Chemical Engineering Science*, 23, 660.

[28] Rowe P N and Everett D J, 1972, "Fluidized bed bubbles viewed by X-rays, Part I-Experimental details and the interactions of bubbles with solid surfaces", *Trans. Inst. Chem. Engrs.*, 50, 55.

[29] Grace J R and Harrison D, 1969, "The behaviour of freely bubbling fluidized beds", *Chemical Engineering Science*, 24, 497-508.

[30] Kelsey J R, Masters in Science - Thesis, University of Bradford, 1970.

[31] Mcgrath L and Streatfield R E, 1971, "Bubbling in shallow gas-fluidized beds of large particles", *Trans.Inst. Chem. Engrs.*, 49, 70.

[32] Geldart D and Cranfield R R, 1972, "The gas fluidization of large particles", *The Chemical Engineering Journal*, 3, 211-231.

[33] Davidson J F and Harrison D, 1966, "The behavior if a continuously bubbling fluidized bed", *Chemical Engineering Science*, 21, 731-738.

[34] Lockett M J, Davidson J F and Harrison D, 1967, "On the two-phase theory of fluidization", *Chemical Engineering Science*, 22, 1059-1066.

[35] Avedesian M M and Davidson J F, 1973, "Two phase theory of fluidization to the batch combustion of char and coke particles in a hot bed of inert material fluidized by air", *Trans. Inst. Chem. Engg.*, 51,121.

[36] Kunii D and Levenspiel O, 1968, "Bubbling bed model for kinetic processes in fluidized beds", *Ind. Engg. Chem. Process Des.,* 7, 481-492.

[37] Chen T P and Saxena S C, 1977, "Mathematical modeling of coal combustion in fluidized beds with sulphur emission control by limestone or dolomite", *Fuel*, 56, 401-413.

[38] Sriramulu S, Sane S, Agarwal P and Mathews T, 1996, "Mathematical modeling of fluidized bed combustion: 1. Combustion of carbon in bubbling bed", *Fuel*, 75, 1351-1362.

[39] Arena U, Chirone R, Damore M and Salatino P, 1995, "Some issues of modeling bubbling and circulating fluidized bed combustors", *Powder Technology*, 82, 301-316.

[40] Horio M and Wen C Y, 1978, "Simulation of fluidized bed combustors Part-I, combustion efficiency and temperature profile", AIChE *Symp. Ser. – Fluidization, Application to Coal Conversion Process*, 74, 112.

[41] Rajan R R, Krishnan R and Wen C Y, 1978, "Simulation of fluidized bed combustors Part-II, coal devolatization and sulphur oxides retention", AIChE *Symp. Ser. – Fluidization, Application to Coal Conversion Process*, 74, 176.

[42] Rajan R R and Wen C Y, 1980, "A comprehensive model for fluidized bed coal combuators", *AIChE*, 26, 642-655.

[43] Gordon A L, Caram H S and Amundson N R, 1978, "Modeling of fluidized bed reactors-V. Combustion of carbon particles – an extension", *Chemical Engineering Science*, 33, 713-722.

[44] Bukur D B and Amundson N R, 1982, "Fluidized bed combustion kinetic models", *Chemical Engineering Science*, 37, 17-25.

[45] Bukur D B and Nasif N, 1985, "The effect of bubble size variation on the performance of fluidized bed reactors", *Chemical Engineering Science*, 40, 1925-1933.

[46] Orcutt J C, Davidson J F and Pigford R L, 1962, "Reaction time distributions in fluidized catalytic reactors", *Chemical Engineering Symposium,* 58, 1-15.

[47] Darton R C, Lanauze R D, Davidson J F and Harrison D, 1977, "Bubble growth due to coalescence in fluidized beds", *Transactions of the Institute of Chemical Engineers,* 55, 274-280.

[48] Khan A A, Jong W D, Gort D R and Spliethoff H, 2007, "A fluidized bed biomass combustion model with discretized population balance", *Energy and fuels,* 21, 2346-2356.

[49] Chavarie, C and Grace J R, 1975, "Performance of a fluidized bed reactor: Visible flow behaviour", *Industrial and Engineering Chemistry,* 14, 75-78.

[50] Okasha F, 2007, "Staged combustion of rice straw in a fluidized bed", *Experimental Thermal and Fluid Science,* 32, 52-59.

[51] Reddy G V and Mohapatra S K, 1994, "A mathematical model for exit gas composition in a 10 MW fluidized bed coal combustion power plant", *Energy Conversion and Management,* 35, 1049-1060.

[52] Cano G, Salatino P and Scala F, 2007, "A single particle model of the fluidized bed combustion of a char particle with a coherent ash skeleton: Application to granulated sewage sludge", *Fuel Processing Technology,* 88, 577-584.

[53] Komatina M, Manovic V and Saljnikov A, 2007, "Temperature of coal particle during devolatization in fluidized bed combustion reactor", *Energy Sources, Part A: Recovery, Utilization and Environmental Effects,* 28, 1387-1396.

[54] Ergudenler A, Ghaly A E, Hamdullahpur F and Al-taweel A M, 1997, "Mathematical modeling of a fluidized bed straw gasifier: Part I- Model development", *Energy Sources,* 19, 1065-1084.

[55] Okasha F, 2007, "Modeling combustion of straw-bitumen pallets in a fluidized bed", *Fuel Processing Technology*, 88, 281-293.

[56] Singh R I, Mohapatra S K and Gangacharyulu D, 2008, "Studies in an atmospheric fluidized bed combustor of 10 MW power plant based on rice husk", *Energy Conversion and Management*, 49, 3086-3103.

[57] Natale G, Galgano A and Blasi C D, 2014, "Modeling particle population balances in fluidized bed gasifiers", *Biomass and Bioenergy*, 62, 123-137.

[58] Aljundi, I H, 2009, "Energy and exergy analysis of a steam power plant in Jordan", *Applied Thermal Engineering*, 29, 324–328.

[59] Rosen M A, 2001, "Energy and exergy-based comparison of coal-fired and nuclear steam power plants", *International Journal of Exergy,* 1, 180–192.

[60] Thakur T, Deshmukh S G and Kaushik S C, 2006, "Efficiency evaluation of the state owned electric utilities in India", *Energy Policy,* 34, 2788–2804.

[61] Hashem H H, 1991, "Thermal-economic analysis of industrial gas turbine cogeneration plant", *Energy Conversion Management,* 32, 419-424.

[62] Ganapathy T, Gakkhar R P, Murugesan K, Alagumurthi N and Seran M, 2009, "Energy and exergy analysis of operating thermal power plant at 50MWe grid load", *Journal on Future Engineering and Technology*, 4, 34-40.

[63] Ganapathy T, Alagumurthi N, Gakkhar R P and Murugesan K, 2009, "Exergy analysis of operating lignite fired thermal power plant", *Journal of Engineering Science and Technology Review,* 2, 123-130.

[64] Dincer I, Hussain M M and Al-Zaharnah I, 2004, "Analysis of sectoral energy and exergy use of Saudi Arabia", *International Journal of Energy Research*, 28, 205-243.

[65] Wright D R M, Hunag Y, Rezvani S, Redpath D, Anderson M, Dave A and Hewitt N J, 2013, "A technical and economic analysis of three large scale biomass combustion plants in the UK", *Applied Enegry*, 112, 396-404.

[66] Rosen M A, 2001, "Energy- and Exergy-based comparison of coal-fired and nuclear steam power plants", *Exergy, An International Journal*, 1, 180-192.

[67] Kwak H Y, Kim D J and Jeon J S, 2003, "Exergetic and thermoeconomic analyses of power plants", *Energy*, 28, 343-360.

[68] Sengupta S, Datta A and Duttagupta S, 2007, "Exergy analysis of a coal-based 210 MW thermal power plant", *International Journal of Energy Research*, 31, 14-28.

[69] Peng S, Wang Z, Hong H, Xu D and Hongguang J, 2014, "Exergy evaluation of a typical 300 MW solar-hybrid coal-fired power plant in China", *Energy Conversion and Management*, 85, 848-855.

[70] Verkhivker G P and Kosoy B V, 2001, "On the exergy analysis of power plants", *Energy Conversion and Management*, 42, 2053-2059.

[71] Oktay Z, 2009, "Investigation of coal fired power plants in Turkey and a case study: Can plant", *Applied Thermal Engineering*, 29, 550–557.

[72] Kopac M and Hilalci A, 2007, "Effect of ambient temperature on the efficiency of the regenerative and reheat Catalagzı power plant in Turkey", *Applied Thermal Engineering*, 27, 1377–1385.

[73] Mitrovic D, Zivkovic D and Lakovic M S, 2010, "Energy and Exergy Analysis of a 348.5 MW steam power plant", *Energy Sources, Part A: Recovery, Utilization, and Environmental Effects*, 32, 1017-1027.

[74] Erdem H H, Akkaya A V, Cetin B, Dagdas A, Sevilgen S H, Sahin B, Teke I, Gungor C and Atas S, 2009, "Comparative energy and exergy performance analyses for coal-

fired thermal power plants in Turkey", *International Journal of Thermal Sciences,* 48, 2179–2186.

[75] Regulagadda P, Dincer I and Naterer G F, 2010, "Exergy analysis of a thermal power plant with measured boiler and turbine losses", *Applied Thermal Engineering,* 30, 970–976.

[76] Bryant J, 2007, "Thermodynamic theory of economics", *International Journal of Exergy,* 4, 302-337.

[77] Liu C H, Lin S J and Charles L, 2010, "Evaluation of thermal power plant operation performance in Taiwan by data envelopment analysis", *Energy Policy,* 38, 1049–1058.

[78] Nakano M and Managi S, 2008, "Regulatory reforms and productivity: an empirical analysis of the Japanese electricity industry", *Energy Policy,* 36, 201–209.

[79] Shrivastava N, Sharma S and Chauhan K, 2012, "Efficiency assessment and benchmarking of thermal power plants in India", *Energy policy,* 40, 159-176.

[80] Scala F, Chirone R and Salatino P, 2003, "The influence of fine char particles burnout on bed agglomeration during the fluidized bed combustion of a biomass fuel," *Fuel Processing Technology*, 84, 229–241.

[81] Mettanant V, Basu P and Butler J, 2009, "Agglomeration of biomass fired fluidized bed gasifier and combustor," *The Canadian Journal of Chemical Engineering,* 87, 656-684.

[82] Lin W, Johansen K D and Frandsen F, 2003, "Agglomeration in bio-fuel fired fluidized bed combustors," *Chemical Engineering Journal,* 96,171–185.

[83] Basu P, 2006, "Combustion and gasification in fluidized beds," CRC Press, Chapter 2.1.

[84] Chirone R, Miccio F and Scala F, 2006, "Mechanism and prediction of bed agglomeration during fluidized bed combustion of a biomass fuel: effect of the reactor scale," *Chemical Engineering Journal*, 123,71–80.

[85] Visser H J M, Lith V S and Kiel J H A, 2002, "Biomass ash-bed material interactions leading to agglomeration in fluidized bed combustion and gasification," *12th European conference on Biomass for Energy, Industry and Climate Protection*, Amsterdam, The Netherlands.

[86] Ohman M, Nordin A, Skrifvars B J, Backman R and Hupa M, 2000, "Bed agglomeration characteristics during fluidized bed combustion of biomass fuels," *Energy and Fuels*, 14, 169–178.

[87] Hulkkonen S, Fabritius M and Enestam S, 2003 "Application of BFB technology for biomass fuels: technical discussions and experience from recent project," *17th International Conference on Fluidized Bed Combustion*, S. Pisupatis, Eds., Jacksonville, FL, U.S.A.

[88] Fernandez M J, 2000 "Reduccion de la sinterizacion en la ceniza de biomasa en combustion. Aplicacion al lechl fluidizado burbujeante", Ph.D. thesis [in Spanish], Valladolid University.

[89] Werther J, Saenger M, Hartge E U, Ogada T and Siagi Z, 2000, "Combustion of agricultural residues," *Progress in Energy and Combustion Science*, 26, 1–27.

[90] Brus E, Ohman M, Nordin A and Bostrom D, 2004, "Bed agglomeration characteristics of biomass fuels using blast-furnace slag as bed material," *Energy and Fuels*, 18, 1187–1193.

[91] Ohman M and Nordin A, 2000, "The role of kaolin in prevention of bed agglomeration during fluidized bed combustion of biomass fuels," *Energy and Fuels*, 14, 618–624.

[92] Ohman M, Nordin A, Lundholm K, Bostrom D, Hedman H and Lundburg M, 2003, "Ash transformations during combustion of meat-, bonemeal, and RDF in a (bench-scale) fluidized bed combustor," *Energy and Fuels*, 17, 1153–1159.

[93] Saleh K, Steinmetz D and Hemati M, 2003, "Experimental study and modeling of fluidized bed coating and agglomeration," *Powder Technology*, 130, 116–123.

[94] Natarajan E, Ohman M, Gabra M, Nordin A, Liliedahl T and Rao N A, "Experimental determination of bed agglomeration tendencies of some common agricultural residues in fluidized bed combustion and gasification," *Biomass and Bioenergy*, 15, 163–169.

[95] Vesilind P A, 1980, "The Rosin–Rammler particle size distribution", *Resource Recovery Conservation*, 5, 275-277.

[96] Stamboltzis G A, 1983, "Modification of Rosin–Rammler and Gates–Gaudin–Schuhmann equations in repeated single fracture of brittle materials", *Mineral Metall Annals*, 54, 36–44.

[97] Bond F C, 1985, "Mineral Processing Handbook", *SME American Institute of Mining, Metallurgical and Petroleum Engineers*: New York, 16–27.

[98] Lynch A J and Less M J, 1985, "Mineral Processing Handbook" *SME American Institute of Mining, Metallurgical and Petroleum Engineers*: New York, 28–53.

[99] Fang Z, Patterson B R and Turner M E, 1993, "Modeling particle size distributions by the Weibull distribution function", *Material Characterization*, 31, 177–182.

[100] Chitester D C, Kornosky R M, Fan L S and Danko J P, 1984, "Characteristics of fluidization at high pressure", *Chemical Engineering Science*, 39, 253–261.

[101] Bird R B, Stewart W E and Lightfoot F N, 2008, "Transport Phenomenon", Wiley India Publications, India.

[102] Stubington J F, Barret D and Lowry G, 1984, "Bubble size measurements and correlation in a fluidized bed at high temperature", *Chemical Engineering Resource Des*, 62, 173–178.

[103] Yagi S and Aochi T, cited in Kunii D and Levenspiel O, 1991, *Fluidization Engineering*. Butterworth- Heinmenn: USA, 178–179.

[104] Wen C Y and Hashinger R F, 1960, "Elutriation of solid particles from a dense-phase fluidized bed", *AIChE*, 6, 220–226.

[105] Tanaka I, Shinohara H, Hirouse H and Tanaka Y, 1972, "Elutriation of fines from fluidized beds", *Journal of Chemical Engineering – Japan*, 5, 51–57.

[106] Merrick D and Highley J, 1974, "Particle size reduction and elutriation in fluidized bed process", *AIChE Symposium Series*, 70, 366–378.

[107] Geldart D, Cullinan J, Georghiades S, Gilvray D and Pope D J, 1979, "The effect of fines on entrainment from gas fluidized beds", *Transitions of Institute of Chemical Engineers*, 57, 269–275.

[108] Colakyan M and Levenspiel O, 1984, "Elutriation from fluidized beds", *Powder Technology*, 38, 223–232.

[109] Kato K, Takarada T, Tarnura T and Nishino K. cited in Kunii D and Levenspiel O, 1991, *Fluidization Engineering*, Butterworth-Heinmenn: USA, 178–179.

[110] Saxena S C and Rehmat A, 1980, *6th Conference on Fluidized Bed Combustion*, 3, 1138–1150.

[111] Avedesian M M and Davidson J F, 1973, "Combustion of carbon particles in a fluidized bed", *Transactions of Institute of Chemical Engineers*, 51, 121–128.

[112] Wen C Y and Ishida M, 1968, "Comparison of kinetic and diffusional models for solid–gas reactions", *AIChE*, 14, 311–317.

[113] Wen C Y and Wang S C, 1970, "Oxidation of carbon in porous solids", *National Meeting of the American Chemical Society*, Chicago, 14, 80–89.

[114] Chirone R, Salatino P, Scala F, Solimene R and Urciuolo M, 2008, "Fluidized combustion of palletized biomass and waste derived fuels", *Combustion and Flame*, 155, 21–36.

[115] Turnbull E, Kossakowaski E R, Davidson J F, Hopes R B, Blackshaw H W and Goodyer P Y T, "Effect of pressure on combustion of char in fluidized beds", *Chemical Engineering Research and Design*, 62, 223–234.

[116] Parker A S and Hotel H C, 1936, "Combustion rate of carbon study of gas film structure by microsampling", *Industrial and Engineering Chemistry Research*, 28, 1334–1341.

[117] Park D, 1989, "Estimation of temperature difference between char particles and the fluidized bed in char combustion", *Fuel*, 68, 1320–1324.

[118] Campbell E K and Davidson J F, 1975, "The combustion of coal in fluidized beds", *Institute of Fuel, Symposium Series 1*, 1–9.

[119] Krishnaiah K and Shahabudeen P, 2012, "Applied design of experiments and Taguchi methods", New Delhi – PHI Learning Private Limited.

[120] Mohapatra S K, 1996, "Modeling of fluidized bed coal combustion process", *Ph D thesis*, Indian School of Mines, Dhanbad, India.

[121] Reddy GV, Parsad S and Mohapatra S K, 1995, "Mathematical model for coal combustion in a fluidized bed combustor: particle size distribution effect", *Industrial Journal of Engineering and Materials Science*, 2, 224–230.

[122] Subramani H, Balaiyya M B and Miranda L, 2007, "Minimum fluidization velocity at elevated temperatures for Geldart's group - B powders", *Experimental Thermal and Fluid Science*, 32, 166-173.

[123] Rathore M M, 2010, "Thermal Engineering", Tata McGraw-Hill Education, New Dehli.

[124] Cengel Y A and Boles A B, 2008, "Thermodynamics-An Engineering Approach", The McGraw-Hill companies, New York.

[125] Rashad A and Maihy A E, 2009, "Energy and exergy analysis of a steam power plant in Egypt", *13th International Conference on Aerospace Sciences and Aviation Technology, Egypt,* 1-12.

[126] Motghare V S and Cham R K, 2014, "Generation cost calculation for 660 MW thermal power plants", *International Journal of Innovative Science, Engineering & Technology,* 1, 660-664.

[127] Moffat R J, 1988, "Describing the uncertainties in experimental results", *Experimental Thermal and Fluid Science,* 1, 3-17.

[128] Kline S J and McClintock F A, "Describing uncertainties in single sample experiments", *Mechanical Engineering,* 75, 3-8.

PUBLICATIONS RELATED TO THIS WORK

Journal Publications

1. Sharma, R K, and Mohapatra, S K, "Thermo-economic analysis of a biomass-fired bubbling fluidized bed thermal power plant", *International Journal of Exergy,* (*SCI, Inderscience*), vol. 21, 1, pp. 1-20.
2. Sharma, R K, and Mohapatra, S K, "Study of particle size distribution and oxygen mass balance in a bubbling fluidizing combustor using cotton stalk", *Asia-Pacific Journal of Chemical Engineering* (*SCI, John Wiley*), vol. 11, 2, pp. 187-199.

Conference Publications

1. Mohapatra, S K, and Sharma, R K, "Study of particle size distribution on fluidization parameters in a 5 MW AFBC power plant using cotton stalk", 28th International Conference on Solid Waste Technology and Management, Widener University, Philadelphia, March 10-13, 2013, pp. 1145-1155.